# The Role of α-Sheet Structure in Bacterial and Mammalian Amyloidogenesis and its Implication in the Microbial Alzheimer's Disease Hypothesis

Tatum Soleil Prosswimmer

A dissertation

submitted in partial fulfillment of the

requirements for the degree of

Doctor of Philosophy

University of Washington

2023

Reading Committee:

Valerie Daggett, Chair

James Bryers

Steven Kahn

Champak Chatterjee

Program Authorized to Offer Degree:

Molecular Engineering and Sciences

University of Washington

## Abstract

The Role of α-Sheet Structure in Bacterial and Mammalian Amyloidogenesis and its Implication in the Microbial Alzheimer's Disease Hypothesis

Tatum Soleil Prosswimmer

Chair of the Supervisory Committee:
Valerie Daggett, Professor
Department of Bioengineering

Mammalian amyloidogenesis is implicated in over 50 diseases and its formation is typically considered inherently pathological. Conversely, many bacteria utilize amyloid fibrils as a structural scaffold to fortify a surface bound 3D matrix known as a biofilm. Bacterial and mammalian amyloidogenesis involves the production of toxic, soluble α-sheet oligomers prior to the formation of nontoxic β-sheet fibrils. The existence of a conserved conformation in the toxic intermediates formed during amyloidogenesis presents a strategy to inhibit aggregation in the context of mammalian amyloid disease and bacterial infection. Here, *de novo* peptides that stably adopt α-sheet conformation are employed to inhibit bacterial and mammalian amyloid formation, neutralize the oligomeric toxicity of mammalian amyloid peptides, and structurally destabilize bacterial biofilms, rendering them more susceptible to antibiotics. The knowledge of a conserved amyloid inhibition mechanism by α-sheet peptides is also used to investigate the microbial Alzheimer's disease hypothesis, providing insight into the molecular mechanisms that govern the role of amyloid-β in the innate immune response and positing an evolutionary role for mammalian amyloidogenesis in the defense against microbial infection.

# TABLE OF CONTENTS

# LIST OF FIGURES

# LIST OF TABLES

# ACKNOWLEDGEMENTS

The author would like to thank Dr. Valerie Daggett for support and mentorship throughout her graduate career, as well as Dr. James Bryers, Dr. Steven Kahn, and Dr. Champak Chatterjee for their service on the supervisory committee. She is also thankful to Dr. Alissa Bleem, Dr. Matthew Childers, Dr. Dylan Shea, Sarah Nick, and Anthony Heng for experimental guidance, informative discussions, and moral support. Finally, the author would like to thank the Molecular Engineering and Sciences Program, the Department of Bioengineering, and the National Institutes of Health for financial support.

# DEDICATION

To my family, both innate and chosen,

for your unwavering support and belief in me.

I would not be here without you.

# Chapter 1. Introduction

## 1.1 Introduction to Amyloid Proteins

Amyloidogenic proteins and peptides undergo conformational changes from their native structure, misfold, and self-aggregate to form amyloid fibrils[1,2]. These self-aggregating proteins have been identified in both mammalian and bacterial species[1,3,4]. Mammalian amyloid proteins are associated with over 50 diseases, including Alzheimer's Disease (AD), Parkinson's Disease (PD), and type 2 diabetes (T2D)[5,6]. Bacteria can also form amyloid fibrils using programmed machinery, and they incorporate the fibrils into their extracellular biofilms to protect the organism from the surrounding environment, including the host immune response and antibiotics[3,4]. Regardless of the function and native structure of an amyloidogenic protein, the corresponding fibrils form cross-β-sheet structure[7]. A growing body of evidence demonstrates that toxicity associated with amyloid diseases is due to the soluble oligomeric species rather than the fibrillar plaques[8–11]. Furthermore, there is increasing evidence that both mammalian and bacterial toxic oligomers are composed of a nonstandard protein secondary structure known as α-sheet[11–16]. The elucidation of a nonstandard oligomeric secondary structure that is conserved between species presents a unique strategy to target both mammalian and bacterial amyloid.

## 1.2 The Amyloid Aggregation Pathway

The amyloid aggregation pathway has been studied extensively, primarily in the context of human disease pathology. Aggregation occurs via a nucleation-dependent mechanism with three main phases of aggregation: lag, exponential, and plateau (**Figure 1.1**)[17]. The lag phase begins when a protein or peptide undergoes conformational changes to form an aggregation-

competent monomer[18]. This aggregation competent species alone has a low propensity for oligomerization, although small aggregates have the capacity to form over time[1,18]. The lag phase ends with the formation of an aggregation nucleus, the structure from which amyloid fibrils assemble[1,19]. The exponential phase is characterized by rapid oligomerization, resulting in the formation of fibrils composed of β-sheet structure[18]. The plateau phase describes the end of the aggregation pathway when fibrils, or plaques, are deposited in surrounding tissues (mammals) or extracellular space (bacteria)[6].

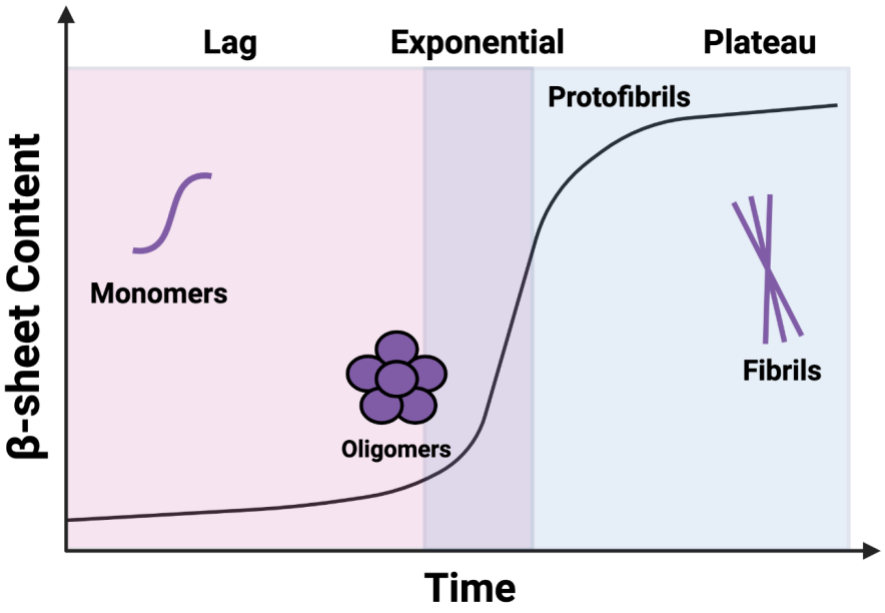


**Figure 1.1. Amyloid aggregation pathway.** Aggregation begins with the lag phase which is characterized by the formation of an aggregation-competent monomer and subsequent oligomerization. In the exponential phase, the amyloid protein changes structure and forms β-sheet protofibrils. Finally, the plateau phase describes the stage at which fibrils have rearranged to adopt highly ordered cross-β-sheet structure.

## 1.3 Mammalian Amyloidogenesis is Disease-Associated

Amyloid fibrils and plaques are the pathological hallmarks of amyloid diseases. As such, amyloid research has historically focused on the study and characterization of the fibrils, rather than the oligomers or the misfolded monomers. One of the most extensively studied amyloid systems is the amyloid-β peptide (Aβ), an intrinsically disordered peptide that is associated with AD[20]. Notably, extensive studies of Aβ and other amyloid fibrils show that the fibrils, or amyloid state, are not responsible for disease-related pathology[9–11,20,21]. Instead, studies of Aβ oligomers indicate that the low molecular weight oligomers (~8-70 kDa) are the toxic species linked to hippocampal long-term potentiation impairment, microglial activation, and synaptic dysfunction[9,10,21]. Higher molecular weight oligomers, protofibrils, and plaques display little to no cytotoxicity in biological assays[10,11]. In fact, plaque formation may serve a protective function by removing toxic oligomers from surrounding tissue[9].

The toxicity of low molecular weight soluble oligomers is not unique to Aβ and AD; studies show that the insoluble fibrils of many amyloid proteins are stable and nontoxic, while oligomers are the primary toxic species[9–11,22–25]. Islet amyloid polypeptide (IAPP), for example, is an intrinsically disordered peptide[26] whose amyloid formation is associated with T2D[27–29]. Electron microscopy experiments in which an aqueous solution of IAPP was applied to cultured islet cells demonstrated small IAPP oligomers disrupting the cell membranes, resulting in apoptosis[30]. This finding suggests that β-cell apoptosis associated with T2D is likely also caused by small, low-molecular weight IAPP oligomers, rather than fibrils[30]. Given that oligomers are thought to be the trigger responsible for downstream pathology in amyloid-associated diseases, a deeper understanding of the structural characteristics of these low molecular weight species is necessary and may inform novel diagnostic and therapeutic strategies.

## 1.4 Functional Amyloid Fortifies Bacterial Biofilms

While mammalian amyloid formation is considered inherently pathological, many bacteria utilize amyloid fibrils, often referred to as "functional amyloid", to fortify the biofilm (**Figure 1.2**). Biofilms are microbe-generated, surface-associated extracellular matrices (ECMs) composed of cells and secreted insoluble extracellular molecules (proteins, polysaccharides, and extracellular DNA) that facilitate cell communication and protect cells from the surrounding environment (i.e., host immune response and antibiotics)[31]. Biofilm cells are 10-1000 times less susceptible to antibiotics than free-floating, or planktonic, cells[32]. Decreased susceptibility is attributed to (1) the physical ECM barrier that restricts penetration, (2) limited nutrient sources within the biofilm causing reduced growth rates and metabolic activity, and (3) differences in global gene expression between sessile and planktonic bacteria[33–35]. Biofilm-associated infections are difficult to treat due to reduced antibiotic sensitivity, and current treatment strategies typically involve intense antibiotic administration which can result in the development of multidrug resistant pathogens[16,36].

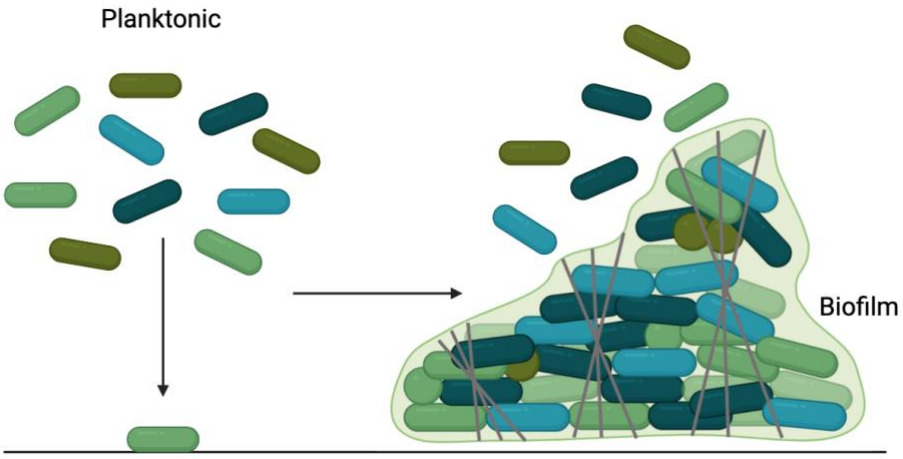


**Figure 1.2. Functional amyloid fortifies the surface-associated biofilm matrix.** Biofilms form when planktonic cells adhere to a surface and build an extracellular matrix composed of proteins, polysaccharides, and extracellular DNA. Many bacteria, including both gram-negative and gram-positive species, incorporate mature amyloid fibrils (represented here by gray cross structures) into their extracellular biofilms to reinforce the biofilm as a structural support and to resist dispersion by chemical or mechanical agents.

Functional bacterial amyloid fibrils are biochemically similar to those involved in mammalian amyloid diseases, revealing the conservation of the amyloid fold over millions of years of evolution[37]. Because functional amyloid is produced in the extracellular space and is not required for cell growth, amyloid fibrils represent an attractive target for the disarming of bacterial pathogens and the clearance of biofilm infections without the increased risk of resistance invoked by selective pressure.

## 1.5 Toxic Oligomers Adopt α-Sheet Structure

Recent studies suggest that toxic oligomers formed by bacterial and mammalian species adopt a nonstandard secondary structure, known as α-sheet, prior to the conversion to β-sheet structure[11–16,38–41]. α-Sheet was first identified in molecular dynamics (MD) simulations of several structurally and functionally unrelated amyloid proteins[41–53]. α-Sheet structure is stabilized by hydrogen bonding between individual α-strands, similar to the formation of the standard β-sheet secondary structure[41,42,54–57]. Amino acids that form the strands are locally helical, occupying the left- ($\alpha_L$) and right-handed ($\alpha_R$) helical regions of Ramachandran space (**Figure 1.3A**)[41,54,56,58]. Sequential alternation between $\alpha_L$ and $\alpha_R$ backbone ($\Phi$, $\Psi$) dihedral angles results in the formation of an elongated strand (**Figure 1.3B**)[41,55,56,58]. Sheets are formed through bifurcated hydrogen bonding between individual residues in adjacent strands (**Figure 1.3C**)[41,56,59]. Bifurcated hydrogen bonding is also seen in α-helices, but not in β-sheet structures, and it can significantly increase structural stability[41,56]. α-Sheet is also unique in that the amide groups are aligned along one side of the peptide backbone, while the carbonyl groups are located along the other[13,38,41,56,60]. The alignment of NH groups on one side of the sheet and CO groups on the opposite forms a strong molecular dipole across the sheet which may assist in oligomerization through monomer–monomer interactions[40,41,56,61].

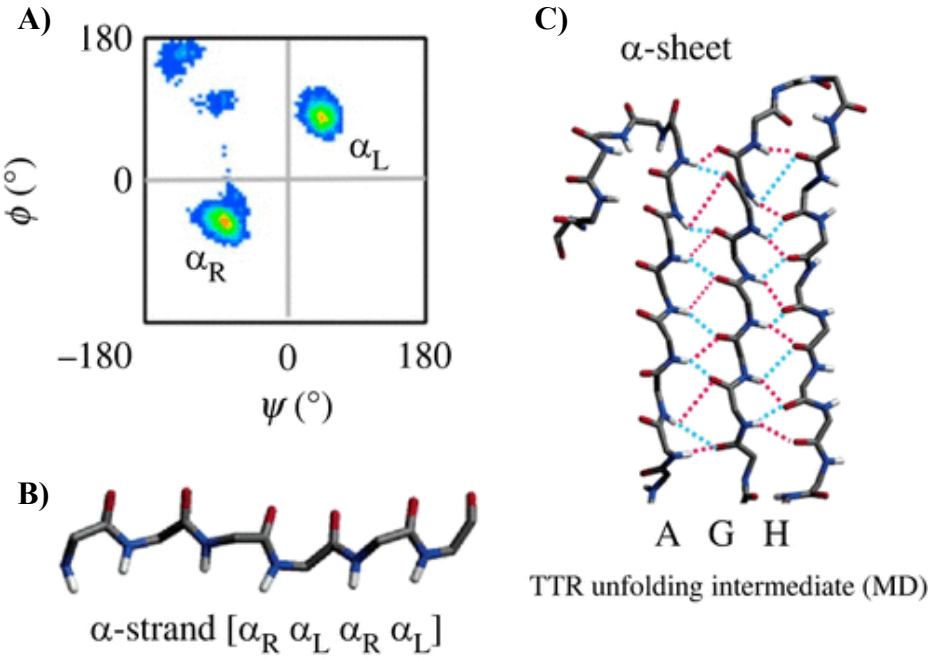


**Figure 1.3. α-Sheet structure. A)** Sequential amino acids in the α-strand conformation have backbone $\Phi$ and $\Psi$ angles that alternately occupy the $\alpha_R$ and $\alpha_L$ regions of Ramachandran space. **B)** The sequential alternation between $\alpha_R$ and $\alpha_L$ conformation results in the alignment of carbonyl groups on one side of the peptide backbone, and the alignment of the peptide's amide groups on the other side of the backbone. **C)** Bifurcated hydrogen bonding between the A, G and H strands of transthyretin (TTR) stabilize the peptide in α-sheet conformation. Figure reproduced with permission[2,13,41].

To experimentally probe the structure of soluble oligomers and further characterize the toxic species associated with mammalian amyloid, *de novo* hairpin peptides were designed and engineered through MD simulations and produced by solid-phase peptide synthesis. These peptides were designed to adopt a conformation complementary to the non-standard α-sheet structure that was observed in MD simulations, and the designed peptides are themselves α-sheet. The designed peptides were hypothesized to selectively bind to the toxic oligomers of

amyloid proteins regardless of the protein's native structure to facilitate isolation and characterization of the nonstandard structure[13,15].

The *de novo* hairpin peptides (APs) were designed using the Structural Library of Intrinsic Residue Properties (SLIRP) associated with the Dynameomics project[62–64]. SLIRP was used to measure the propensities for various combinations of amino acids to occupy the desired regions of conformational space observed in MD[62–68] (**Figure 1.4A**). It was determined that sequential alternation between L- and D-amino acids would produce an extended sheet structure that mimics the α-sheet conformational signature observed in MD simulations of amyloid proteins containing all L-amino acids[13] (**Figure 1.4B**). A variety of sequences were chosen according to these criteria and the sequences were used to engineer a library of *de novo* peptides predicted to adopt stable α-sheet structure.

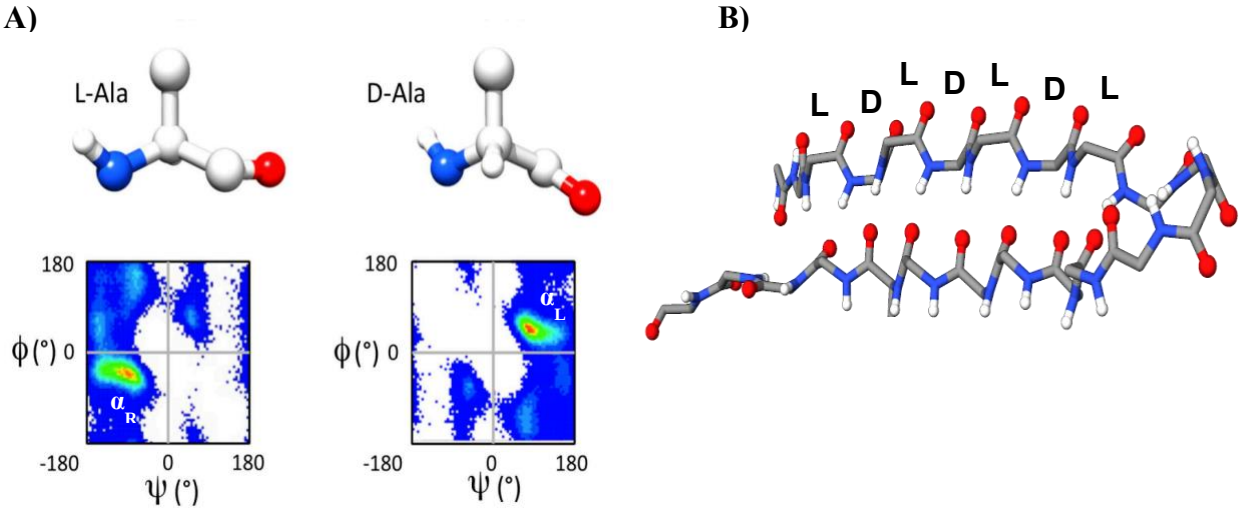


**Figure 1.4. *De novo* α-sheet peptide design. A)** Intrinsic residue propensities for L- and D-alanine were calculated from MD simulation of a GGXGG peptide system[62]. **B)** Sequential alternation between L- and D-amino acids produces elongated strand conformation in which sequential residues alternate between $\alpha_R$ and $\alpha_L$ propensity, templating the structure observed in MD simulations[13,15]. Figure reproduced with permission[13,15].

α-Sheet structure can be readily visualized using circular dichroism spectroscopy (CD), a technique which utilizes right- and left-handed circularly polarized light to determine protein secondary structure[69]. Because of the alternating $\alpha_L$ and $\alpha_R$ chirality residues that compose α-sheet structure and *de novo* α-sheet peptides, the nonstandard conformation produces a relatively flat and featureless spectrum by CD. As predicted, *de novo* hairpin peptides, such as AP5, AP401, and AP516, which each have alternating L- and D-amino acids but different sequences, produce relatively flat and featureless CD spectra, confirming that the designed peptides adopt stable α-sheet structure (**Figure 1.5**).

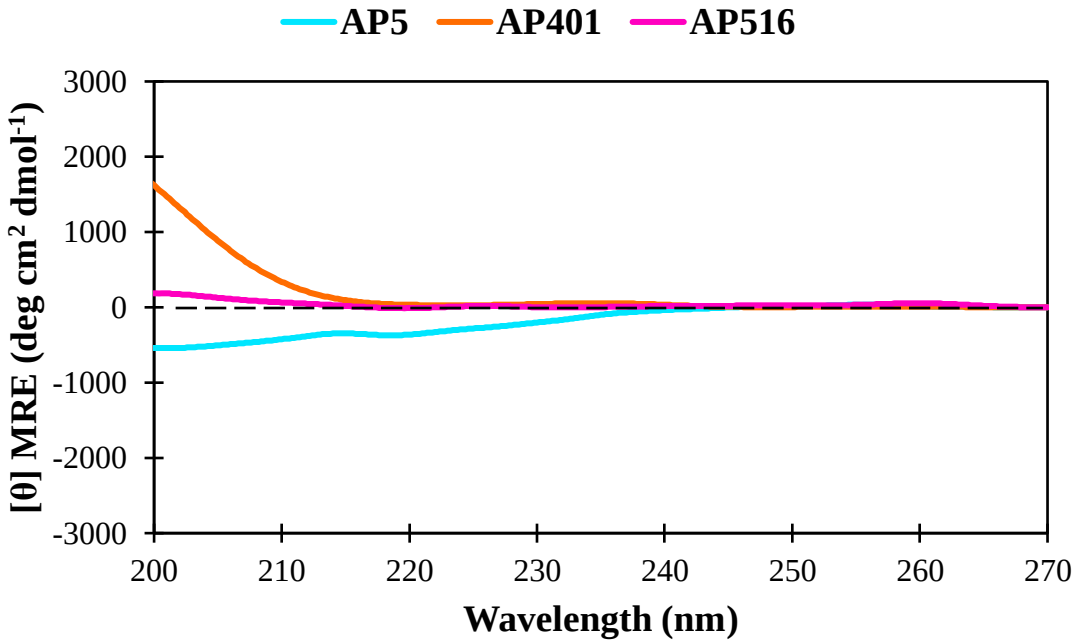


**Figure 1.5. CD spectroscopy of AP5, AP401, and AP516.** *De novo* hairpin peptides (25 μM) with alternating L- and D- amino acids produce relatively flat and featureless CD spectra, representative of the α-sheet conformation. AP5 (blue) has predominantly L-amino acids, resulting in slightly reduced CD signal at lower wavelengths. AP401 and AP516 (orange and pink, respectively) are composed of predominantly D-amino acids, and a slight CD signal increase is observed at lower wavelengths.

This Dissertation explores the role of α-sheet structure in both mammalian (Aβ and IAPP) and bacterial (*E. coli* and *S. aureus*) amyloidogenesis and investigates the capacity for *de novo* α-sheet peptides to inhibit amyloid formation by each of these species. Various experimental techniques are employed to characterize the aggregation of Aβ and IAPP and to determine the secondary structures sampled by each peptide throughout the course of aggregation. Experiments described here confirm that α-sheet oligomers are the primary toxic species, while random coil monomers and β-sheet fibrils are relatively nontoxic. Various *de novo* hairpin peptides, including AP5, AP90, and AP401 are shown to inhibit aggregation and neutralize oligomeric toxicity of both Aβ and IAPP, as well as to inhibit bacterial amyloid formation in *E. coli* and *S. aureus*. Additionally, α-sheet peptides are employed as a strategy to weaken biofilm ECM structure and promote antibiotic susceptibility, revealing a novel strategy to target biofilm infections. The work described in this Dissertation uncovers a shared conformation between mammalian and bacterial oligomers and provides evidence for an inhibitory strategy that can be used to defend against pathological mammalian amyloid and functional biofilm-associated amyloid.

## 1.6 Microbial Alzheimer's Disease Hypothesis

The aggregation of Aβ is associated with AD, a disease which is characterized by progressive cognitive dysfunction and that is the 6$^{th}$ leading cause of death in the United States[70]. During amyloidogenesis, Aβ forms toxic, soluble α-sheet oligomers – implicated in neuronal death and disease pathology – prior to the deposition of mature fibrils[9–11,23,71,72]. Previously, Aβ aggregation was considered an inherently aberrant process, but recent studies suggest that

aggregation may be triggered as a protective mechanism to target microbial infection in the brain.

The microbial AD hypothesis was derived from numerous studies that observed colocalization between Aβ plaques and microbial pathogens in various brain regions of AD patients[73–81]. Pathogens discovered directly colocalized with Aβ plaques include herpes simplex virus 1 (HSV1), *Chlamydia pneumoniae* (*C. pneumoniae*), bacterial lipopolysaccharide (LPS), *Borrelia burgdorferi* (*B. burgdorferi*), *Porphyromonas gingivalis* (*P. gingivalis*), and more[74,82–85]. In one study, *B. burgdorferi*, a spirochete implicated in Lyme disease, was found in 25.3% of analyzed AD cases and was 13 times more prevalent in AD samples as compared to controls[84]. Another study found the presence of *C. pneumoniae* in 89% of AD samples tested, and only 9% of controls[85]. The discovery of pathogens in AD brain samples calls into question the widely held belief that Aβ aggregation is inherently disease-associated and suggests that oligomerization and subsequent fibrilization of Aβ may be employed as an innate immune response to an invading infection.

Overwhelming evidence of the implication of microbial pathogens in AD pathology promoted investigation into the possible role of Aβ as an antimicrobial peptide. As hypothesized, Aβ demonstrates antimicrobial activity against numerous pathogens including *E. coli, Candida albicans (C. albicans), S. aureus, Pseudomonas aeruginosa (P. aeruginosa),* and more[86,87]. These observations resulted in the development of the microbial AD hypothesis, which suggests that Aβ aggregates to protect against infection present in the brain. However, a chronic inflammatory response coupled with the accumulation of toxic α-sheet oligomers results in neuronal death and AD pathology. The classification of Aβ as an antimicrobial peptide has the

potential to revolutionize the understanding of AD and may inform novel therapeutic and early intervention strategies.

Aβ is believed to function as an antimicrobial peptide by entrapping pathogens such as bacteria, fungi, and viruses in extracellular fibrillar proteins, thereby protecting the host cells from the invading infection[88,89]. This Dissertation investigates whether the oligomeric form of Aβ functions as the first defense against pathogens (as they are the primary toxic species) prior to 'entrapment' by fibrils[9–11,23,71]. In this hypothesis, Aβ oligomers combat pathogens by inhibiting their amyloid formation, therefore weakening the infection, and rendering the bacteria more susceptible to the host immune response and subsequent entrapment by Aβ plaques (**Figure 1.6**).

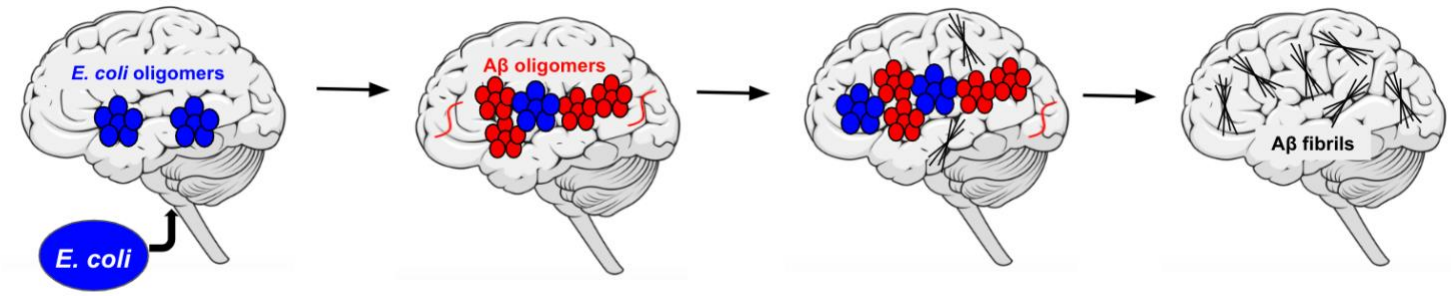


**Figure 1.6. The α-sheet-mediated microbial Alzheimer's disease hypothesis.** First, *E. coli* crosses the blood brain barrier and deposits in brain tissue. The bacteria begin to form a surface-associated biofilm, and secrete toxic, α-sheet containing oligomers (blue) in the process of forming amyloid. Exposure to these toxic oligomers elicits Aβ oligomerization (red) to inhibit curli formation through α-sheet interactions. Overaccumulation of toxic, α-sheet containing Aβ oligomers causes cell death, resulting in AD progression. Finally, Aβ forms mature fibrils (gray).

Previous studies suggest that bacterial and mammalian amyloid proteins can inhibit one another's aggregation, and inhibition is likely mediated by the oligomeric species[90]. In one study, TTR, a mammalian protein involved in various amyloid diseases including familial amyloidotic cardiomyopathy[38,90,91], was shown to inhibit CsgA fibrilization by sequestering the bacterial amyloid protein formed by *E. coli* into 'dead-end' oligomers[90]. Monomeric TTR (M-TTR), which rapidly oligomerizes into α-sheet aggregates[13,15,38,90], was also shown to significantly inhibit uropathogenic *E. coli* biofilm formation[90]. As discussed in **Chapter 1.5**, soluble oligomers of various amyloid species, including Aβ, IAPP, CsgA, PSMα1, and TTR adopt a nonstandard secondary structure known as α-sheet[11–13,15,16]. Further, *de novo* peptides that adopt stable α-sheet structure successfully inhibit amyloid formation and oligomeric toxicity by binding to aggregates with the same structure[11–16]. Bacterial amyloid inhibition by *de novo* α-sheet peptides has also been shown to reduce biofilm density in *E. coli* and *S. aureus*, rendering the bacteria more susceptible to various antibiotics[16]. This Dissertation investigates the effect of amyloid formation by uropathogenic *E. coli* on Aβ aggregation in neuroblastoma cells and probes the capacity for Aβ oligomers to inhibit *E. coli* biofilm formation.

## 1.7 Overview of Chapters

The conservation of nonstandard α-sheet secondary structure in the soluble oligomeric species of bacterial and mammalian amyloid proteins represents a novel strategy to target biofilm-associated infection and human amyloid disease, while also revealing the existence of a molecular mechanism that may explain the previously observed interactions between amyloid proteins. This Dissertation explores the universality of α-sheet structure in the toxic oligomers

produced during amyloidogenesis and investigates whether the conservation of the amyloid fold across species suggests a physiological role for the formation of mammalian amyloid.

Amyloid diseases, such as Alzheimer's disease and type 2 diabetes, afflict millions and incur a significant financial burden. The toxic oligomeric intermediates of Aβ and IAPP produced prior to the deposition of β-sheet fibrils are the primary toxic species responsible for cell death and disease progression. In **Chapter 2**, synthetic α-sheet peptides are employed to inhibit the aggregation of Aβ and IAPP and neutralize the toxicity of the oligomeric α-sheet intermediates of each species. A library of *de novo* α-sheet peptides, each with sequentially alternating L- and D-amino acids but varied sequences, exhibit inhibitory properties toward both Aβ and IAPP. Further, the designed α-sheet peptides neutralize oligomeric toxicity in relevant cell models via selective binding of the α-sheet conformation present in the oligomeric species of each amyloidogenic peptide. These insights provide experimental evidence for the existence of a conserved nonstandard conformation in Aβ and IAPP and suggest that *de novo* α-sheet peptides may serve as an effective strategy to inhibit amyloidogenesis and neutralize toxicity in mammalian amyloid diseases.

The role of amyloid fibrils in the fortification of extracellular biofilms and in the reduction of *E. coli* and *S. aureus* sensitivity to antibiotics is investigated in **Chapter 3**. In this chapter, α-sheet peptides are employed against both bacteria and are shown to inhibit amyloid formation, reduce biofilm density, and improve biofilm susceptibility to multiple different antibiotics. The findings reported in this chapter elucidate a strategy to promote biofilm sensitivity to antibiotics without invoking selective pressure and increasing the risk of acquired resistance. Further, the results described in this chapter provide evidence for the presence of a

conserved nonstandard conformation in the oligomers of both bacterial and mammalian amyloid proteins.

**Chapter 4** employs the knowledge of a conserved oligomeric conformation and amyloid inhibition mechanism to the microbial Alzheimer's disease hypothesis. The effect of amyloid formation by *E. coli* on Aβ aggregation is quantified in human neuroblastoma cells. Further, the role of Aβ oligomers in the innate immune response is probed using *E. coli* biofilm inhibition and antibiotic susceptibility studies. The findings reported in this chapter suggest that the production of toxic Aβ α-sheet oligomers may be employed to protect against bacterial infection via specific α-sheet interactions, positing a role for Aβ in the innate immune response.

# Chapter 2. Characterization of the α-Sheet Conformation in Mammalian Amyloid

## 2.1 Summary

Aβ and IAPP, associated with AD and T2D, respectively, were experimentally characterized using fibrilization kinetic assays and circular dichroism spectroscopy (CD) to investigate how each peptide changes conformation throughout the course of aggregation. Studies with *de novo* α-sheet peptide inhibitors showed that amyloid inhibition is not sequence specific, but rather conformation dependent. Cellular viability studies confirmed that oligomers of both Aβ and IAPP are the primary toxic species formed during amyloidogenesis, and designed α-sheet peptides successfully neutralized oligomeric toxicity in relevant cell models. These findings reveal a novel strategy to inhibit amyloid formation in mammalian disease systems.

## 2.2 Background and Motivation

Mammalian amyloid formation is associated with over 50 diseases, including Alzheimer's disease (AD) and type 2 diabetes (T2D)[5,6]. AD is the 6$^{th}$ leading cause of death in the United States and is characterized by neuronal death and progressive loss of cognitive function[70,72]. Disease progression involves the aggregation of the 42-amino acid amyloid-β peptide (hereafter referred to as Aβ), which is intrinsically disordered in its 'normal' biologically active monomeric state[11]. During amyloidogenesis, Aβ forms toxic, soluble oligomers – implicated in neuronal death and disease pathology – prior to the deposition of mature fibrils[11,71,92–94].

Diabetes is the 7th leading cause of death in the United States, afflicting approximately 37 million people[95,96]. An estimated 90-95% of these cases are T2D[95,96]. T2D is characterized by insufficient insulin secretion and reduced response by insulin-sensitive tissues caused by pancreatic islet β-cell dysfunction and death[97]. β-cell death is attributed to multiple factors, including islet amyloid production[97]. Islet amyloid polypeptide (IAPP) is a 37-residue peptide hormone that is synthesized in β-cells and co-secreted with insulin[98]. Unlike IAPP in species such as mice and rats, human IAPP is amyloidogenic and forms fibrillar amyloid deposits[99,100]. Human IAPP is intrinsically disordered; under amyloidogenic conditions, it aggregates to form a heterogeneous distribution of soluble oligomers prior to forming insoluble and nontoxic β-sheet fibrils[101–107]. IAPP fibrils are present in over 90% of T2D cases[97,101,107], and the soluble oligomers that are formed prior to β-sheet fibrils are reported to be cytotoxic and responsible for β-cell death[106].

The development of a new strategy to inhibit amyloid formation and oligomeric toxicity is desirable, as doing so would aid in the treatment of amyloid disease. Decades of research on various methods aimed at clearing amyloid plaques proved fruitless, as β-sheet fibrils are stable and nontoxic[11]. Instead, the primary species responsible for toxicity and pathology in amyloid diseases are the low molecular weight soluble oligomers that are formed prior to insoluble fibrils[10,11,22,23,27,30,71,97,108,109]. Therefore, treatment strategies should focus on targeting the toxic oligomers rather than the mature fibrils.

An attempt to elucidate the structure composing toxic Aβ oligomers by Glabe, Kayed, and coworkers revealed the existence of a conserved conformation between the oligomers formed by amyloidogenic proteins during aggregation[22,110,111]. A polyclonal antibody, now known as A11, was raised against molecular mimics of soluble Aβ oligomers in effort to produce

a molecule that targets the soluble toxic aggregates of Aβ with no specificity toward the monomeric or fibrillar forms[22,110,111]. While they successfully produced an antibody with specificity for Aβ oligomers, they found that A11 also binds to many oligomeric species, regardless of the amyloid protein's native structure or amino acid sequence. Additionally, A11 does not exhibit specificity toward the corresponding monomers or amyloid fibrils of these proteins[22,110,111]. A11 was also shown to inhibit oligomeric toxicity[22,110,111], suggesting that the low molecular weight species also share a conserved mechanism of toxicity that is inherently related to oligomeric structure.

The cross-reactivity of the A11 antibody led to the elucidation of α-sheet structure through MD simulations[41,42,44–53,58,112–115] and the production of *de novo* α-sheet peptides for experimental characterization of the nonstandard conformation[13,15,40]. As was observed with A11, *de novo* α-sheet peptides were designed to bind to oligomers with the same conformation and exhibit no specificity toward the monomeric or fibrillar forms of an amyloidogenic peptide[11,13,15,40]. This chapter explores the role of α-sheet structure in the amyloidogenesis of Aβ and IAPP. The capacity for *de novo* α-sheet peptides to inhibit aggregation and neutralize toxicity of these two amyloid peptides is also investigated.

## 2.3 Results

### *2.3.1 Aβ Oligomers Adopt α-Sheet Structure*

A standard Thioflavin T (ThT) study was conducted to visualize the aggregation of Aβ. ThT is a fluorescent dye that binds to β-sheet rich structures, and it is frequently employed to measure the extent of amyloid formation over time[116]. Aβ aggregated at 75 μM in phosphate buffered saline (PBS; pH 7.6) and 25°C exhibited a lag phase of approximately 30 hours (**Figure**

**2.1A**). The relatively flat ThT signal observed in the lag phase is followed by a rapid exponential signal increase, indicating that the formation of an aggregation competent species is a significant rate limiting step in Aβ aggregation. The production of stable β-sheet rich fibrils is evident at approximately 50 hours, when the ThT signal reaches a plateau (**Figure 2.1A**). Aggregation studies shown in **Figure 2.1A** were utilized to inform subsequent spectroscopy and toxicity experiments.

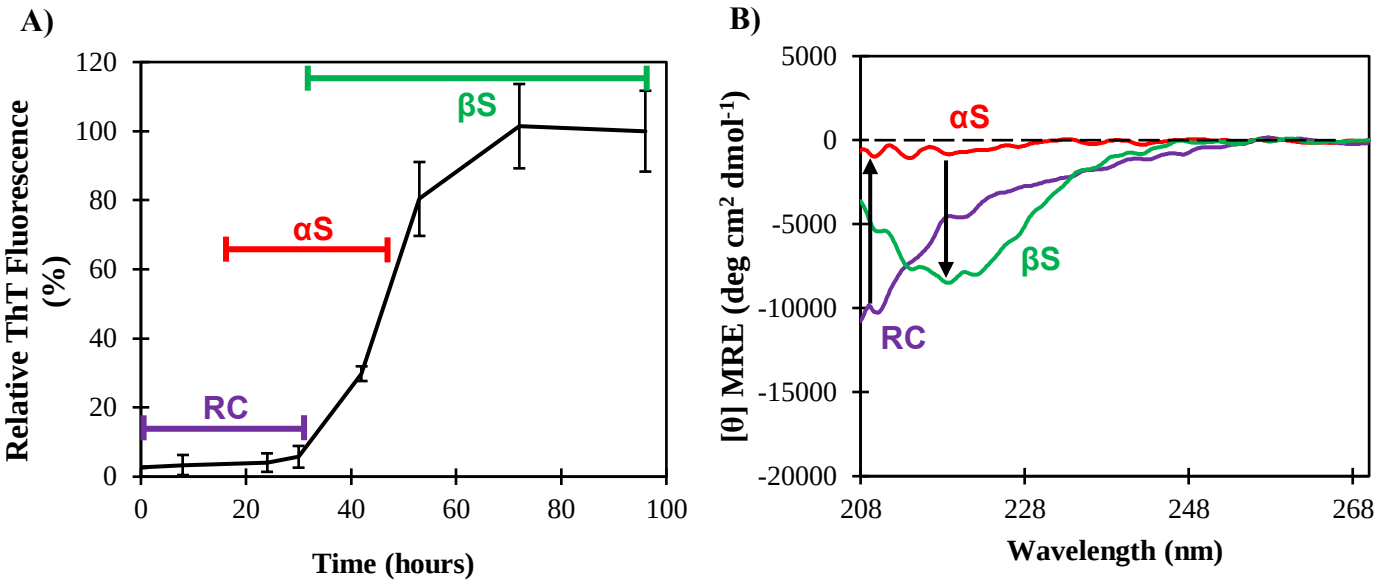


**Figure 2.1. Aβ Characterization. A)** ThT signal is measured over time and is indicative of β-sheet fibril formation. Aβ has random coil structure at the beginning of aggregation (purple) and transitions to α-sheet structure (red) at the end of the lag phase. The ThT signal plateaus when Aβ forms fibrils with β-sheet structure (green) at the end of aggregation. Values are mean ± SD for three replicates. **B)** CD spectra of three pre-incubated Aβ samples that are representative of the secondary structures populated by Aβ throughout aggregation. Aβ has random coil structure at t=0 hours (purple). α-Sheet structure (red) is present in Aβ at t=30 hours and is representative of a late lag phase sample. β-sheet structure is found in Aβ at t=72 hours (green) and corresponds to a sample in the plateau phase of aggregation. While random coil, α-sheet, and β-sheet

conformers are enriched in the aggregation stages described above, mixed populations are likely present.

CD spectroscopy was conducted to investigate the structural conformations sampled by Aβ during aggregation. CD utilizes right- and left-handed circularly polarized light to determine protein secondary structure[69], and this spectroscopic technique can be used in parallel with kinetic data to monitor conformational changes over time. A sample obtained at the beginning of aggregation (t=0 hours) produced CD spectra indicative of random coil structure (**Figure 2.1B**). Aβ is intrinsically disordered in its monomeric form, and the CD spectra produced by the t=0 sample is representative of this. To isolate an Aβ sample late in the lag phase of aggregation where α-sheet structure is predicted to be present, Aβ was incubated statically for 30 hours as informed by **Figure 2.1A**. The late lag phase Aβ aggregation sample produced a relatively flat and featureless spectra by CD (**Figure 2.1B**). Because the nonstandard structure is composed of amino acids whose backbone dihedral angles sequentially alternate between $\alpha_L$ and $\alpha_R$ regions of Ramachandran space, flat CD spectra is predicted for the α-sheet conformation. The CD spectrum obtained in **Figure 2.1B** is similar to the spectra produced by *de novo* α-sheet peptides (**Figure 1.4**) and therefore confirms that Aβ adopts α-sheet structure at the end of the lag phase. Finally, Aβ was incubated for 72 hours to isolate a sample in the plateau phase of aggregation. This sample produced a CD spectrum with a minimum at approximately 220 nm (**Figure 2.1B**), which is indicative of β-sheet structure and aligns with the high ThT signal produced by Aβ during the plateau phase (**Figure 2.1B**). The data reported in **Figure 2.1** was obtained from the same Aβ stock solution, allowing conclusions to be made regarding the structural changes

observed by Aβ throughout aggregation. CD data confirms that Aβ is largely unstructured at the beginning of aggregation. In amyloidogenic conditions (low temperature), Aβ then transitions to α-sheet conformation at the end of the lag phase (30 hours for the conditions reported here), and by 72 hours the peptide has deposited into β-sheet-rich amyloid fibrils. The characterization of aggregation kinetics and conformational changes sampled by Aβ throughout aggregation was then used to inform future inhibition and cellular toxicity studies.

### *2.3.2 Aβ α-Sheet Oligomers are Toxic to Human Neuroblastoma Cells*

Cell viability experiments with human neuroblastoma cells (SH-SY5Y) were conducted to determine the relative toxicity associated with the monomeric, oligomeric, and fibrillar forms of Aβ. An MTT assay was used to measure cell viability of human neuroblastoma cells treated with Aβ. MTT is a yellow tetrazolium salt (3-(4,5-dimethylthiazol-2-yl)-2,5-diphenyltetrazolium bromide) that is reduced to purple formazan crystals by NADH-dependent oxidoreductase enzymes present in metabolically active cells during glycolysis[117]. Following cell lysis and solubilization of the formazan crystals, a colorimetric assay was used to quantify formazan and determine the relative metabolic activity, and viability, of the cells.

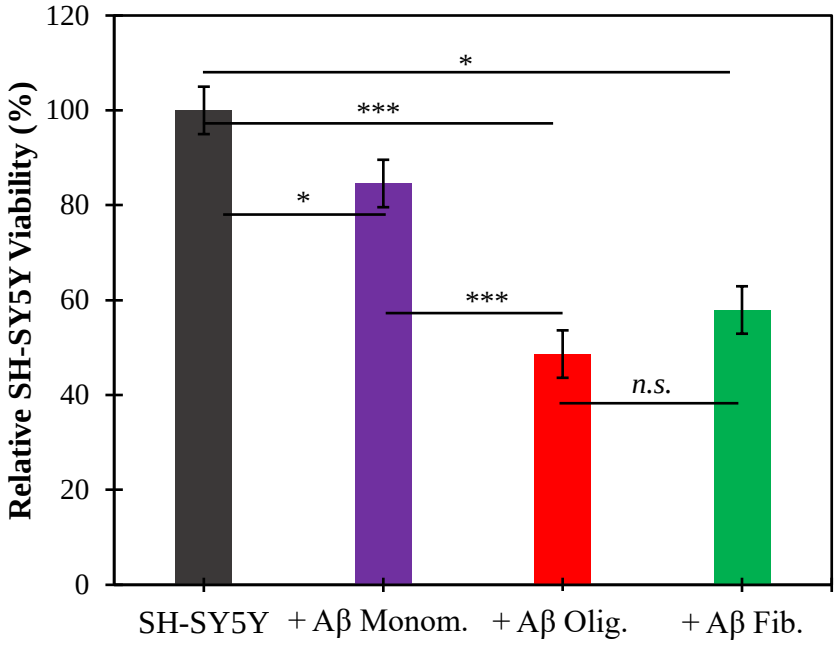


**Figure 2.2. Oligomeric Aβ is toxic to SH-SY5Y human neuroblastoma cells.** Cell viability is measured relative to the control, which is SH-SY5Y in the absence of Aβ. Aβ samples were incubated at 75 µM and diluted to 25 µM in cell media prior to administration to human neuroblastoma cells. A 0-hour monomeric Aβ sample caused a 15% reduction in cell viability (*p=0.02*). Incubation of neuroblastoma cells with a late lag phase oligomeric sample (t=30 hours) caused a 51% reduction in cell viability (*p=0.0005*). An Aβ sample incubated for 48 hours resulted in a 42% drop in cell viability with respect to the control (*p=0.001*). Values are mean ± SD for three replicates.

Three Aβ samples (t=0, t=30, and t=48 hours) were isolated using the same methods described above (**Figure 2.1B)** and applied to SH-SY5Y cells. Aβ was incubated at 75 µM and diluted 1:3 in cell media prior to application to human neuroblastoma cells, resulting in a final concentration of 25 µM (**Figure 2.2**). The random coil sample (t=0) was minimally toxic to the human neuroblastoma cells, resulting in a 15% reduction in cell viability with respect to the

untreated control (**Figure 2.2**). The late lag phase α-sheet sample caused a 51% reduction in MTT signal with respect to the untreated control, corresponding to the largest drop in cellular viability by the Aβ samples (**Figure 2.2**). The plateau sample (t=48 hours) caused a 42% reduction in relative cell viability, indicating that neuroblastoma cells grown in the presence of the plateau Aβ sample were approximately 9% more viable than those grown with the late lag phase sample (**Figure 2.2**). The toxicity of the 48hr sample is likely due to incomplete fibrilization of Aβ, as this sample corresponds to Aβ at the beginning of the plateau (**Figure 2.1A**). It is likely that toxic oligomers were still present in the 48hr sample, in addition to the β-sheet fibrils, although at a smaller concentration than in the 30hr sample due to continued aggregation. The data reported in **Figure 2.2** confirm that soluble oligomeric Aβ, which has α-sheet structure (**Figure 2.1B**), is the primary toxic species formed during amyloidogenesis. This correlates with previous research demonstrating that the monomeric and fibrillar conformers of amyloidogenic peptides are largely nontoxic, while the low molecular weight oligomers are responsible for cellular toxicity and AD pathology[8–11].

*2.3.3 De novo α-Sheet Peptides Inhibit Aβ Aggregation and Oligomeric Toxicity*

With knowledge that α-sheet oligomers are the primary species responsible for cellular toxicity observed in AD pathology, inhibition studies with *de novo* peptides were conducted. A library of 22 α-sheet peptides (APs), each with varying amino acid sequences and stable α-sheet conformation (**Figure 1.5; Appendix A, Table A.1**), was utilized to determine the significance of primary sequence, if any, in preventing Aβ aggregation. An 'endpoint inhibition' study was employed, such that Aβ was co-incubated with each AP (1:1; 75 μM) until aggregation reached a plateau (as determined by **Figure 2.1A**). After 120 hours, ThT was added to each co-incubation

solution, and the ThT fluorescence was measured. Each of the 22 tested *de novo* peptides successfully inhibited Aβ aggregation, but to varying extents. AP501, AP505, AP510, and AP532 were the most potent inhibitors, resulting in almost complete inhibition of Aβ fibrilization (**Figure 2.3**). Each experimental peptide inhibited Aβ aggregation by at least 50%, with exception to AP90 and AP504 which inhibited the production of Aβ fibrils by only 38% and 24%, respectively (**Figure 2.3**). The results reported here indicate that inhibition by *de novo* α-sheet peptides is not sequence dependent, although the varied inhibitory effects observed suggest that primary sequence may affect the potency of the α-sheet peptides against a particular amyloidogenic peptide. While the results reported in **Figure 2.3** indicate that the α-sheet conformation itself is responsible for promoting inhibition of Aβ aggregation, optimization of the *de novo* inhibitors' primary sequences may result in increased effect.

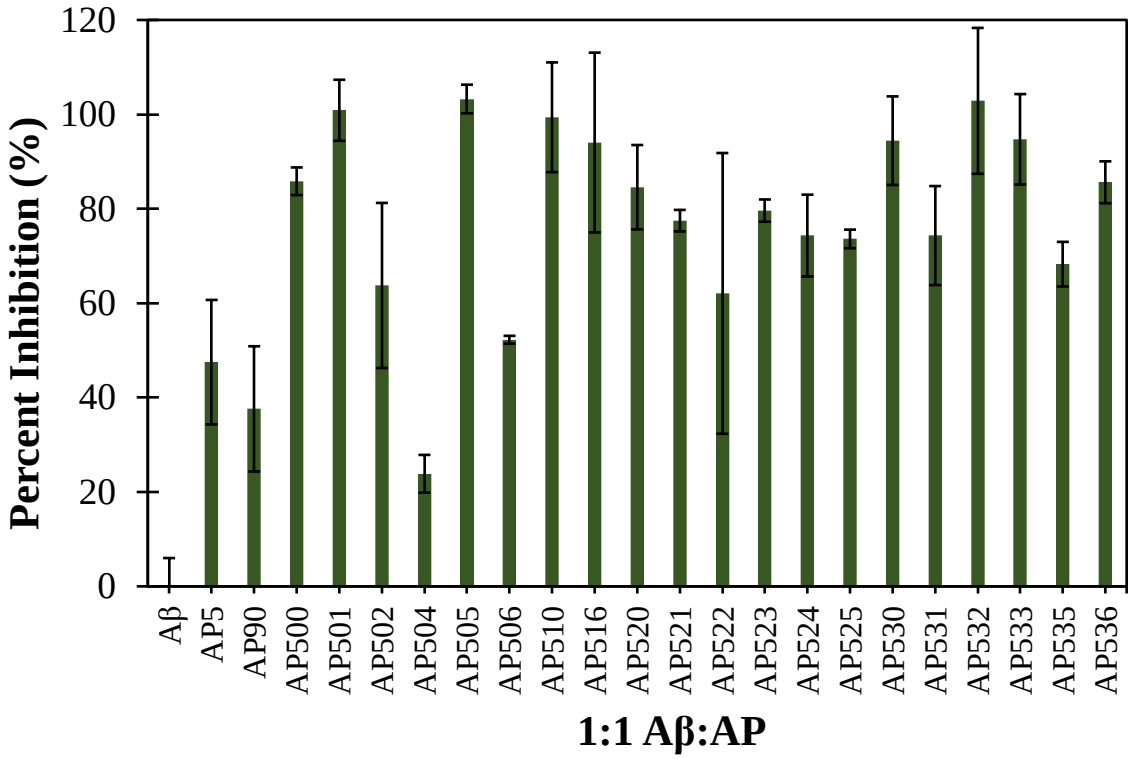


**Figure 2.3. *De novo* α-sheet peptides inhibit Aβ aggregation regardless of sequence.** An endpoint inhibition study with 22 α-sheet peptides (APs) that have varying amino acid sequences was conducted to demonstrate that Aβ fibrilization is inhibited by APs regardless of primary sequence. AP501, AP505, AP510, and AP532 were the most potent inhibitors, resulting in almost complete inhibition of Aβ fibrilization. Aβ and α-sheet peptides were incubated at a 1:1 ratio (75 μM). Values are mean ± SD for three replicates.

Cellular toxicity studies were then conducted to measure the capacity for the peptides to neutralize oligomeric toxicity. AP5 and AP90 (4:1 AP:Aβ) were incubated with Aβ for 30 hours to isolate the toxic oligomeric conformation (as informed by **Figure 2.1** and **Figure 2.2**). In this study, 25 μM Aβ reduced SH-SY5Y cell viability by 44%, as measured by MTT (**Figure 2.4**). When co-incubated with AP5 or AP90, cell viability increased to 83% and 77%, respectively

(**Figure 2.4**). Inhibition of Aβ by AP5 and AP90 caused a significant increase in neuroblastoma cell viability but did not promote complete recovery of SH-SY5Y viability (**Figure 2.4**). The results reported in **Figure 2.4** indicate that *de novo* α-sheet peptides inhibit toxicity of Aβ oligomers, and inhibition is conformation specific and primary sequence independent.

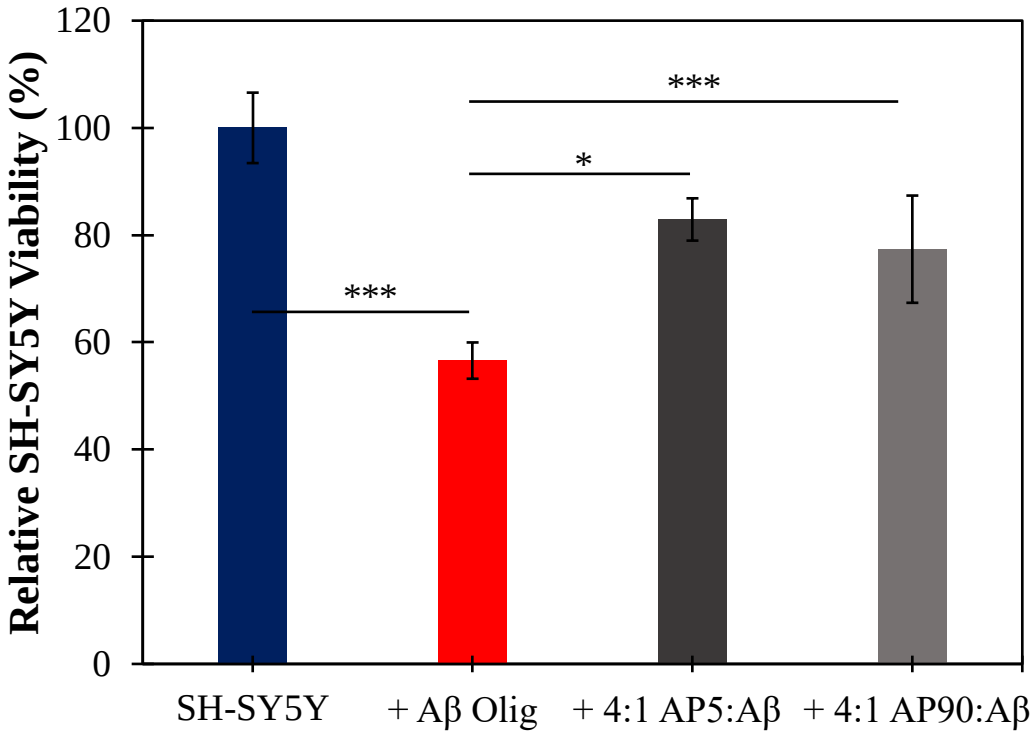


**Figure 2.4. α-Sheet peptides ameliorate cellular toxicity associated with Aβ oligomers in human neuroblastoma cells.** Cell viability is measured relative to the control, which is SH-SY5Y in the absence of Aβ and APs. Incubation with Aβ oligomers resulted in 44% reduction in SH-SY5Y viability (*p=0.0005*). The addition of AP5 (4:1 AP5:Aβ) improved cell viability, corresponding to 83% viability with respect to the control (*p=0.0009*). AP90 (4:1 AP90:Aβ) improved cell viability to a lesser extent, resulting in 77% viability with respect to the control (*p=0.03*). Values are mean ± SD for three replicates.

*2.3.4 IAPP Oligomers Adopt α-Sheet Structure*

Aggregation studies with human islet amyloid polypeptide (hereafter referred to as IAPP) were conducted at 25°C with 25 μM peptide in PBS (pH 7.6). IAPP aggregated significantly faster than Aβ, resulting in a lag phase of approximately 3.5 hours (**Figure 2.5A**). Following a rapid increase in ThT signal, aggregation plateaued at approximately 10 hours, indicating that IAPP formed β-sheet rich fibrils (**Figure 2.5A**). The relatively short lag phase of IAPP suggests that the peptide begins to form low molecular weight oligomers almost immediately. Rapid oligomerization makes isolating a monomeric species more challenging, and it is therefore possible that samples isolated at the beginning of aggregation (t=0 hours) are also composed of a small number of low molecular weight oligomeric species.

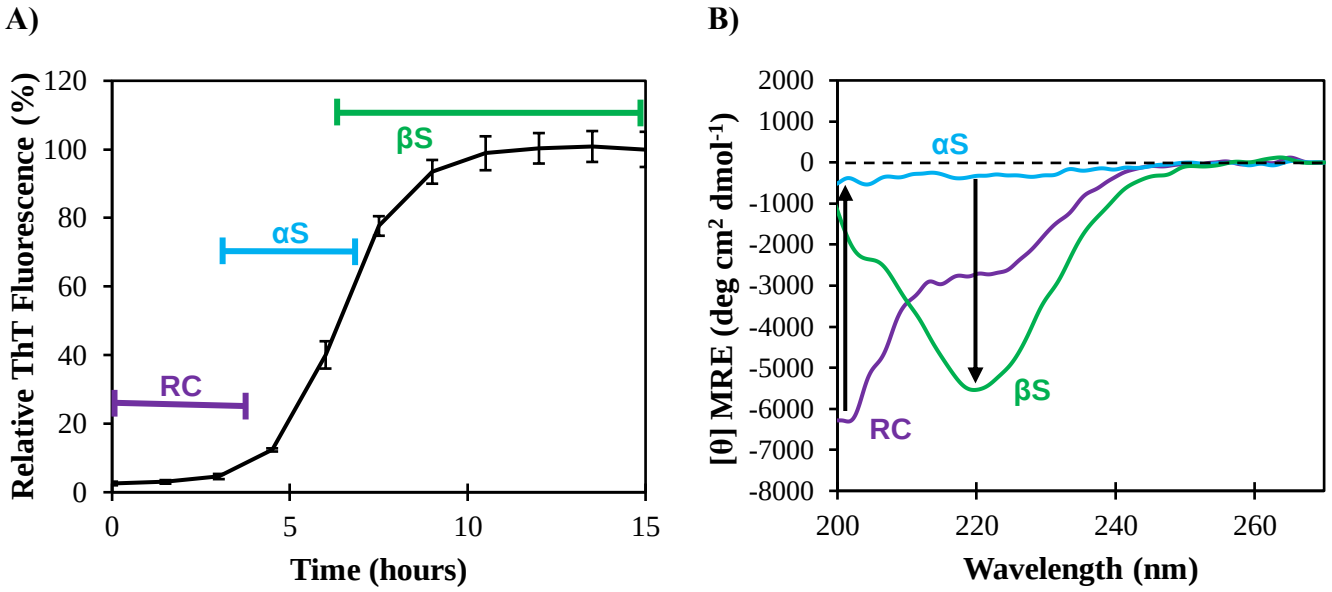


**Figure 2.5. IAPP characterization. A)** ThT signal is measured over time and is indicative of β-sheet (fibril) formation. IAPP has random coil structure at the beginning of aggregation (purple) and transitions to α-sheet structure (blue) at the end of the lag phase. The ThT signal plateaus when IAPP forms fibrils with β-sheet structure (green) at the end of aggregation. Values are

mean ± SD for three replicates. **B)** CD spectra of three pre-incubated IAPP samples, representative of the three secondary structures populated by IAPP throughout aggregation. IAPP has random coil structure at t=0 (purple). α-Sheet structure (blue) is present in IAPP at t=3.5 hours and is representative of a late lag phase sample. β-sheet structure is found in IAPP at t=53 (green) and corresponds to a sample in the plateau phase of aggregation.

Three IAPP samples (t=0, t=3.5, and t=53 hours) were isolated to visualize the conformational changes observed by IAPP over the course of aggregation by CD. IAPP isolated at t=0 hours produced a CD signal indicative of random coil structure, although at lower wavelengths, the signal is lifted slightly above what is expected for random coil monomeric IAPP (**Figure 2.5B**). As discussed above, this may be indicative of the presence of a small concentration of α-sheet oligomers influencing a slight lift in the predominantly random coil (monomeric) signal. An IAPP sample isolated after 3.5 hours of aggregation produced a relatively flat and featureless CD signal, indicating that IAPP adopts α-sheet structure toward the end of the lag phase (**Figure 2.5B**). The CD spectrum of an IAPP sample collected late in the plateau (t=53 hours) is indicative of β-sheet structure, evident by the strong minimum at 220 nm (**Figure 2.5B**).

### *2.3.5 IAPP α-Sheet Oligomers are Toxic to Rat Insulinoma Cells*

Cell viability studies were conducted with rat insulinoma INS-1 cells to measure the relative toxicity of the conformations sampled by IAPP during aggregation. Three 25 μM IAPP samples were prepared based on the data obtained in **Figure 2.5** and diluted to 10 μM in cell

media prior to their addition to the insulinoma cells. A random coil, monomeric IAPP sample (t=0 hours) caused INS-1 viability to drop 56%. The α-sheet IAPP oligomers exhibited significant toxicity to the cells, corresponding to a 75% reduction in INS-1 viability. β-Sheet fibrils reduced cell viability by only 29% (**Figure 2.6**).

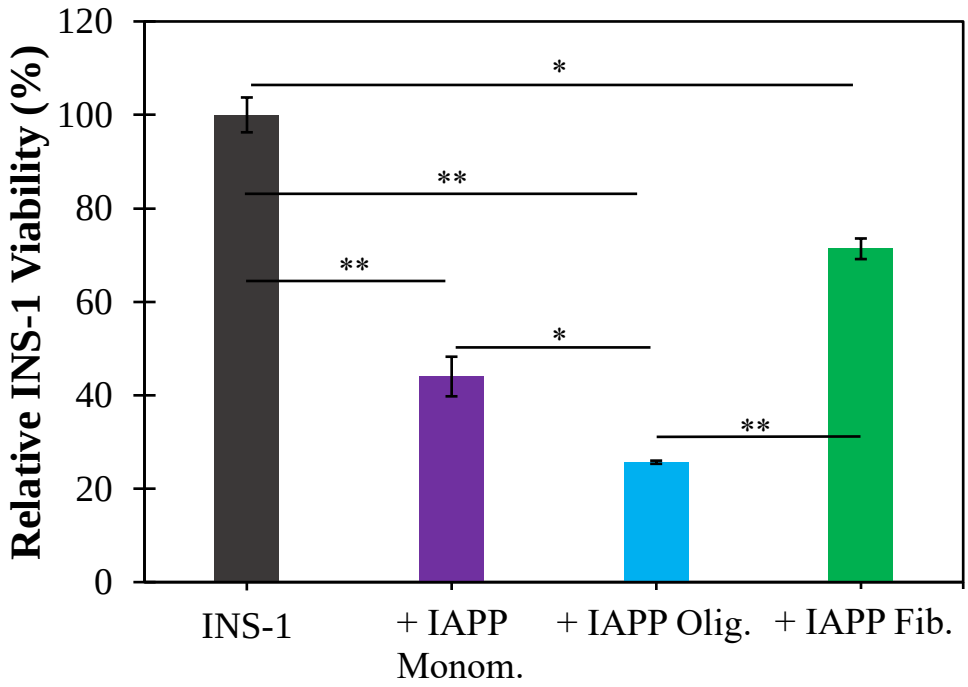


**Figure 2.6. IAPP oligomers are toxic to INS-1 rat insulinoma cells.** Cell viability is measured relative to the control (INS-1 cells in the absence of IAPP). IAPP samples were incubated at 25 μM and diluted to 10 μM in cell media prior to application to rat insulinoma cells. A 0-hour monomeric IAPP sample caused a 56% reduction in cell viability (*p=0.005*). Incubation of insulinoma cells with a late lag phase oligomeric sample (t=3.5 hours) caused a 75% reduction in cell viability (*p=0.001*). An IAPP sample incubated for 24 hours resulted in a 29% drop in cell viability with respect to the control (*p=0.01*). Oligomeric IAPP was 19% more toxic than monomeric IAPP (*p=0.03*) and 46% more toxic than the fibrillar species (*p=0.001*). Values are mean ± SD for three replicates.

*2.3.6 De novo α-Sheet Peptides Inhibit IAPP Aggregation and Neutralize Oligomeric Toxicity*

Aggregation inhibition studies were conducted with IAPP and several *de novo* peptides with various sequences but stable α-sheet structure (**Figure 1.5; Appendix A, Table A.1**) to assess the capacity for peptides with α-sheet conformation to prevent IAPP fibrilization regardless of amino acid sequence. Co-incubation samples were prepared with 25 μM IAPP and 100 μM AP (excess AP 4:1). ThT signal was read after 72 hours to ensure IAPP aggregation had plateaued. Of the 27 inhibitor peptides tested, more than half (14 of 27 – AP500, AP504d, AP505d, AP510d, AP521, AP522, AP522d, AP523d, AP524, AP524d, AP530, AP533, AP533d, and AP534) inhibited IAPP fibrilization by 90% or greater with respect to the control (IAPP without inhibitor) (**Figure 2.7**). Although elevated potency was observed with the inhibitors listed above, every peptide tested inhibited IAPP fibrilization by 50% or greater (**Figure 2.7**).

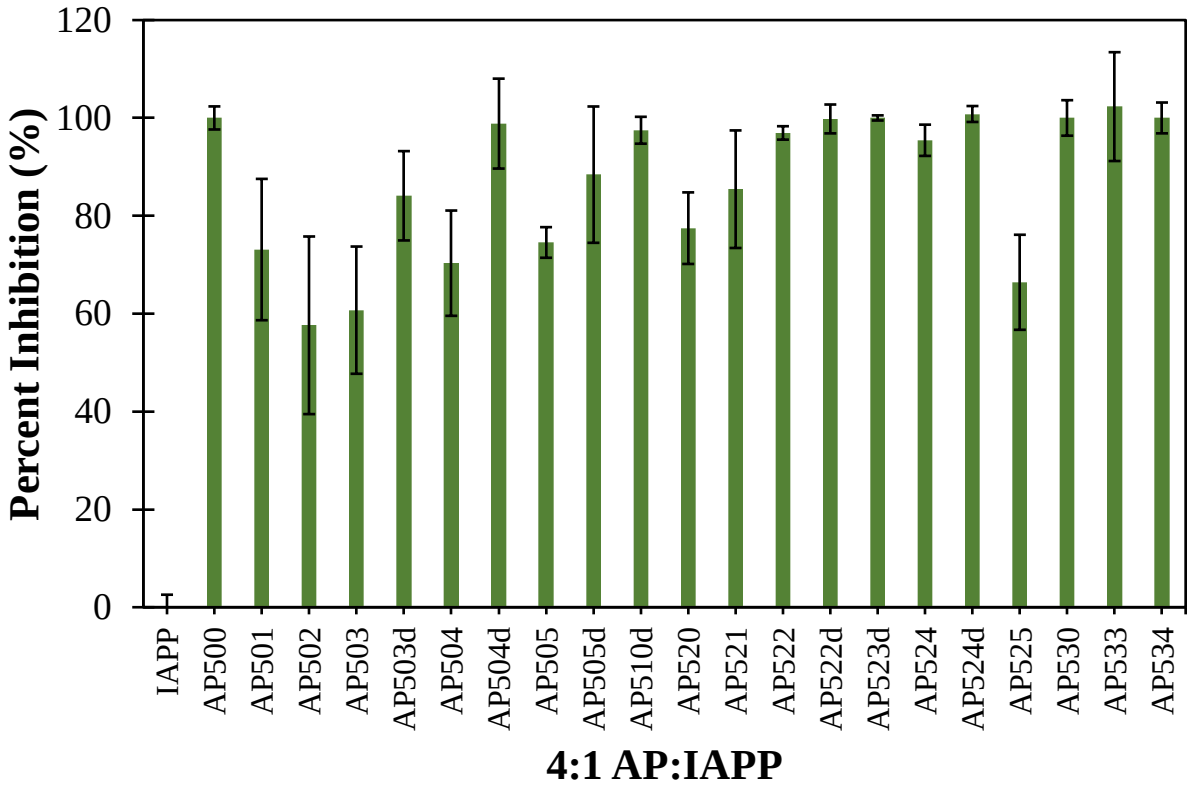


**Figure 2.7. *De novo* α-sheet peptides inhibit IAPP aggregation regardless of sequence.** An endpoint inhibition study with 27 α-sheet peptides (APs) that have various sequences was conducted. Inhibition greater than 90% was observed for more than half of the inhibitors tested. The assay was conducted with AP in excess to IAPP 4:1 (100 to 25 μM). Values are mean ± SD for three replicates.

Following the aggregation inhibition study, which demonstrated that α-sheet peptides prevent IAPP aggregation regardless of amino acid sequence, cell viability studies were conducted to determine whether the *de novo* peptides can also neutralize IAPP oligomeric toxicity. SH-SY5Y human neuroblastoma cells were used for this assay, along with IAPP that had been incubated at 150 μM and diluted to 50 μM in cell media prior to application to the

cells. The altered concentration was used because a new lot of IAPP produced different aggregation kinetics, allowing for a higher concentration to be used while maintaining a sufficient lag phase. The kinetic and CD corresponding to the IAPP used in **Figure 2.8** is shown in **Appendix B.1** (**Figure B.1**). When applied to human neuroblastoma cells, IAPP oligomers caused an 89% drop in cell viability, as measured by MTT (**Figure 2.8**). Cellular viability was significantly recovered when co-incubated with AP5, corresponding to only 17% toxicity with respect to the SH-SY5Y control (**Figure 2.8**).

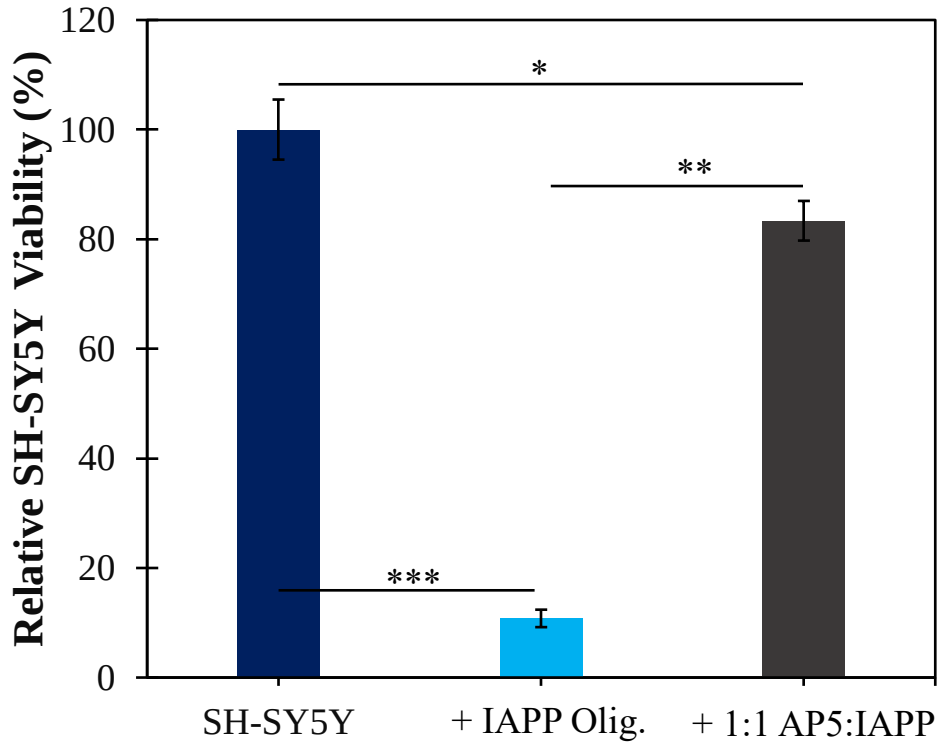


**Figure 2.8. AP5 inhibits IAPP oligomeric toxicity in human neuroblastoma cells.** Cell viability is measured relative to the control, which is SH-SY5Y in the absence of IAPP and AP5. Incubation with IAPP oligomers resulted in 89% reduction in SH-SY5Y viability (*p=0.0002*). The addition of AP5 (1:1 AP5:Aβ) improved cell viability (*p=0.0004*), corresponding to 83% viability with respect to the control (*p=0.015*). Values are mean ± SD for three replicates.

## 2.4 Discussion

Aβ and IAPP are amyloidogenic peptides whose toxic oligomers are involved in diseases that are the 6th and 7th leading causes of death in the United States, respectively. Strategies to prevent the aggregation and oligomeric toxicity of these peptides are desirable to mitigate the pathology of AD and T2D. The findings reported in **Chapter 2** elucidate the structural changes that Aβ and IAPP undergo during amyloidogenesis. As both peptides are intrinsically disordered, they are largely unstructured in their monomeric form and produce CD spectra indicative of random coil structure (**Figure 2.1B** and **2.5B**). In amyloidogenic conditions, both peptides transition to α-sheet structure at the end of their respective lag phases. Finally, Aβ and IAPP form insoluble, nontoxic β-sheet-rich fibrils at the end of aggregation.

Notably, previous CD studies have reported that IAPP produces α-helical intermediates prior to the transition to β-sheet[118]. The CD spectra for the monomeric starting conformation of IAPP reported in **Figure 2.5B** may be consistent with a minor population of α-helix, but others have obtained much more pronounced helical spectra in the presence of, and/or after extended treatment with, helix-promoting alcohols, including Tris buffer, and fluorinated alcohols such as HFIP[118]. The helix-promoting effect of Tris is evident by comparing the monomeric starting structure of IAPP in Tris and PBS (**Appendix B**, **Figure B.2**), explaining the discrepancies observed between the CD spectra reported here and in other studies[118] while also emphasizing the impact that various buffers can have on experimental results.

Isolation of Aβ and IAPP samples enriched in the random coil, α-sheet, and β-sheet conformations demonstrated that α-sheet oligomers are the primary toxic species formed during amyloidogenesis (**Figure 2.2** and **Figure 2.6**). This is consistent with previous studies that determined that the low molecular weight oligomers formed prior to mature fibrils are

responsible for toxicity in amyloid diseases[8,10,11,27,30,105,106,108,111]. Further, *de novo* peptides that adopt stable α-sheet conformation were shown to inhibit aggregation and neutralize toxicity of both Aβ and IAPP, regardless of the *de novo* peptide's amino acid sequence (**Figure 2.4** and **Figure 2.8**). The capacity for α-sheet peptides of varying sequences to inhibit aggregation and neutralize oligomeric toxicity of both Aβ and IAPP suggests that inhibition and toxicity neutralization is conformation, rather than sequence, dependent. The findings reported in **Chapter 2** are consistent with the studies conducted by Glabe, Kayed, and coworkers in which the A11 antibody exhibited specificity for several oligomers produced by amyloidogenic proteins that have various sequences, structures, and physiological functions[22,110,111]. The elucidation of a conserved oligomeric secondary structure and amyloid inhibition mechanism can inform novel therapeutic strategies in the treatment and prevention of amyloid diseases.

## 2.5 Conclusions

This chapter investigates the conformational changes observed by Aβ and IAPP, each of which are implicated in prevalent mammalian amyloid diseases. Both peptides were shown to transition from random coil structure to the nonstandard α-sheet conformation at the end of their respective lag phase and prior to transitioning to β-sheet fibrils. MTT studies confirmed that α-sheet oligomers are the predominantly toxic species produced during the aggregation of Aβ and IAPP. Finally, *de novo* α-sheet peptides significantly inhibited aggregation and oligomeric toxicity of the amyloid peptides, revealing that amyloid inhibition is conformation dependent, and not sequence specific. The results reported here elucidate a novel strategy to target amyloid formation associated with several mammalian diseases, regardless of the native structure or function of the peptide or protein.

## 2.6 Materials and Methods

### *2.6.1 Preparation of Aβ Stock*

Aβ(1-42), hereafter referred to as Aβ, was obtained from ERI Amyloid Laboratory, LLC (Oxford, CT) and stock solution was prepared as discussed in Shea et al., 2019[11]. Aβ was solubilized using hexafluoroisopropanol (HFIP, Sigma-Aldrich; St. Louis, MO) to 1 mg/mL. The Aβ solution was sonicated in a water bath sonicator for 5 minutes, then incubated on ice for 25 minutes. The sonication and icing incubation process was repeated a second time. The HFIP was then evaporated under a gentle $N_2$ stream, and the Aβ was concentrated using a SpeedVac concentrator (Savant ISS110, Thermo Fisher Scientific; Waltham, MA) for two hours on low setting. The monomerized Aβ film was stored at -20°C until use. Aβ stock was prepared by removing the aliquoted film from -20°C and allowing it to equilibrate to room temperature for approximately 5 minutes. The film was dissolved to 0.75 mg/mL in 6 mM NaOH (pH 11.6, Sigma-Aldrich; St. Louis, MO) solution and sonicated in a water bath sonicator in 5-minute intervals until fully solubilized. The solution was centrifuged at 7,000 rpm for 2 minutes in a 0.22 µm Costar Spin-X cellulose acetate centrifuge filter (Sigma-Aldrich; St. Louis, MO) to remove any remaining seeds. The solution was then transferred to an Eppendorf LoBind microcentrifuge tube (Sigma-Aldrich; St. Louis, MO) and the concentration was measured using a NanoDrop 2000 Spectrometer (Thermo Fisher Scientific; Waltham, MA) at 280 nm using an extinction coefficient of 1490 $M^{-1}$ $cm^{-1}$. The stock solution was incubated at 25°C for 4 hours to promote complete monomerization and was either used immediately or stored at 4°C for up to one week.

*2.6.2 Aβ Aggregation*

Stock Aβ was aliquoted into Eppendorf LoBind microcentrifuge tubes (Sigma-Aldrich; St. Louis, MO) and diluted using phosphate buffered saline (PBS) buffer (10 mM phosphate, 130 mM NaCl, and 2.7 mM KCl; Sigma-Aldrich, St. Louis, MO) to 75 µM. One tube was prepared for each time point that was to be measured by ThT. First, a portion of the stock Aβ was aliquoted into a LoBind tube. PBS buffer was then added gently to the side of the tube for a final volume of 185 µL and final concentration of 75 µM and the solution was gently mixed 3x by pipette. Aliquots were statically incubated at 25°C. At the desired time point, a single tube was removed from the incubator for measurement by ThT. Concentrated stock ThT (Thermo Fisher Scientific; Waltham, MA) was prepared monthly by dissolving ThT powder to 5 mg/ml in $H_2O$. Concentration was measured of 1:10 dilutions of the stock using a NanoDrop 2000 Spectrometer at 412 nm using an extinction coefficient of 36,000 $M^{-1}$ $cm^{-1}$. Concentrated ThT stock was added to the Aβ solution, with the calculated volume corresponding to a final concentration of 24 µM ThT for aggregation studies (typically ~1.0 µL). The resulting solution was gently mixed once by pipette, and 60 µL was added to a single well (in triplicate) in a black 384-well plate and read on a multimode plate reader (Perkin Elmer; Waltham, MA). Relevant parameters include: $\lambda_{ex}$ 438 nm, $\lambda_{em}$ 495 nm, measurement height 7.5 mm, 8 flashes.

*2.6.3 Peptide Synthesis*

Synthetic α-sheet peptide inhibitors were designed *in silico*[13,15,40]**,** using backbone dihedral angle constraints derived from MD simulations[41,42,44–46,49–53,58,62,63,112,113] and synthesized using solid phase peptide synthesis (SPPS)[13,15,40]. The designed peptides contain two α-strands of seven residues each, with amino acids alternating sequentially between L-

conformation and D-conformation in each of the strands. The α-strands are connected by a five-residue turn comprised of either all L- or all D-amino acids, which gives the peptide a hairpin shape. Finally, the tail of each strand consists of a Gly and an Arg residue, followed by acetyl and amide caps at the N- and C-terminus, respectively. Peptides were assembled by solid phase peptide synthesis on Rink amide resin with Fmoc chemistry and HBTU activation. Peptides were cleaved from the resin and side chain deprotected by TFA/TIPS/H2O (95:2.5:2.5) and precipitated by cold ether. Crude peptides were purified to >95% by RP-HPLC using 5 μM C12 or C18 100 Å columns (Phenomenex; Torrance, CA) and atomic masses were confirmed by electrospray mass spectrometry on a Bruker Esquire Ion Trap (Bruker; Billerica, MA). All peptides were lyophilized after purification and stored at -80°C until use. Dimeric α-sheet peptides were produced using a previously established protocol[119]. Briefly, 0.25 mg of the respective lyophilized monomeric peptide was dissolved in 4 μL DMSO and then diluted in 300 μL 50 mM sodium carbonate buffer (pH 9.6) for a final monomer concentration of 250 μM. The peptide solution was incubated at 37°C for 2 hours, facilitating complete oxidation of disulfide bonds and promoting dimerization. Dimerization was confirmed by a lack of absorption at 412 nm by Ellman's reagent (Thermo Fisher Scientific; Waltham, MA) as measured by a NanoDrop 2000 Spectrometer. Sequences for the α-sheet designs described in this study are listed in **Appendix A** (**Table A.1**).

### *2.6.4 Aβ Inhibition by α-Sheet Peptides*

Endpoint aggregation studies were conducted for Aβ inhibition experiments. Aβ stock was prepared as discussed in **Chapter 2.6.1** and aliquoted into Eppendorf LoBind microcentrifuge tubes (Sigma-Aldrich; St. Louis, MO) with the calculated volume corresponding

to a final concentration of 75 µM in 185 µL. APs were synthesized in house according to the methods described in **Chapter 2.6.3** and prepared by removing the aliquoted, lyophilized pure peptide from -80°C and allowing it to equilibrate to room temperature for approximately 5 minutes. The lyophilized AP was then solubilized to 2 mg/mL in $H_2O$, thoroughly mixed, and the concentration was measured using a NanoDrop 2000 Spectrometer (Thermo Fisher Scientific; Waltham, MA) at 280 nm using the respective extinction coefficient (**Appendix A, Table A.1**). APs were diluted to 75 µM in PBS (1:1 Aβ:AP) in a separate Eppendorf LoBind microcentrifuge tube. Concentrated ThT stock was prepared as described in **Chapter 2.6.2** and added to the AP + PBS solution, with the calculated volume corresponding to a final concentration of 24 µM ThT for aggregation studies (typically ~1.0 µL). Finally, the AP + PBS + ThT solution was added – gently – along the side of the Aβ-containing tube and gently mixed 3x by pipette. In the case of controls, $H_2O$ was used in place of the AP. 60 µL was added to a single well (in triplicate) in a black 384-well plate and read on a multimode plate reader in 24-hour intervals for 14 total readings (~two weeks) (Tecan; Mannendorf, Switzerland). Relevant parameters include: $\lambda_{ex}$ 438 nm, $\lambda_{em}$ 495 nm, measurement height 7.5 mm, 8 flashes. Between readings, the 384-well plate was covered in foil to prevent photobleaching of the ThT fluorescent dye and was incubated statically at 25°C. Relative ThT fluorescence values were obtained by first subtracting the ThT blank value from each signal, then subtracting the Aβ or Aβ + AP starting value from the respective endpoint value (i.e., $A\beta_{final} - A\beta_{initial}$ or $[A\beta + AP]_{final} - [A\beta + AP]_{initial}$, and dividing the corrected initial Aβ values by each of the adjusted values (i.e., $[[A\beta + AP]_{final} - [A\beta + AP]_{initial}]/[A\beta_{final} - A\beta_{initial}]]$). Percent inhibition values were obtained by multiplying the relative ThT values by 100 and subtracting the multiplied value from 100.

*2.6.5 Preparation of IAPP Stock*

Human IAPP (referred to hereafter as IAPP) was obtained from ERI Amyloid Laboratory, LLC (Oxford, CT) and solubilized using hexafluoroisopropanol (HFIP, Sigma-Aldrich; St. Louis, MO) to 1 mg/mL. The IAPP solution was sonicated in a water bath sonicator for 5 minutes, then incubated on ice for 25 minutes. The sonication and icing incubation process was repeated a second time. The HFIP was then evaporated under a gentle $N_2$ stream, and the IAPP was concentrated using a SpeedVac concentrator (Savant ISS110, Thermo Fisher Scientific; Waltham, MA) for two hours on low setting. The monomerized IAPP film was stored at -20°C until use. IAPP stock was prepared by removing the aliquoted film from -20°C and allowing it to equilibrate to room temperature for approximately 5 minutes. The film was dissolved in chilled PBS buffer (10 mM phosphate, 138 mM NaCl, 2.7 mM KCl, pH 7.4, Sigma-Aldrich; St. Louis, MO) to 1 mg/mL and sonicated in an ice-chilled cold-water bath for 1 minute. The aliquots were placed on ice after sonication and the stock concentration was measured using a NanoDrop 2000 Spectrometer (Thermo Fisher Scientific; Waltham, MA) at 280 nm using an extinction coefficient of 1520 $M^{-1}$ $cm^{-1}$. The stock solution was prepared fresh for each experiment and used immediately.

*2.6.6 IAPP Aggregation*

Stock IAPP was aliquoted into Eppendorf LoBind microcentrifuge tubes (Sigma-Aldrich; St. Louis, MO) and diluted using PBS buffer to 25 µM (used for **Figures 2.5-2.7**) or 150 µM (used for **Figure 2.8** and **Appendix B, Figure B.1**). One tube was prepared for each time point that was to be measured by ThT. First, a portion of the stock IAPP was aliquoted into a LoBind tube (Sigma-Aldrich; St. Louis, MO). PBS buffer was then added gently to the side of the tube

for a final volume of 185 µL and gently mixed 1x by pipette. Aliquots were incubated at 25°C. At the desired time point, a single tube was removed from the incubator for measurement by ThT. Concentrated stock ThT (Thermo Fisher Scientific; Waltham, MA) was prepared monthly as described in **Chapter 2.6.2** and added to the IAPP solution, with the calculated volume corresponding to a final concentration of 24 µM ThT for aggregation studies (typically ~1.0 µL). The resulting solution was gently mixed 1x by pipette, and 60 µL was added to a single well (in triplicate) in a black 384-well plate and read on a multimode plate reader (PerkinElmer; Waltham, MA). Relevant parameters include: $\lambda_{ex}$ 438 nm, $\lambda_{em}$ 495 nm, measurement height 7.5 mm, 8 flashes.

*2.6.7 Circular Dichroism Spectroscopy*

Circular dichroism (CD) studies were conducted to determine Aβ and IAPP secondary structure. Aβ and IAPP stocks were prepared and pre-incubated as described in **Chapter 2.6.1** and **Chapter 2.6.5**, respectively. Pre-incubated Aβ at 75 µM was diluted in PBS to a concentration of 25 µM, and the timepoints were informed by **Fig. 2.1a**. Pre-incubated IAPP at 25 µM was diluted in PBS to a concentration of 10 µM, and the timepoints were informed by Fi**gure 2.5a**. Dilutions were performed by first adding a portion of the peptide solution to a LoBind tube (Sigma-Aldrich; St. Louis, MO). Buffer volume was calculated to achieve a final concentration of 25 µM (Aβ) or 10 µM (IAPP) in a final volume of 310 µL. The calculated volume of buffer was added gently – along the side of the tube – to the peptide-containing LoBind tube and mixed 1x by pipette to ensure adequate mixing. 300 µL of the resulting solution was added to a 1 mm pathlength quartz cuvette (Starna Cells; Atascadero, CA) and scans were collected using a Jasco J-720 CD machine. All experiments aggregated 8 scans and used a

Savitzky-Golay smoothing protocol, followed by reduction of noise by an FFT filter. The mean residual ellipticity (MRE) was calculated by first subtracting the peptide signal from the blank signal, and the curve zeroed against the value at 270 nm.

*2.6.8 IAPP Inhibition by α-Sheet Peptides*

Endpoint aggregation studies were conducted for IAPP inhibition experiments. IAPP stock was prepared as discussed in **Chapter 2.6.5** and aliquoted into Eppendorf LoBind microcentrifuge tubes (Sigma-Aldrich; St. Louis, MO) with the calculated volume corresponding to a final concentration of 25 µM in 185 µL. APs were synthesized in house according to the methods described in **Chapter 2.6.3** and prepared as described in **Chapter 2.6.4**. APs were diluted to 100 µM in PBS (4:1AP:IAPP) in a separate Eppendorf LoBind microcentrifuge tube. Concentrated ThT stock was prepared as described in **Chapter 2.6.2** and added to the AP + PBS solution, with the calculated volume corresponding to a final concentration of 24 µM ThT for aggregation studies (typically ~1.0 µL). Finally, the AP + PBS + ThT solution was added – gently – along the side of the tube IAPP-containing tube and gently mixed 1x by pipette. In the case of controls, $H_2O$ was used in place of the AP. 60 µL was added to a single well (in triplicate) in a black 384-well plate and read on a multimode plate reader at t=0, 3.5, 6, 8, 24, and 30 hours (Tecan; Mannendorf, Switzerland). Relevant parameters include: $\lambda_{ex}$ 438 nm, $\lambda_{em}$ 495 nm, measurement height 7.5 mm, 8 flashes. Between readings, the 384-well plate was covered in foil to prevent photobleaching of the ThT fluorescent dye and incubated statically at 25°C. Relative ThT values were obtained by first subtracting the ThT blank value from each signal, then subtracting the IAPP or IAPP + AP starting value from the respective endpoint value (i.e., $IAPP_{final} - IAPP_{initial}$ or $[IAPP + AP]_{final} - [IAPP + AP]_{initial}$, and dividing the initial IAPP values

by each of the adjusted values (i.e., $[[IAPP + AP]_{final} – [IAPP+ AP]_{initial}]/[IAPP_{final} – IAPP_{initial}]]$). Percent inhibition values were obtained by multiplying the relative ThT values by 100 and subtracting the multiplied value from 100.

*2.6.9 SH-SY5Y Toxicity Experiments*

SH-SY5Y cell viability was determined using a 3-(4,5-dimethylthiazol-2-yl)-2,5-diphenyltetrazolium bromide (MTT) assay[117]. SH-SY5Y human neuroblastomas (American Type Culture Collection; Manassas, VA) were cultured in 1:1 DMEM:F12 (Invitrogen; Carlsbad, CA) supplemented with 10% FBS (Invitrogen; Carlsbad, CA), 100 units/mL penicillin (Invitrogen; Carlsbad, CA), and 100 µg/mL streptomycin (Invitrogen; Carlsbad, CA). The cells were seeded in a 96-well sterile tissue culture-treated plate (Corning; Glendale, AZ) at $2.4x10^5$ cells per well and cultured in $CO_2$ water-jacketed incubator (37°C, 5% $CO_2$; Thermo Fisher Scientific; Waltham, MA) for 24 hours. For the samples reported in **Figure 2.4**, Aβ (75 µM) was pre-incubated statically at 25°C for 0, 30, or 48 hours to isolate samples enriched in the random coil, α-sheet, and β-sheet conformations, respectively. For the samples tested in **Figure 2.6**, Aβ (75 µM) was pre-incubated statically at 25°C for 30 hours alone or with AP5/AP90. IAPP (150 µM) was incubated alone or with AP5 for 1.9 hours for the experimented described in **Figure 2.8**. In the case of controls (Aβ or IAPP incubated alone), $H_2O$ was used in place of APs. After 24 hours of cell seeding, the cell culture media was removed and replaced with 100 µL preincubated Aβ, IAPP, Aβ + AP, IAPP + AP, or vehicle control (NaOH + PBS + $H_2O$ for Aβ or PBS + $H_2O$ for IAPP) samples that had been diluted 1:3 in cell media. The cells were cultured with experimental solution for 24 hours at 37°C before addition of 25 µL MTT (5mg/mL in PBS; Sigma-Aldrich), then incubated for 4 hours at 37°C. After 28 hours of incubation, 100 µL lysis

buffer (50% DMF, 20% SDS, 1% glacial acetic acid, and 0.2% HCl) was added to each well and statically incubated overnight at 25°C covered in foil. The optical density was read at 570nm with a multimode plate reader (Tecan; Mannendorf, Switzerland). Relative cell viability values were determined by first subtracting the MTT + media blank from each signal, and then normalizing the values to the average SH-SY5Y control value.

*2.6.10 INS-1 Toxicity Experiments*

INS-1 cell viability was determined using a 3-(4,5-dimethylthiazol-2-yl)-2,5-diphenyltetrazolium bromide (MTT) assay[117]. INS-1 832/13 cells (immortalized rat pancreatic β-cells) were obtained from the University of Washington Diabetes Research Center. Cells were cultured in RMPI-1640 (Invitrogen; Carlsbad, CA) medium supplemented with 10% fetal bovine serum (Invitrogen; Carlsbad, CA), 1 mM sodium pyruvate (Invitrogen; Carlsbad, CA), 100 units/ml penicillin (Invitrogen; Carlsbad, CA), and 100 μg/ml streptomycin (Invitrogen; Carlsbad, CA). The cells were seeded in a 96-well plate at $8x10^4$ cells per well and cultured in a $CO_2$ water-jacketed incubator (37ºC, 5% $CO_2$; Forma Scientific) for 24 hours. The cell culture medium was removed and replaced with 100 μL pre-incubated IAPP (incubated at 25 μM) that was diluted to 10 μM in INS-1 cell media immediately prior to addition to the cells. The IAPP was incubated at 25ºC without agitation for 0, 3.5, or 24 hours to isolate samples enriched in the random coil, α-sheet, and β-sheet conformations, respectively, as informed by **Figure 2.5**. The cells were cultured with experimental solution for 24 hours at 37°C before addition of 25 μL MTT (5mg/mL in PBS; Sigma-Aldrich), and then incubated for 4 hours at 37°C. After 28 hours of incubation,100 μL lysis buffer (50% DMF, 20% SDS, 1% glacial acetic acid, and 0.2% HCl) was added to each well and incubated overnight at 25°C covered in foil. The absorbance was

measured at 570 nm with a multimode plate reader (Perkin Elmer; Waltham, MA). Relative cell viability values were determined by first subtracting the MTT + media blank from each signal, and then normalizing the values to the average SH-SY5Y control value.

### *2.6.11 Statistics*

All statistical significance values reported were calculated using a two-tailed T-test. A single asterisk indicates a p-value less than 0.05. Two asterisks indicate a p-value less than 0.01. Three asterisks indicate a p-value less than 0.001.

# Chapter 3: Inhibition of Functional Bacterial Amyloid Improves Biofilm Antibiotic Susceptibility

## 3.1 Summary

Many biofilm-associated bacteria, including *Escherichia coli* and *Staphylococcus aureus*, generate amyloid fibrils to reinforce their extracellular matrix[12,16,32,120–122]. Previously, the oligomeric species of CsgA and PSMα1, the primary protein subunits of the amyloid fibrils produced by *E. coli* and *S. aureus*, respectively, were shown to adopt α-sheet structure late in the lag phase of *in vitro* aggregation studies[12,16]. Further, *de novo* synthetic α-sheet peptides successfully inhibit amyloid formation and interrupt biofilm formation in both bacteria[12,16]. Here, the impact of α-sheet peptides on biofilm antibiotic susceptibility is investigated, and the combined administration of antibiotics and α-sheet peptides is hypothesized to increase biofilm antibiotic susceptibility. Two α-sheet peptides, AP90 and AP401, with the same sequence but inverse chirality at every residue were tested to determine the effect of chirality on bacterial amyloidogenesis. AP90 is L-amino acid dominant while AP401 is D-amino acid dominant[16]. For *E. coli*, both peptides increased antibiotic susceptibility and decreased colony forming units as compared to the control when administered with five different antibiotics, with AP401 causing a greater increase in all cases. For *S. aureus*, increased biofilm antibiotic susceptibility was also observed for both peptides, but AP90 outperformed AP401 in four out of five cases. Comparison of these peptides demonstrates how the chirality of the designed inhibitors affects biofilm inhibition of gram-negative *E. coli* and gram-positive *S. aureus*. The observed increase in antibiotic susceptibility highlights the role amyloid formation can play in the tolerance of biofilm

bacteria to specific antibiotics. Thus, the co-administration of α-sheet peptides and antibiotics represents a promising strategy for the treatment of critical biofilm infections.

## 3.2 Background and Motivation

Nosocomial (healthcare-associated) infections afflict approximately 15% of all hospitalized patients[123]. These infections occur in both developed and developing countries, and they often result in prolonged hospital stays, significant financial burden, and disability[123]. Multidrug resistant bacteria are implicated in at least 14% of all nosocomial infections in the United States, and this number continues to rise[124,125]. Increased resistance is accompanied by a sharp decline in the development of new antibiotics, which has resulted in a global healthcare crisis[126]. Antibiotic resistance is caused in part by the overuse and misuse of antibiotics, as selective pressure can accelerate conferred resistance[127]. Bacteria within a biofilm are significantly less susceptible to antibiotics due to numerous complex mechanisms including the structural barrier provided by the extracellular matrix (ECM), ECM-sequestered antibiotic-degrading enzymes, and phenotypic/metabolic changes in sessile bacteria orchestrated by cell-to-cell communication[128].

Biofilms are microbe-generated, surface-associated ECMs composed of cells and secreted insoluble extracellular molecules (proteins, polysaccharides, and extracellular DNA) that facilitate cell communication and protect cells from the surrounding environment (i.e., host immune response and antibiotics)[31]. Biofilm cells are 10-1000 times less susceptible to antibiotics than free-floating, or planktonic, cells[32]. This reduced sensitivity is attributed both to the physical barrier of the ECM and to the capacity for cells present in the nutrient-lacking biofilm to exhibit low growth rates and reduced metabolic activity, effectively resulting in

transient antibiotic resistance[33]. Biofilms can foster "persister" cells that can often lead to recalcitrance and reestablishment of infection, and they are thought to have a significant role in acquired resistance[33].

*Escherichia coli* (*E. coli*) and *Staphylococcus aureus* (*S. aureus*) are robust biofilm-forming bacteria that are often implicated in drug-resistant nosocomial infections. Uropathogenic *E. coli* (UPEC) alone account for approximately 50% of all hospital-acquired infections[120]. Although antibiotic resistance varies between isolates, UPEC strains have exhibited resistance to a wide range of antibiotics including fluoroquinolones, amoxicillin, cephalosporin, and ampicillin[120]. Many *S. aureus* strains have also demonstrated clinical resistance to a vast majority of antibiotics including aminoglycosides, tetracyclines, all β-lactam antibiotics, and more[32,129].

To date, many anti-biofilm efforts have focused on the destabilization of the 3D structure of the biofilm ECM, prompting bacteria to return to the planktonic state and resulting in increased sensitivity of the treated biofilm to antibiotics. Biofilm dispersal can be achieved through various matrix-degrading enzymes such as proteases, deoxyribonucleases, and glycoside hydrolases[130–132]. Other strategies employ antibiofilm peptides, peptide mimetic graphene quantum dots, or oligosaccharides for specific protein or extracellular DNA targets in the extracellular polymeric substance[133–135]. While these techniques can render biofilms more susceptible to antibiotic treatment, some biofilms have shown resistance to various dispersion agents. Further, small molecule agents can be degraded by bacteria or can rapidly diffuse away from biofilms. Thus, the identification of new extracellular targets, such as amyloid proteins, and the development of novel inhibition or dispersion methods is desirable.

Multidrug resistance of *E. coli* and *S. aureus* is partially attributed to their ability to form biofilms that are structurally reinforced by the incorporation of insoluble amyloid fibrils[12,32,120–

[122]. Mature amyloid fibrils serve as structural scaffolds and mediate dispersion of chemical or mechanical agents[12,16,31,121,136,137]. *E. coli,* a gram-negative bacterium, produces amyloid fibrils known as curli in its biofilm[121,138]. Curli biogenesis involves seven genes that are transcribed by two separate operons: csgBAC and csgDEF[121]. CsgA and CsgB form the amyloid fibrils, and CsgC, CsgD, CsgE, and CsgF are involved either in the secretion-assembly machinery or function to activate transcription of the csgBAC operon[121]. This complex machinery has evolved to tightly regulate curli biogenesis to avoid unnecessary resource expenditure and to protect the cell from self-toxicity associated with the accumulation of intracellular aggregates[121]. The toxicity risk is minimized by secreting precursors to the growing curli fibers outside of the cell thereby restricting amyloid formation to the cell surface alone.

In *S. aureus*, a gram-positive bacterium, phenol soluble modulins (PSMs) aggregate to form amyloid fibrils that fortify the biofilm matrix[12,136,137]. PSMs are surfactant-like peptides that, in the monomeric form, are responsible for the promotion of biofilm disassembly[137]. However, during biofilm assembly, PSMα3 forms small aggregates capable of seeding fibrilization that then undergo secondary nucleation by PSMα1, PSMα3 and PSMβ1[136]. Notably, mutant strains lacking the machinery to produce PSMs are more susceptible to biofilm degradation[137]. Although the mechanisms of amyloid formation in *S. aureus* are not fully characterized, the regulation of PSM aggregation has a clear and significant role in biofilm assembly and disassembly[137].

Previous studies demonstrate that by inhibiting amyloid fibrilization, *de novo* α-sheet peptides (APs) can weaken bacterial biofilms and significantly reduce biofilm density in various bacteria, including *E. coli* and *S. aureus*[12,16]. Importantly, *in vitro* aggregation studies with CsgA and PSMα1 indicate that both proteins form α-sheet structure at the end of the lag phase of

aggregation and that α-sheet peptides significantly inhibit the aggregation of CsgA and PSMα1[12,16]. Therefore, the *in vitro* aggregation studies suggest that amyloid inhibition by α-sheet peptides in *E. coli* and S. aureus is mediated by interactions between the oligomeric species formed by CsgA and PSMα1, respectively, that have the same conformation.

Interestingly, amyloid and biofilm inhibition by APs does not cause cell death, eliminating the concern of selective pressure leading to acquired resistance[16]. Instead, amyloid inhibition facilitates a shift in cells from the biofilm to the planktonic state, rendering the bacteria more susceptible to antibiotics[16]. In a previous study, AP401 is shown to significantly increases the susceptibility of uropathogenic *E. coli* to gentamicin[16]. In this chapter, previous work is expanded upon to investigate the capacity for AP90 and AP401, two 23-residue α-sheet peptides with identical sequences but opposite chirality at each residue (**Appendix A**, **Figure A.1**), to increase the susceptibility of both *E. coli* and *S. aureus* to five different antibiotics, each with different mechanisms of action. *E. coli* and *S. aureus* clinical isolates (UTI89 and MN8, respectively) were used for the following studies (**Appendix A**, **Table A.2**).

## 3.3 Results

### *3.3.1 E. coli UTI89 and S. aureus MN8 are multidrug resistant*

Preliminary experiments were first conducted to quantify the susceptibility of mature *E. coli* UTI89 and *S. aureus* MN8 biofilms to five different antibiotics: amoxicillin (an amino-penicillin effective against many uropathogenic *E. coli* and *Staphylococcus* species[139]), ciprofloxacin (a broad spectrum fluroquinolone active against both gram-positive and gram-negative bacteria[140]), erythromycin (a macrolide primarily effective against gram-positive bacteria[141]), gentamicin (an aminoglycoside primarily effective against gram-negative

bacteria[142]), and vancomycin (a tricyclic glycopeptide used against gram-positive bacteria[143]). Four concentrations were tested per antibiotic (100 µg/mL, 300 µg/mL, 500 µg/mL, 1,000 µg/mL) and the total biofilm colony forming units (CFUs) of the antibiotic conditions were compared to the non-antibiotic control condition to determine the CFU fold reduction upon antibiotic addition after 24 (*S. aureus*) or 48 (*E. coli*) total hours. Fold reductions were calculated by dividing the control biofilm CFU in the absence of antibiotic by the experimental biofilm condition CFU in the presence of antibiotic. Biofilm resistance was observed to varying extents for both bacteria as measured by CFU fold reduction (**Table 3.1** and **Table 3.2**).

*E. coli* exhibited the highest susceptibility to gentamicin at each of the tested concentrations (40,789-fold CFU reduction at 1,000 µg/mL) and showed very little susceptibility to the other tested antibiotics (**Table 3.1**). Erythromycin and vancomycin were predicted to have minimal effect on *E. coli*, as they are primarily effective against gram-positive bacteria[141,143]. However, the lack of effect of ciprofloxacin and amoxicillin on biofilm CFUs indicates that UTI89 biofilms exhibit multidrug resistance.

UTI89 Antibiotic Fold Reductions

| | Antibiotic Concentration (µg/mL) | | | |
|---|---|---|---|---|
| | 100 | 300 | 500 | 1000* |
| Amoxicillin | 1.6±0.6 | 4.5±3.0 | 8.3±6.5 | 2.3+1.0 |
| Ciprofloxacin | 1.8±0.4 | 3.4±1.9 | 4.8±3.7 | 2.5±0.7 |
| Erythromycin | 1.9±0.5 | 1.7±0.5 | 1.7±0.5 | 1.9±0.6 |
| Gentamicin | 96.9±55 | 775±301 | 7045±2276 | 40789±18290 |
| Vancomycin | 1.6±1.2 | 1.7±0.8 | 1.9±0.8 | 2.1±1.1 |

**Table 3.1. Fold reductions for the addition of antibiotics to UTI89 WT for CFUs measured after 48 hours.** Fold reductions were calculated as the control UTI89 biofilm CFU in the absence of antibiotics divided by the condition biofilm CFU in the presence of antibiotics. Values are mean ± standard error. *Some antibiotics (amoxicillin and ciprofloxacin) are not fully soluble in media at concentrations of 1000 µg/mL.

*S. aureus* exhibited the highest susceptibility to vancomycin at each concentration (**Table 3.2**). Interestingly, the highest CFU fold reduction (8.5-fold) was observed with 300 µg/mL rather than 500 or 1,000 µg/mL. Ciprofloxacin was also effective against *S. aureus*, resulting in a 5.4-fold reduction at 1,000 µg/mL (**Table 3.2**). *S. aureus* was minimally susceptible to amoxicillin, erythromycin, and gentamicin with the highest fold reduction of only 2.7-fold for 1000 µg/mL gentamicin (**Table 3.2**). As gentamicin is primarily effective against gram-negative bacteria[142], the antibiotic was expected to have minimal effect against *S. aureus*. However, the lack of susceptibility to amoxicillin and erythromycin indicates that MN8 biofilms exhibit multidrug resistance.

MN8 Antibiotic Fold Reductions

| | Antibiotic Concentration (µg/mL) | | | |
|---|---|---|---|---|
| | 100 | 300 | 500 | 1000* |
| Amoxicillin | 1.9±1.0 | 1.5±0.7 | 1.4±0.6 | 1.2±0.5 |
| Ciprofloxacin | 1.7±0.5 | 2.2±0.6 | 3.5±2.0 | 5.4±2.4 |
| Erythromycin | 1.2±0.4 | 1.8±0.6 | 1.6±0.5 | 2.0±1.1 |
| Gentamicin | 1.8±0.9 | 2.1±1.0 | 2.5±1.1 | 2.7±1.2 |
| Vancomycin | 2.4±1.1 | 8.5±5.8 | 7.3±5.3 | 7.8±3.3 |

**Table 3.2. Fold reductions for the addition of antibiotics to MN8 biofilms for CFUs measured after 24 hours.** Fold reductions were calculated as the control MN8 biofilm CFU in the absence of antibiotics divided by the condition biofilm CFU in the presence of antibiotics. Values are mean ± standard error.

Based on these results, an antibiotic concentration of 300 µg/mL was used for the following studies incorporating the α-sheet peptides. This concentration was selected because a reduction in biofilm formation was observed for all antibiotics and both bacteria at this concentration. Additionally, this antibiotic concentration falls within the range of known minimum biofilm inhibitory concentrations (bMICs) for uropathogenic *E. coli* and methicillin susceptible *S. aureus* (MSSA) for the five antibiotics tested[144–153] (**Appendix C**).

*3.3.2 a-Sheet peptides inhibit amyloid formation and reduce biofilm density*

UTI89 and MN8 biofilms were then grown with α-sheet peptides (no antibiotics) to determine the effect of the peptides on amyloid formation and biofilm density. The amyloid dye

ThT was used an indicator of amyloid fibril content as it fluoresces upon binding β-sheet fibrils[116]. As ThT also binds nonspecifically to the bacterial cell surface[12], UTI89 experiments included a non-amyloid forming control mutant strain, UTI89 ΔCsgA, as an estimate of nonspecific ThT fluorescence.

For UTI89 experiments, a significant reduction in ThT fluorescence was observed for all peptide conditions except for 20 μM AP90 (**Figure 3.1A**). The 40 μM AP401 condition had the largest reduction (49.3%) as compared to the UTI89 control ($p<0.0001$). This reduction was comparable to that of the UTI89 ΔCsgA control, indicating complete inhibition of amyloid fibril formation. For MN8 experiments, a significant reduction in ThT fluorescence was also observed for all peptide conditions except for 25 μM AP401 (**Figure 3.1B**). The 125 μM AP401 condition showed the greatest reduction with an 18.2% fluorescence reduction as compared to the MN8 control ($p=0.01$).

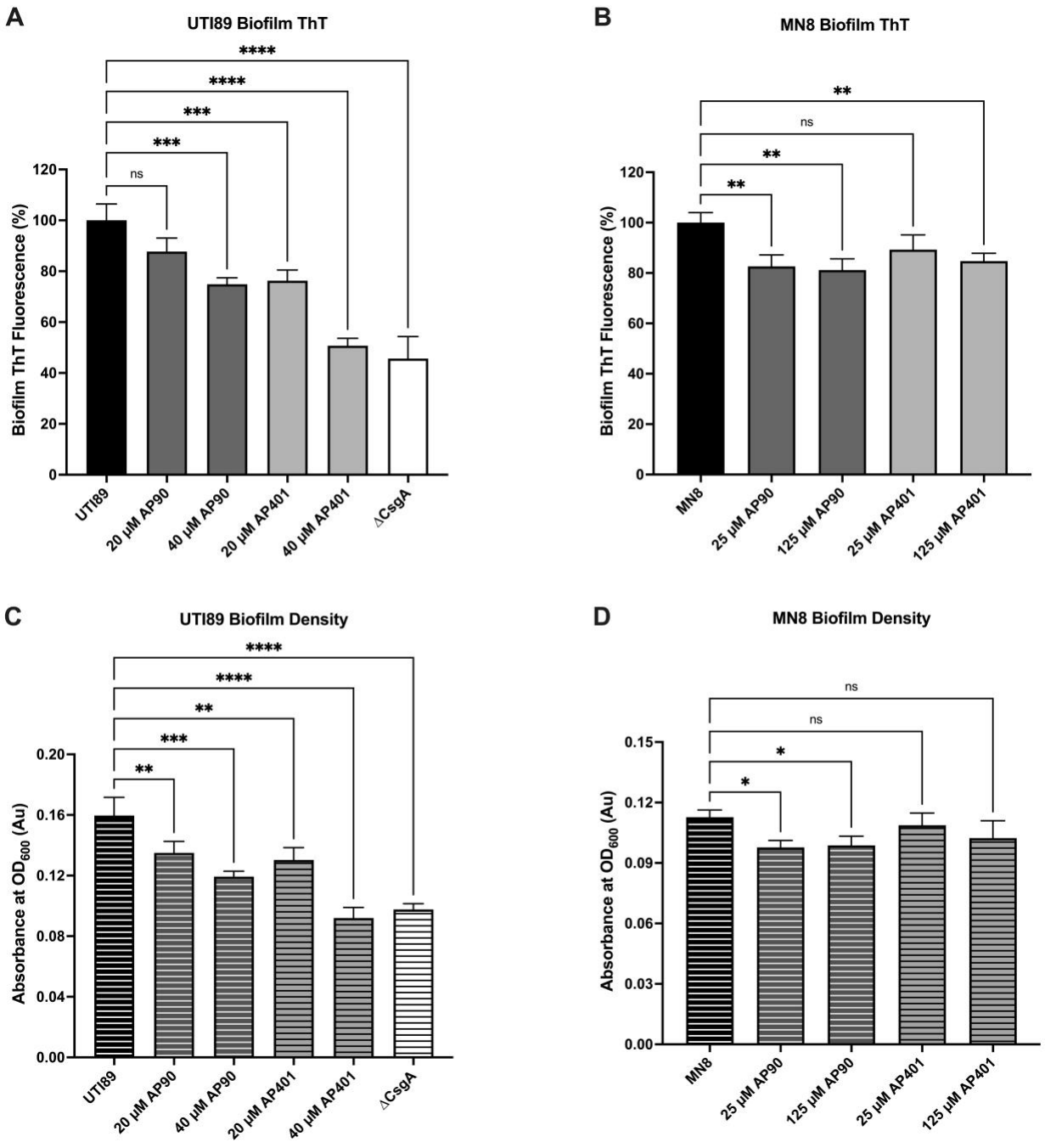


**Figure 3.1. α-Sheet peptides inhibit amyloid formation and reduce biofilm cell density.** Both α-sheet peptides inhibited amyloid formation as indicated by reduced ThT fluorescence. Biofilm ThT fluorescence values are reported as percent of the average UTI89 or MN8 peptide-free control fluorescence. For UTI89 (**A**), 40 μM AP401 caused the greatest reduction in fluorescence

of 49% as compared to the UTI89 control (*p<0.0001*). For MN8 (**B**), the 125 µM AP401 condition caused the greatest reduction of 18.2% as compared to the MN8 control (*p=0.01*). Significant reductions in biofilm formation as quantified by indirect cell density measurements ($OD_{600}$) were also observed for both peptides and bacteria. For UTI89 (**C**), 40 µM AP401 reduced biofilm formation to the level of the control UTI89 ΔCsgA strain (*p<0.0001*). For MN8 (**D**), both AP90 conditions significantly reduced biofilm formation (*p=0.0334* and *p=0.0485* for 25 µM and 125 µM, respectively) while neither AP401 condition caused a significant reduction. All values are mean and standard deviation for three replicates.

The optical density ($OD_{600}$) of the biofilms was quantified as an indirect measure of bacterial cells in the biofilm. For UTI89, all peptide conditions caused a significant reduction in biofilm density (**Figure 3.1C**). The 40 µM AP401 condition caused a 42% reduction in biofilm density (*p<0.0001*) as compared to the UTI89 control which is equal to the reduction seen for UTI89 ΔCsgA, providing additional evidence of complete inhibition of CsgA fibrilization by AP401. For MN8, a significant reduction in biofilm density was observed only for the AP90 conditions (*p=0.0334* and *p=0.0485* for 25 µM and 125 µM, respectively) (**Figure 3.1D**). These data indicate that the α-sheet peptides inhibit amyloid formation as indicated by ThT fluorescence and that this inhibition correlates to a reduction in biofilm formation as measured by $OD_{600}$. Additionally, variable efficacy by the two peptides was observed for both bacterial strains with AP401 showing increased amyloid inhibition and biofilm reduction for UT89 and AP90 demonstrating a greater effect for MN8.

*3.3.3 Curli inhibition by AP90 and AP401 renders E. coli more susceptible to antibiotics*

After establishing the susceptibility of mature *E. coli* biofilms to the antibiotics (**Table 3.1**) and determining the effect of the α-sheet peptides on curli fibril and biofilm inhibition (**Figure 3.1A and Figure 3.1C**), the effect of the co-administration of the α-sheet peptides and antibiotics on biofilm antibiotic susceptibly was investigated. For each *E. coli* antibiotic condition, the susceptibility of the UTI89 strain was compared to the non-amyloid-forming control mutant strain, UTI89 ΔCsgA. Because the hypothesis is contingent on the understanding that curli fortifies the biofilm and increases antibiotic resistance, the CsgA knockout strain was predicted to be more susceptible than UTI89 to each antibiotic without α-sheet peptide treatment. This was the case for all antibiotics tested except for amoxicillin where a comparable effect was observed (**Figures 3.2-3.6**).

The comparison of antibiotic susceptibility of wild-type UT189 biofilms treated with α-sheet peptides to the antibiotic susceptibility of UTI89 ΔCsgA biofilms also allows for conclusions to be drawn regarding the extent of curli inhibition. Notably, in cases where UTI89 ΔCsgA is not more susceptible to an antibiotic than UTI89 treated with α-sheet peptides, it can be deduced that biofilm fortification by curli does not play a significant role in *E. coli* antibiotic resistance. In these cases, α-sheet peptides would likely have a lesser effect on antibiotic susceptibility. The findings are discussed below and summarized in **Table 3.3**.

*UTI89 Susceptibility: Amoxicillin*

For the non-antibiotic conditions, addition of both peptides significantly reduced biofilm formation as compared to the UTI89 strain with AP401 showing a reduction equal to that of the UTI89 ΔCsgA control strain ($p<0.0001$ for all) (**Figure 3.2A**). For the antibiotic conditions,

AP401 caused a non-significant reduction in biofilm formation (**Figure 3.2A**). Both UTI89 and UTI89 ΔCsgA exhibited a 4-fold reduction in CFUs when exposed to 300 µg/mL amoxicillin, suggesting that curli formation does not have a significant effect on biofilm resistance to this antibiotic (**Figure 3.2B**). It was therefore predicted that the designed peptides would not have a large effect on biofilm clearance by amoxicillin. Interestingly, the CFU fold reduction of UTI89 increased to 12-fold when incubated with AP401 (**Figure 3.2B**). This indicates that UTI89 biofilms are 3x more susceptible to amoxicillin with co-administration of AP401. In contrast, AP90 had a minimal effect on UTI89 biofilm susceptibility to amoxicillin.

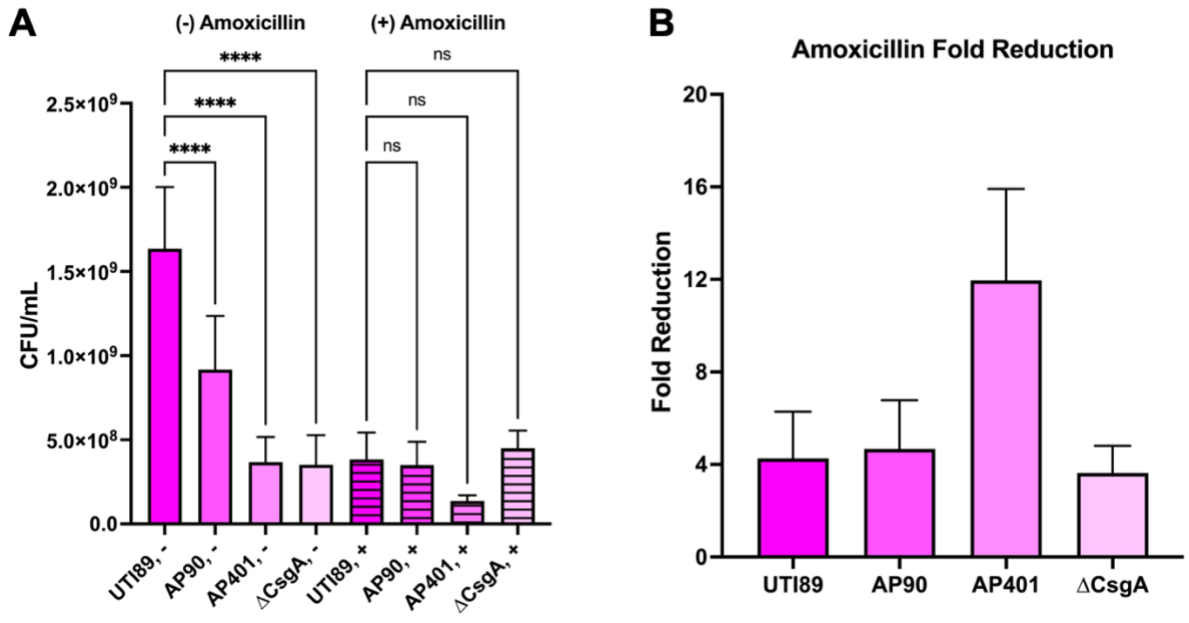


**Figure 3.2. AP90 and AP401 improve UTI89 biofilm susceptibility to amoxicillin. A)** Both synthetic α-sheet peptides inhibited biofilm formation for the non-antibiotic and antibiotic conditions for the *E. coli* strain UTI89. Biofilm formation was quantified as CFU/mL for UTI89 biofilms without (plain bars) and with antibiotics (striped bars) after 48 hours. Values are mean ± standard deviation for three replicates and p-values are indicated as follows: *ns* = not significant; **** $p<0.0001$. **B)** The co-administration of AP401 and amoxicillin demonstrated increased

antibiotic susceptibility for UTI89 biofilms. Fold reductions were calculated from biofilm CFU values after 48 hours as control UTI89 CFU in the absence of antibiotics divided by the condition CFU in the presence of antibiotics. Values are mean ± standard error. AP401 caused a greater fold reduction than AP401, and AP401 increased UTI89 susceptibility beyond the level observed for the control UTI89 ΔCsgA strain.

*UTI89 Susceptibility: Ciprofloxacin*

As previously demonstrated, for the non-antibiotic conditions, addition of both peptides caused a statistically significant reduction in biofilm formation as compared to UTI89, with AP401 causing a greater reduction ($p=0.0020$ for AP90 and $p<0.0001$ for AP401) (**Figure 3.3A**). A significant reduction was observed for both α-sheet peptides as compared to the UTI89 strain for ciprofloxacin treated conditions ($p<0.0001$) (**Figure 3.3A**). Ciprofloxacin applied to UTI89 biofilms resulted in a 1.7-fold reduction in CFUs (**Figure 3.3B**). UTI89 ΔCsgA exhibited an 18-fold CFU reduction upon ciprofloxacin treatment, indicating that amyloid incorporation into UTI89 biofilms has a critical role in establishing resistance to the antibiotic (**Figure 3.3B**). When grown with AP90 and AP401, the UTI89 CFU fold reduction increased to 11 and 28, respectively (**Figure 3.3B**). α-Sheet peptide inhibition of curli formation rendered UTI89 biofilms more susceptible to ciprofloxacin, with AP401 increasing susceptibility beyond that of the non-amyloid forming control strain, UTI89 ΔCsgA.

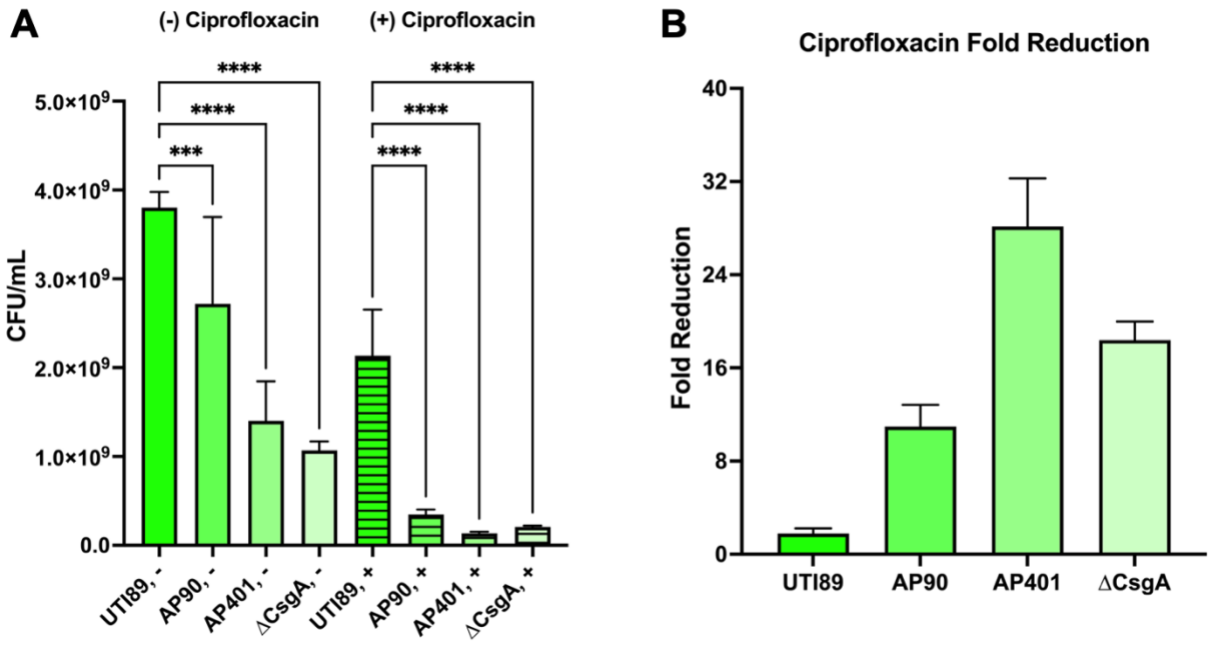


**Figure 3.3. AP90 and AP401 improve UTI89 biofilm susceptibility to ciprofloxacin. A)** Both synthetic α-sheet peptides inhibited biofilm formation for the non-antibiotic and antibiotic conditions for the *E. coli* strain UTI89. Biofilm formation was quantified as CFU/mL for UTI89 biofilms without (plain bars) and with antibiotics (striped bars) after 48 hours. Values are mean ± standard deviation for three replicates and p-values are indicated as follows: *** $p<0.001$, **** $p<0.0001$. **B)** The co-administration of α-sheet peptides and ciprofloxacin resulted in an increased antibiotic susceptibility for UTI89. Fold reductions were calculated from biofilm CFU values after 48 hours as control UTI89 CFU in the absence of antibiotics divided by the condition CFU in the presence of antibiotics. Values are mean ± standard error. AP401 caused a greater fold reduction than AP401, and AP401 increased UTI89 susceptibility beyond the level observed for the control UTI89 ΔCsgA strain.

*UTI89 Susceptibility: Erythromycin*

For the erythromycin conditions, AP401 significantly reduced biofilm formation to the level of the UTI89 ΔCsgA control strain (*p=0.028*) (**Figure 3.4A**). Erythromycin applied to UTI89 biofilms caused a 1.8-fold CFU reduction, and a 5.6-fold reduction with UTI89 ΔCsgA (**Figure 3.4B**). When grown with AP90 or AP401, UTI89 CFU fold reduction increased to 3.6 and 4.8, respectively (**Figure 3.4B**). These CFU fold reduction values are relatively low even with significant amyloid inhibition by AP90 and AP401, but this was expected since erythromycin is not active against gram-negative bacteria[141].

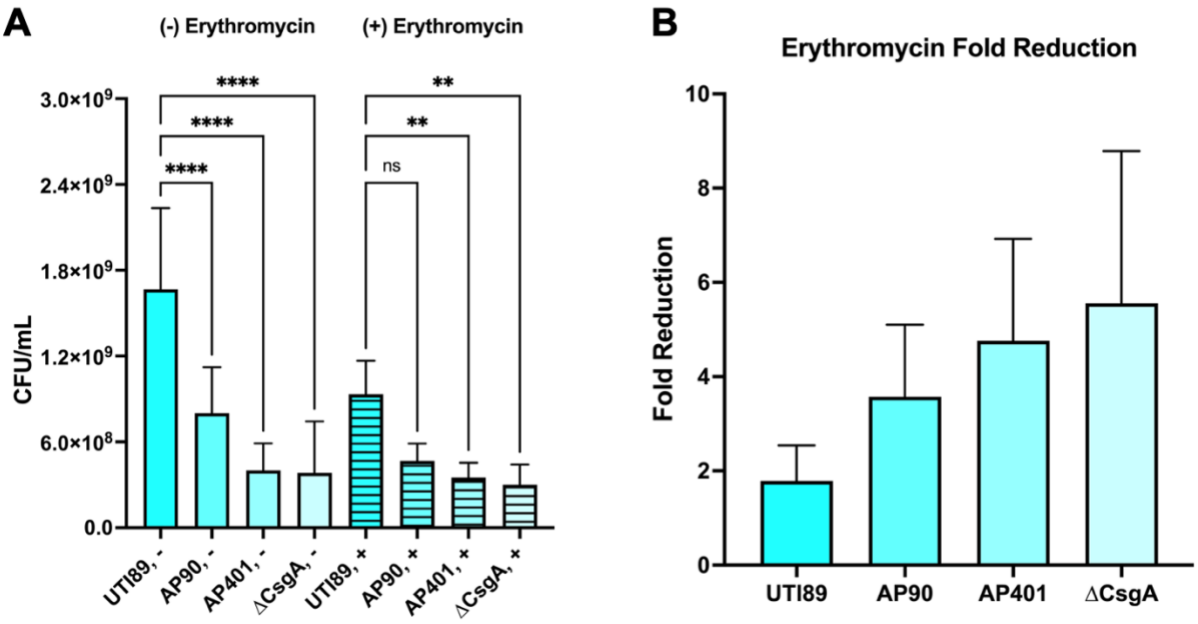


**Figure 3.4. AP90 and AP401 improve UTI89 biofilm susceptibility to erythromycin. A)** Both synthetic α-sheet peptides inhibited biofilm formation for the non-antibiotic and antibiotic conditions for the *E. coli* strain UTI89. Biofilm formation was quantified as CFU/mL for UTI89 biofilms without (plain bars) and with antibiotics (striped bars) after 48 hours. Values are mean ± standard deviation for three replicates and p-values are indicated as follows: *ns* = not significant; ** $p<0.01$, **** $p<0.0001$. **B)** The co-administration of α-sheet peptides and erythromycin

demonstrated increased biofilm antibiotic susceptibility for UTI89. Fold reductions were calculated from biofilm CFU values after 48 hours as control UTI89 CFU in the absence of antibiotics divided by the condition CFU in the presence of antibiotics. Values are mean ± standard error. AP401 caused a greater fold reduction than AP90.

*UTI89 Susceptibility: Gentamicin*

Application of gentamicin caused the greatest reduction in UTI89 biofilm formation of the five antibiotics tested, corresponding to an almost 800-fold reduction in UTI89 biofilm CFUs. Further, UTI89 ΔCsgA showed a $3.8 \times 10^3$-fold reduction to gentamicin, indicating that amyloid formation contributes significantly to UTI89 biofilm resistance to gentamicin (**Figure 3.5B**). Both AP90 and AP401 rendered UTI89 biofilms significantly more susceptible to gentamicin, with CFU fold reductions increasing to $2.6 \times 10^4$ and $5.3 \times 10^4$, respectively (**Figure 3.5B**).

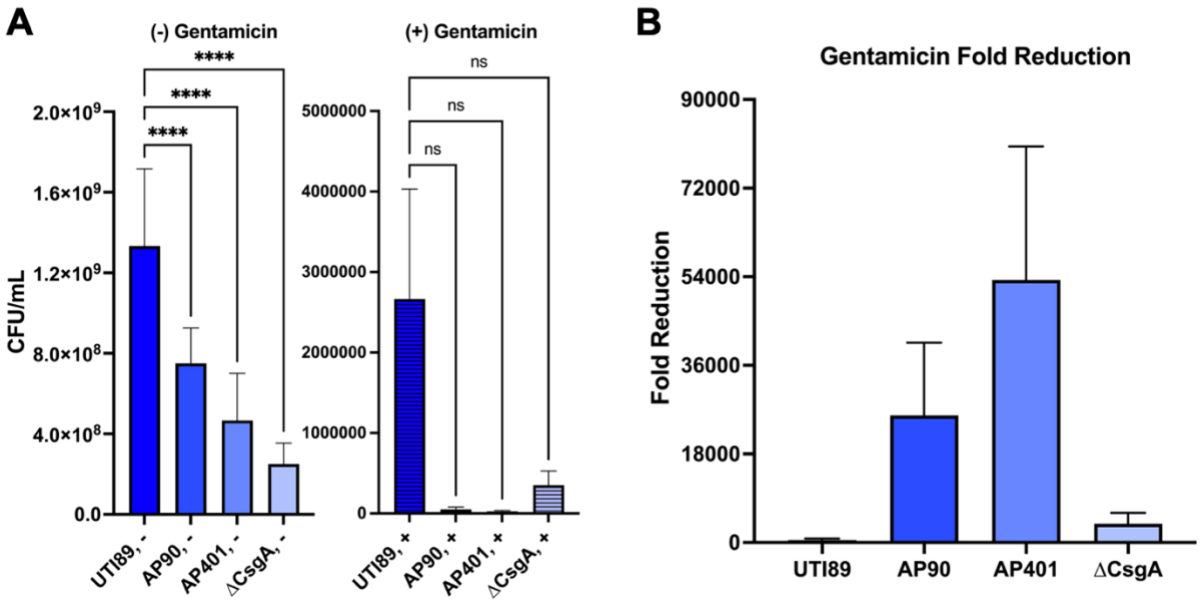


**Figure 3.5. AP90 and AP401 improve UTI89 biofilm susceptibility to gentamicin. A)** Both synthetic α-sheet peptides inhibited biofilm formation for the non-antibiotic and antibiotic conditions for the *E. coli* strain UTI89. Biofilm formation was quantified as CFU/mL for UTI89 biofilms without (plain bars) and with antibiotics (striped bars) after 48 hours. Values are mean ± standard deviation for three replicates and p-values are indicated as follows: *ns* = not significant; **** $p<0.0001$. **B)** The co-administration of α-sheet peptides and gentamicin demonstrated increased antibiotic susceptibility for UTI89 biofilms. Fold reductions were calculated from biofilm CFU values after 48 hours as control UTI89 CFU in the absence of antibiotics divided by the condition CFU in the presence of antibiotics. Values are mean ± standard error. AP401 caused a greater fold reduction than AP90, and AP401 increased UTI89 biofilm susceptibility beyond the level observed for the control UTI89 ΔCsgA strain.

*UTI89 Susceptibility: Vancomycin*

For the vancomycin conditions, both peptides significantly inhibited biofilm formation as compared to UTI89 (*p=0.0019* for AP90 and *p=0.0002* for AP401) and reduced biofilm formation to levels comparable to UTI89 ΔCsgA (**Figure 3.6A**). Vancomycin exposure led to a 1.5-fold CFU reduction in mature UTI89 biofilms, and a 7-fold reduction in UTI89 ΔCsgA biofilms (**Figure 3.6B**). Although vancomycin is primarily used against gram-positive bacteria[143], the fold reduction discrepancy observed between UTI89 and UTI89 ΔCsgA suggests that curli inhibition by α-sheet peptides may result in increased vancomycin biofilm susceptibility. Indeed, AP90 and AP401 increased UTI89 CFU fold reductions to 6.5 and 14.6, respectively (**Figure 3.6B**). Incubation of UTI89 with AP401 therefore resulted in a 10x greater fold reduction by vancomycin. These data are notable in that they demonstrate that amyloid fibril inhibition can improve susceptibility to a wide range of antibiotics, regardless of the antibiotic's specific mechanism of action.

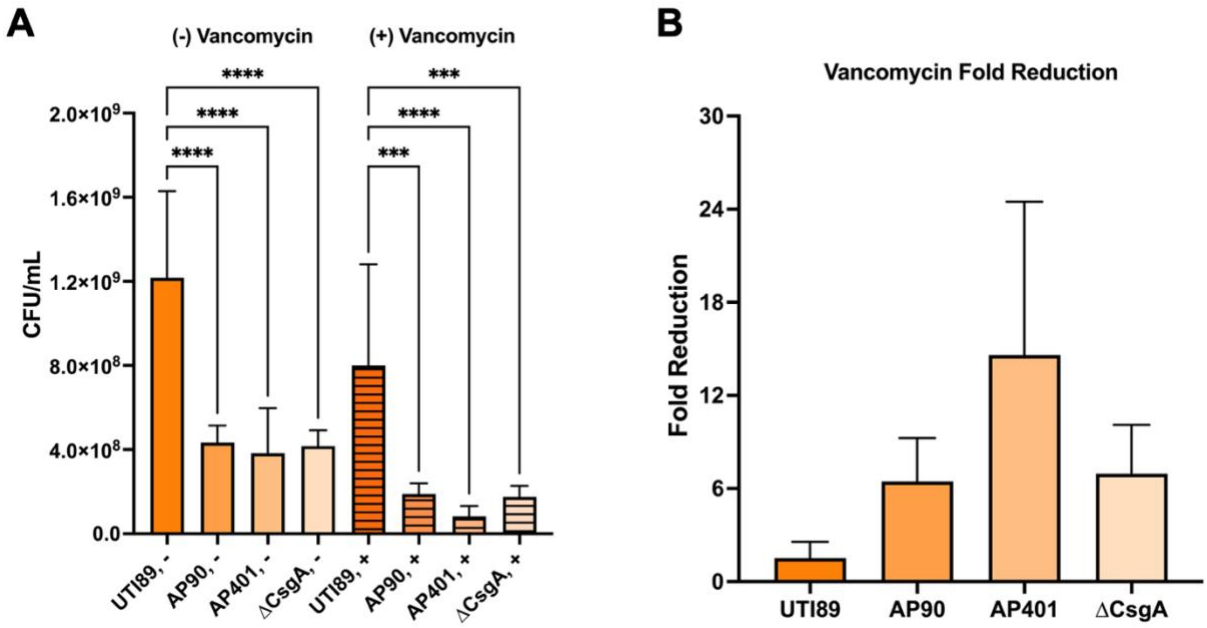


**Figure 3.6. AP90 and AP401 improve UTI89 biofilm susceptibility to vancomycin. A)** Both synthetic α-sheet peptides inhibited biofilm formation for the non-antibiotic and antibiotic conditions for the *E. coli* strain UTI89. Biofilm formation was quantified as CFU/mL for UTI89 biofilms without (plain bars) and with antibiotics (striped bars) after 48 hours. Values are mean ± standard deviation for three replicates and p-values are indicated as follows: *** $p<0.001$, **** $p<0.0001$. **B)** The co-administration of α-sheet peptides and vancomycin demonstrated an increased antibiotic susceptibility for UTI89. Fold reductions were calculated from biofilm CFU values after 48 hours as control UTI89 CFU in the absence of antibiotics divided by the condition CFU in the presence of antibiotics. Values are mean ± standard error. AP401 caused a greater fold reduction than AP401, and AP401 increased UTI89 biofilm susceptibility beyond the level observed for the control UTI89 ΔCsgA strain.

*3.3.4. AP90 and AP401 increase S. aureus biofilm susceptibility to antibiotics*

After establishing the susceptibility of mature *S. aureus* biofilms to the antibiotics (**Table 3.2**) and determining the effect of the α-sheet peptides on MN8 amyloid fibrilization and biofilm formation (**Figure 3.1B** and **Figure 3.1D**), the effect of the co-administration of the α-sheet peptides and antibiotics on MN8 antibiotic susceptibility was investigated.

*MN8 Susceptibility: Amoxicillin*

For the non-antibiotic conditions, both peptides caused a significant reduction in biofilm formation as compared to the MN8 control, with AP90 having a bigger effect than AP401 ($p=0.0038$ for AP90 and $p=0.04$ for AP401) (**Figure 3.7A**). A significant reduction was also observed for both peptides for the antibiotic conditions ($p<0.0001$ for AP90 and $p=0.001$ for AP401) (**Figure 3.7A**). When applied to mature MN8 biofilms, amoxicillin caused a 1.4-fold reduction in total CFUs (**Figure 3.7B**). Incubation with both AP90 and AP401 increased MN8 biofilm susceptibility to the antibiotic, resulting in a 3.3-fold and 2.8-fold CFU reduction, respectively (**Figure 3.7B**). Although the peptides did cause a small increase in antibiotic susceptibility, the magnitude of the change likely indicates that the MN8 biofilm resistance to amoxicillin is largely independent of amyloid formation.

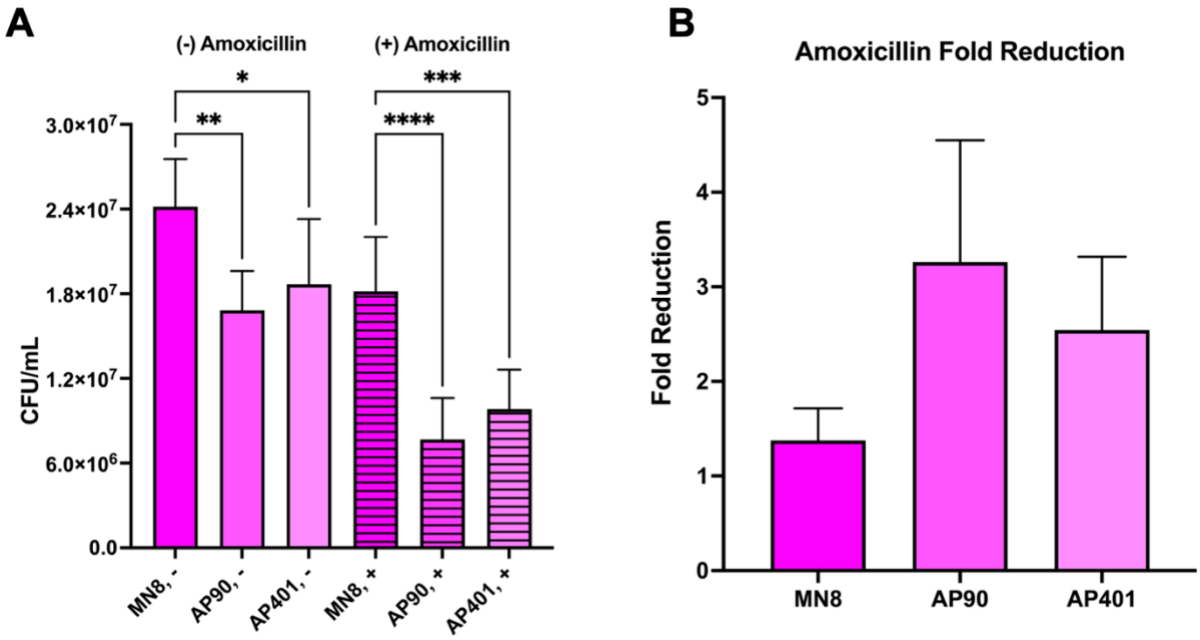


**Figure 3.7. AP90 and AP401 improve MN8 susceptibility to amoxicillin. A)** The α-sheet peptides inhibited *S. aureus* biofilm formation for the non-antibiotic and antibiotic conditions as measured by CFUs. Biofilm formation was quantified as CFU/mL for MN8 biofilms without (plain bars) and with antibiotics (striped bars) after 24 hours of growth. Values are mean ± standard deviation for three replicates and p-values are indicated as follows: * $p<0.05$, ** $p<0.01$, *** $p<0.001$, **** $p<0.0001$. **B)** The co-administration of α-sheet peptides and antibiotics increased amoxicillin susceptibility for MN8 biofilms. Fold reductions were calculated from biofilm CFU values after 24 hours as control MN8 CFU in the absence of antibiotics divided by the condition CFU in the presence of amoxicillin. Values are mean ± standard error. Both peptides increased susceptibility to amoxicillin, and a larger effect was observed with AP90.

*MN8 Susceptibility: Ciprofloxacin*

As previously shown, for the non-antibiotic conditions, both peptides caused a reduction in biofilm formation with AP90 causing a greater reduction (*p=0.0016* for AP90) (**Figure 3.8A**). For the ciprofloxacin conditions, only AP90 caused a reduction in biofilm formation (**Figure 3.8A**). The addition of ciprofloxacin caused a 2.8-fold reduction in CFUs for the MN8 control while the AP90 and AP401 conditions showed a 5.1-fold and 2.1-fold reduction, respectively (**Figure 3.8B**). The small fold change with AP90 indicates that amyloid formation contributes to but is not the primary factor in MN8 biofilm ciprofloxacin resistance.

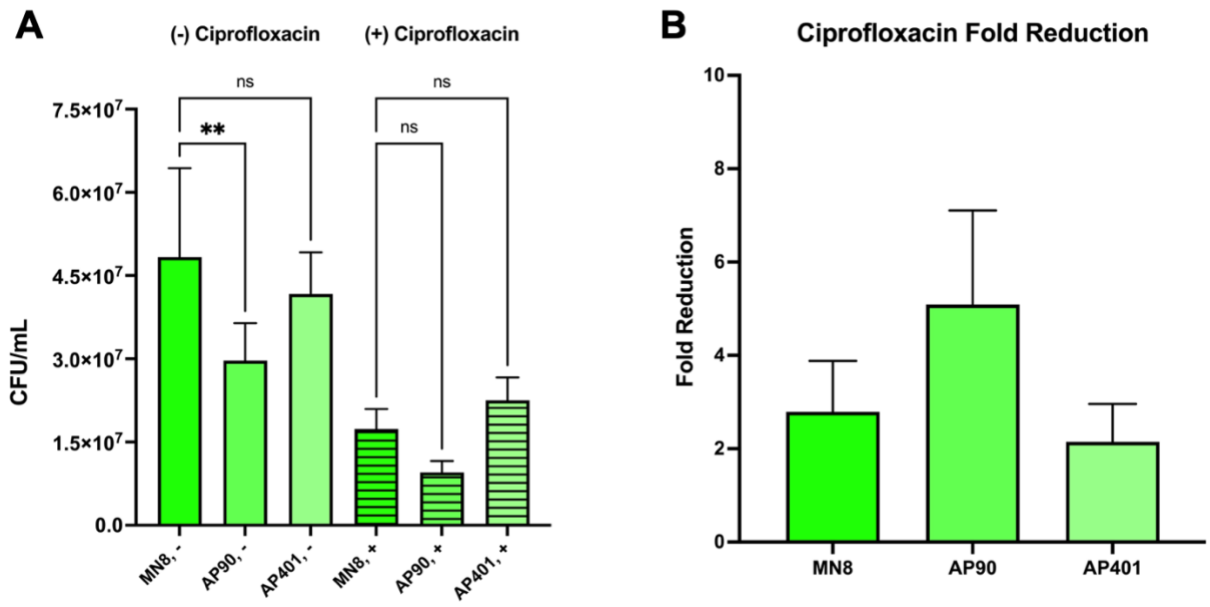


**Figure 3.8. AP90 and AP401 improve MN8 susceptibility to ciprofloxacin. A)** Both α-sheet peptides inhibited *S. aureus* biofilm formation for the non-antibiotic conditions and AP90 inhibited *S. aureus* biofilm formation for the antibiotic conditions as measured by CFUs. Biofilm formation was quantified as CFU/mL for MN8 biofilms without (plain bars) and with antibiotics (striped bars) after 24 hours of growth. Values are mean ± standard deviation for three replicates and p-values are indicated as follows: *ns* = not significant and ** $p<0.01$. **B)** The co-

administration of AP90 and ciprofloxacin increased antibiotic susceptibility for MN8 biofilms. Fold reductions were calculated from biofilm CFU values after 24 hours as control MN8 CFU in the absence of antibiotics divided by the condition CFU in the presence of antibiotics. Values are mean ± standard error. AP401 had no significant effect on MN8 susceptibility to ciprofloxacin.

*MN8 Susceptibility: Erythromycin*

The addition of erythromycin to mature MN8 biofilms caused a 2.5-fold reduction in biofilm CFUs (**Figure 3.9A**). For the antibiotic conditions, both peptides caused a significant reduction in CFUs (*p=0.02* and *p=0.035* for AP90 and AP401, respectively) with fold reductions of 9.4 for AP90 and 7.8 for AP401 (**Figure 3.8B**). These improvements in fold reductions suggest that amyloid formation is a factor in MN8 biofilm resistance to erythromycin.

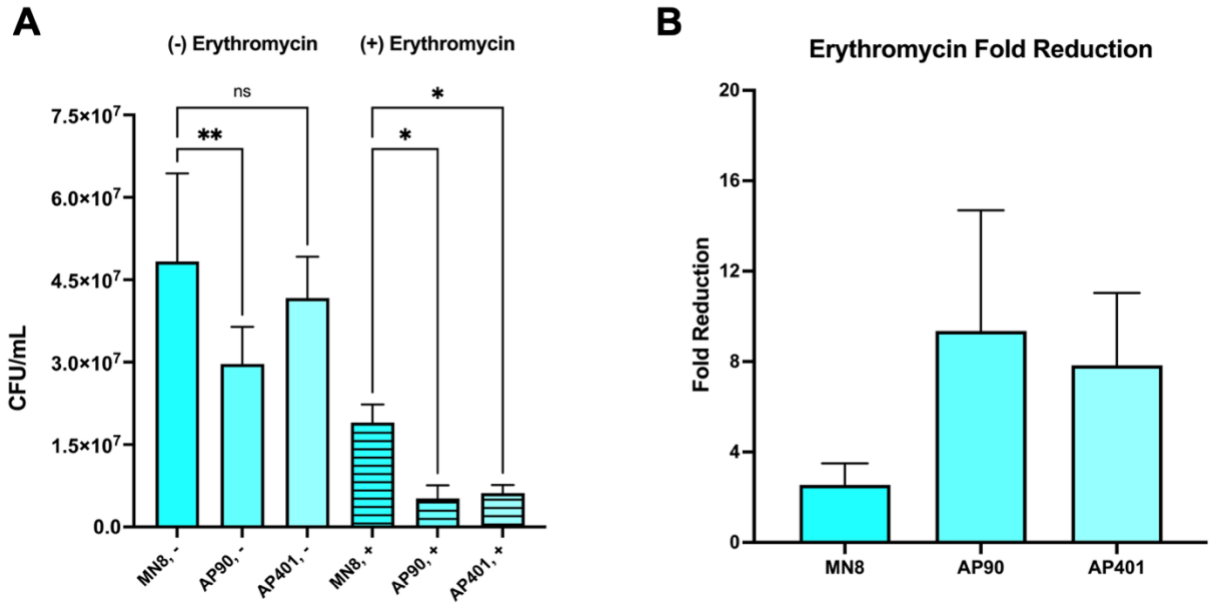


**Figure 3.9. AP90 and AP401 improve MN8 susceptibility to erythromycin. A)** The α-sheet peptides inhibited *S. aureus* biofilm formation for the non-antibiotic and antibiotic conditions as

measured by CFUs. Biofilm formation was quantified as CFU/mL for MN8 biofilms without (plain bars) and with antibiotics (striped bars) after 24 hours of growth. Values are mean ± standard deviation for three replicates and p-values are indicated as follows: *ns* = not significant; * $p<0.05$, ** $p<0.01$. **B)** The co-administration of α-sheet peptides and antibiotics increased erythromycin biofilm susceptibility for MN8. Fold reductions were calculated from biofilm CFU values after 24 hours as control MN8 CFU in the absence of antibiotics divided by the condition CFU in the presence of erythromycin. Values are mean ± standard error. Both peptides increased susceptibility to erythromycin, and a larger effect was observed with AP90.

*MN8 Susceptibility: Gentamicin*

Gentamicin was predicted to have a minimal effect on *S. aureus* as it targets aerobic gram-negative bacteria by passing through the gram-negative membrane[142]. Both α-sheet peptides caused a significant reduction in biofilm formation as compared to the MN8 strain with gentamicin only ($p=0.04$ for both peptides) (**Figure 3.10A**). When applied to mature MN8 biofilms, gentamicin reduced CFUs 1.6-fold (**Figure 3.10B**). Incubation with AP90 and AP401 increased MN8 susceptibility, corresponding to a 2.8-fold reduction in biofilm CFUs for both peptides (**Figure 3.10B**). As was observed with *E. coli* UTI89 and both erythromycin and vancomycin, these data are notable in that they demonstrate that amyloid fibril inhibition can improve susceptibility to a wide range of antibiotics, regardless of the antibiotic's specific mechanism of action.

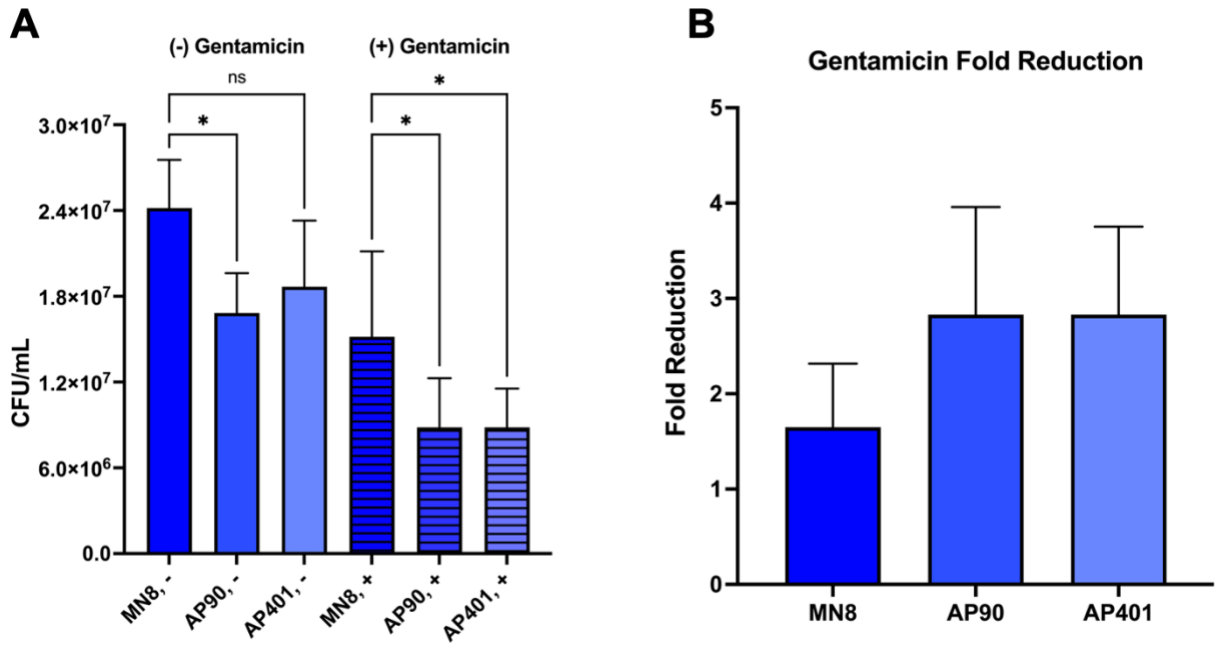


**Figure 3.10. AP90 and AP401 improve MN8 susceptibility to gentamicin. A)** The α-sheet peptides inhibited *S. aureus* biofilm formation for the non-antibiotic and antibiotic conditions as measured by CFUs. Biofilm formation was quantified as CFU/mL for MN8 biofilms without (plain bars) and with antibiotics (striped bars) after 24 hours of growth. Values are mean ± standard deviation for three replicates and p-values are indicated as follows: *ns* = not significant and * $p<0.05$. **B)** The co-administration of α-sheet peptides and antibiotics increased gentamicin susceptibility for MN8 biofilms. Fold reductions were calculated from biofilm CFU values after 24 hours as control MN8 CFU in the absence of antibiotics divided by the condition CFU in the presence of gentamicin. Values are mean ± standard error. Both peptides increased susceptibility to gentamicin to the same extent.

*MN8 Susceptibility: Vancomycin*

For the vancomycin conditions, incubation with AP90 and AP401 led to a non-significant reduction in biofilm CFUs (**Figure 3.11A**). Vancomycin reduced MN8 biofilm CFUs 12-fold, and AP90 and AP401 successfully increased susceptibility further, corresponding to CFU fold reductions of 24 and 16, respectively (**Figure 3.11B**). These data confirm that MN8 amyloid formation increases biofilm resistance to vancomycin and that the amyloid inhibiting peptides improved biofilm antibiotic susceptibility with varying efficacy between the two peptides.

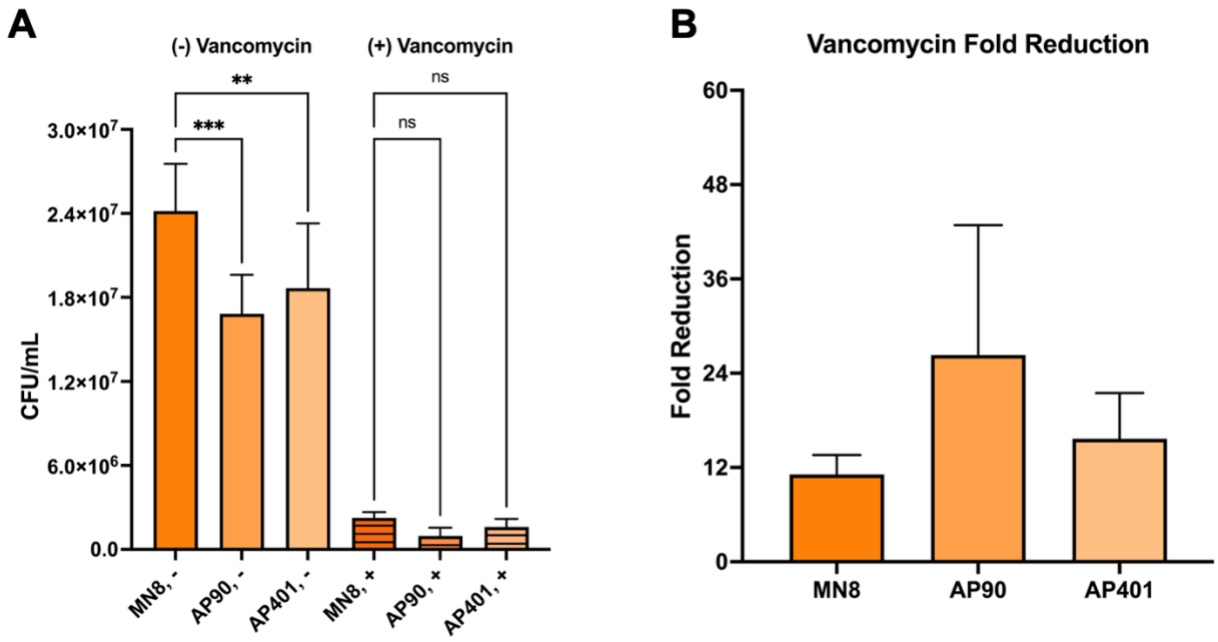


**Figure 3.11. AP90 and AP401 improve MN8 susceptibility to vancomycin. A)** The α-sheet peptides inhibited *S. aureus* biofilm formation for the non-antibiotic and antibiotic conditions as measured by CFUs. Biofilm formation was quantified as CFU/mL for MN8 biofilms without (plain bars) and with antibiotics (striped bars) after 24 hours of growth. Values are mean ± standard deviation for three replicates and p-values are indicated as follows: *ns* = not significant; ** $p<0.01$, *** $p<0.001$. **B)** The co-administration of α-sheet peptides and antibiotics increased vancomycin susceptibility for MN8 biofilms. Fold reductions were calculated from biofilm CFU

values after 24 hours as control MN8 CFU in the absence of antibiotics divided by the condition CFU in the presence of vancomycin. Values are mean ± standard error. Both peptides increased susceptibility to vancomycin, and a larger effect was observed with AP90.

The findings from the UTI89 and MN8 biofilm antibiotic susceptibility experiments are summarized in **Table 3.3**.

**Summary of Findings**

| | | Increased Biofilm Susceptibility? | |
|---|---|---|---|
| | | AP90+abx | AP401+abx |
| ***E. coli* UTI89** | Amoxicillin | ✓ | ✓✓✓ |
| | Ciprofloxacin | ✓✓✓ | ✓✓✓ |
| | Erythromycin | ✓ | ✓ |
| | Gentamicin | ✓✓✓✓ ✓ | ✓✓✓✓✓ |
| | Vancomycin | ✓ ✓ | ✓ ✓ ✓ |
| ***S. aureus* MN8** | Amoxicillin | ✓ | ✓ |
| | Ciprofloxacin | ✓ | ✓ |
| | Erythromycin | ✓✓ | ✓✓ |
| | Gentamicin | ✓ | ✓ |
| | Vancomycin | ✓✓✓ | ✓✓✓ |

**Table 3.3. Summary of findings.** ✓ = 1-5 fold reduction, ✓✓ = 5-10 fold reduction, ✓✓✓=10-100 fold reduction, ✓✓✓✓=100-1000 fold reduction, ✓✓✓✓✓= >1000 fold reduction.

## 3.4 Discussion

Increased rates of antibiotic resistance pose a global threat and there thus exists a significant need to develop novel methodologies to target microbial infections, particularly those

that are biofilm-associated. The ongoing emergence of multidrug resistant strains and the use of some drugs only as antibiotics of last resort disincentives the development of new antibiotics. Approaches like the strategy presented in this Chapter are advantageous as they may facilitate the continued use of existing antibiotics for treatment. Here, a strategy is presented to increase the biofilm susceptibility of amyloid-forming bacteria to antibiotics without introducing selective pressure and invoking the risk of acquired resistance. It has previously been shown that α-sheet peptides inhibit curli formation, increase *E. coli* susceptibility to gentamicin, and improve macrophage clearance[16]. The findings reported here expand on previous research by demonstrating that α-sheet peptides reduce biofilm cell density as reported by CFU quantification (**Figures 3.2A-3.11A**) and $OD_{600}$ (**Figure 3.1 C-D**) and are effective at increasing antibiotic susceptibility of both gram-negative (*E. coli*) and gram-positive (*S. aureus*) bacteria to multiple classes of antibiotics (**Figures 3.2B-3.11B** and **Table 3.3**). The results reported here suggest that the *de novo* α-sheet peptides may be universally effective against amyloid-producing bacteria, although additional bacterial strains must be tested utilizing the outlined methodologies to confirm this hypothesis.

Although the α-sheet peptides proved effective at increasing biofilm antibiotic susceptibility of both *E. coli* and *S. aureus*, the results reported here suggest key differences in the response of the bacteria to amyloid inhibition by APs. A higher peptide concentration was required to achieve a significant increase in *S. aureus* biofilm formation and antibiotic susceptibility (100 μM vs. 30 μM in *E. coli*), and it was hypothesized that the observed differences arise because *E. coli* is a gram-negative bacterium while *S. aureus* is gram-positive. Gram-positive bacteria are encompassed by thick layers of peptidoglycan, while gram-negative bacteria have much thinner peptidoglycan cell walls surrounded by an outer membrane

composed of lipopolysaccharide[154]. Variations in the cell surface may differentially affect the ability for the *de novo* α-sheet peptides to access the growing amyloid fibril located on the cell surface. The observed differences may also be due to variations in the amount of amyloid precursor secreted by and incorporated into the biofilms of *E. coli* and *S. aureus*.

Discrepancies were also observed in the relative potency of AP90 and AP401 in the two bacteria. Previously, it was demonstrated that AP401 is a more potent inhibitor of curli biogenesis than its structural isomer, AP90[16]. AP90 and AP401 have the same amino acid sequence, but every amino acid has the opposite chirality[16], and it was hypothesized that the elevated potency of AP401 in *E. coli* was due to the presence of D-amino acids in the hairpin turn resulting in increased stability to proteases. The results presented here suggest that AP401 is not only a more potent inhibitor of curli formation, but that this elevated inhibition also translates to a larger effect on biofilm antibiotic susceptibility. Interestingly, there was a smaller potency difference between AP90 and AP401 in *S. aureus* with AP90 causing a greater effect for four antibiotics. D-amino acids are frequently incorporated into gram-positive cell walls which are composed of thick peptidoglycan layers[155]. Because *S. aureus* utilizes D-amino acids in its cell wall, the bacteria may also produce proteases that are designed to cleave the peptide bond between D-amino acids. Therefore, AP401 may not be more stable than AP90 to proteases in *S. aureus*, as is hypothesized to be the case in *E. coli*.

The designed peptides employed here improved bacterial biofilm antibiotic susceptibility to varying extents for each antibiotic. The observed variations can be attributed both to the differences between the mechanism of action of each antibiotic, as well as to the mechanism that governs the bacterium's resistance to the antibiotic. AP90 and AP401 are amyloid inhibitors, and the hypothesis presented in this Chapter is contingent on amyloid formation contributing a

significant effect to reduced biofilm antibiotic sensitivity. However, AP90 and AP401 may not have any effect on a bacterium's resistance if the mechanism of resistance is unrelated to biofilm fortification by amyloid fibrils.

Previous studies have identified several other compounds with anti-amyloid activity against bacterial biofilms, including peptides, proteins, curlicides, graphene quantum dots, and polyphenols[156–159]. However, in some cases, such as for the plant flavonoids luteolin, myricetin and quercetin, biofilm inhibition was seen in some bacteria (*E. coli* and *S. aureus*) while an increase or no change in biofilm formation was observed in other bacteria (*P. aeruginosa*)[160]. Additionally, while some compounds have successfully inhibited biofilm formation, most compounds have not been tested with antibiotics, or have in fact been shown to increase antibiotic resistance. In one study, the anti-amyloidogenic polyphenol epigallocatechin gallate (EGCG) caused reduced susceptibility of *S. aureus* to vancomycin, oxacillin, and ampicillin[161]. Another study found that in some conditions, EGCG administration promoted biofilm formation in *P. aeruginosa* and increased antibiotic resistance to tobramycin[162]. A third study reported that co-administration of EGCG and tobramycin had a moderate effect on wildtype *P. aeruginosa* biofilm minimum bactericidal eradication concentrations, but a larger effect was observed when the functional amyloid fibril Fap was overexpressed[163]. Thus, it is critical to test the efficacy of potential bacterial amyloid inhibitors in combination with antibiotics, as was done in this Chapter.

## 3.5 Conclusions

Nosocomial infections caused by biofilm-dwelling microbes are often difficult to eradicate due to antibiotic resistance and therefore present a major healthcare risk. Novel

strategies to target and treat multidrug resistant pathogens without inducing resistance are required. The findings reported in **Chapter 3** represent a method through which to structurally weaken bacterial biofilms by inhibiting amyloid formation using designed α-sheet peptides, thereby improving bacterial clearance by antibiotics without introducing selective pressure and triggering acquired resistance.

## 3.6 Materials and Methods

### *3.6.1 Peptide Synthesis*

Peptide synthesis was conducted in house as described in **Chapter 2.6.3**.

### *3.6.2 E. coli Biofilm Cultures*

A uropathogenic clinical isolate strain, UTI89[164], and a control strain with a chromosomal deletion of the CsgA gene, UTI89 ΔCsgA[138], were used for all *E. coli* experiments (**Appendix A, Table A.2**). Overnight cultures were grown in Luria Broth (LB, Miller, Thermo Fisher Scientific; Waltham, MA) for 16-18 hours at 37°C with shaking (180 rpm). Cultures were then "refreshed" by replacing 5 mL of culture with 5 mL fresh LB medium and grown for an additional 3 hours to ensure bacteria were in the exponential phase. Overnight cultures were then spun down and diluted to an optical density ($OD_{600}$) of 0.1 (~$8x10^7$ cells/mL) in YESCA broth supplemented with 4% DMSO (Corning; Glendale, AZ), medium known to promote increased curli formation[165]. Lyophilized peptide stock was dissolved to 2 mg/mL in $H_2O$, thoroughly mixed, and the concentration was measured using a NanoDrop 2000 Spectrometer (Thermo Fisher Scientific; Waltham, MA) at 280 nm using the respective extinction coefficient (**Appendix A, Table A.1**). The APs were then diluted to 300 μM in $H_2O$. Diluted bacteria

culture (180 µL) was plated with 20 µL peptide (or water, in the case of controls) and aliquoted in triplicate into wells of a sterile, clear 48-well polystyrene plate (Corning; Glendale, AZ). The final peptide concentration was 0 or 30 µM (1.2 pg/CFU at the time of plating, assuming $8x10^7$ cells/mL). Plates were covered, sealed in a plastic bag, and statically grown at 26°C for 48 hours.

### *3.6.3 S. aureus Biofilm Cultures*

*S. aureus* MN8 (clinical isolate; urogenital tract[166]; **Appendix A, Table A.2**) was grown for 16-18 hours in trypticase soy broth (TSB; 10g/L; Becton, Dickinson and Company; Sparks, MD) at 37°C with shaking (180 rpm). Overnight cultures were "refreshed" by replacing 5 mL of culture with 5 mL of fresh TSB medium and grown for an additional six hours. Cells were then spun down and re-suspended in peptone-NaCl-glucose (PNG) media (Thermo Fisher Scientific; Waltham, MA)[137]. Resuspended cells were diluted to an optical density of 0.1 ($OD_{600}$). Peptides were synthesized as described in **Chapter 2.6.3**, prepared as discussed in **Chapter 3.6.2**, and diluted to 1000 µM in $H_2O$. Diluted bacteria culture (180 µL) was plated with 20 µL peptide (or water, in the case of controls) and aliquoted in triplicate into wells of a sterile, clear 48-well polystyrene plate (Corning; Glendale, AZ). The final peptide concentration was 0 or 100 µM (4 pg/CFU at the time of plating, assuming $8x10^7$ cells/mL)). Plates were covered, sealed in a plastic bag, and grown at 37°C for 24 hours with shaking (250 rpm).

### *3.6.4 Antibiotic Susceptibility*

UTI89 and MN8 biofilms were grown according to the methods described in **Chapter 3.6.2** and **Chapter 3.6.3**, respectively. Five different antibiotics were tested per bacterium: amoxicillin (MP Biomedicals; Solon, OH), ciprofloxacin hydrochloride (MP Biomedicals;

Solon, OH), erythromycin (Thermo Fisher Scientific; Waltham, MA), gentamicin sulfate (Thermo Fisher Scientific; Waltham, MA), and vancomycin hydrochloride (Thermo Fisher Scientific; Waltham, MA). Antibiotics were dissolved in YESCA (*E. coli*) or PNG medium (*S. aureus*) at a concentration of 900 µg/mL. 100 µL of antibiotic or control (YESCA or PNG media) was added to each well after 42 (*E. coli*) or 18 (*S. aureus*) hours of incubation without disturbing the biofilm for a final well concentration of 300 µg/mL. Following 6 additional hours of biofilm growth (48 or 24 hours total), planktonic cells were removed by gentle pipetting and discarded. The biofilms were rinsed with 250 µL PBS (Sigma Aldrich; St. Louis, MO) by gentle pipetting, and the rinse was discarded. Biofilms were homogenized in 200 µL PBS by vigorous pipetting (30x per well), and the biofilm suspensions were transferred to an Eppendorf tube. The biofilm suspensions were then ultra-sonicated for 5 seconds on ice and diluted in tenfold increments. The serial dilutions were then plated on agar plates (LB agar or TSB agar) using the drop plate method[167]. Six replicates were plated per condition. Colonies were grown for 16 hours at 37°C and CFUs were counted. Total CFUs of the biofilm suspensions were calculated using the dilution number and the number of CFUs counted in the respective dilution. CFU fold reductions were calculated as the control UTI89 or MN8 biofilm CFU in the absence of antibiotics divided by the condition biofilm CFU in the presence of antibiotics.

### *3.6.5 Statistics*

All statistical significance values reported are One-Way ANOVA with post-hoc comparisons and a Bonferroni multiple comparison correction performed in GraphPad Prism. A single asterisk indicates a p-value less than 0.05. Two asterisks indicate a p-value less than 0.01.

Three asterisks indicate a p-value less than 0.001. Four asterisks indicate a p-value less than 0.0001.

# Chapter 4. Microbial Alzheimer's Disease Hypothesis

## 4.1 Summary

Evidence of the colocalization of microbial pathogens and the β-amyloid peptide (Aβ) in the brain of Alzheimer's disease (AD) patients suggests that microbial infection may play a role in sporadic AD[73,74,76,79,80,87,89]. Aβ exhibits antimicrobial activity against numerous pathogens, positing a role for Aβ in the innate immune response[86,87]. While mammalian amyloid formation is disease-associated, many bacteria form amyloid fibrils to fortify the extracellular biofilm and protect cells from the surrounding environment[3,12,14,16,90,121,122,136,138,156,159,168,169]. In the microbial AD hypothesis, Aβ aggregates in response to infection to combat the pathogen. This Chapter investigates whether this response occurs through toxic Aβ oligomers. Oligomers adopt α-sheet structure prior to fibrilization[11–13,15,16,39,40], and *de novo* α-sheet peptides specifically bind to the oligomeric aggregates of bacterial and mammalian amyloid proteins to neutralize toxicity and inhibit aggregation[11–16,40]. Here, the soluble oligomer binding assay (SOBA) is employed to measure the effect of *E. coli* amyloid, or curli, formation on Aβ aggregation. SOBA is an ELISA-like assay that uses a *de novo* designed dimeric α-sheet peptide (AP510d) as the capture agent (**Figure 4.1**), thereby exhibiting specificity for α-sheet species without binding to the monomeric, random coil Aβ or fibrillar, β-sheet conformations of Aβ[39]. Additionally, Aβ enriched in each of the conformations sampled during aggregation (random coil monomer, α-sheet oligomer, and β-sheet protofibril) was isolated based on methods and findings discussed in **Chapter 2** to determine the effect of Aβ secondary structure on curli biogenesis and *E. coli* biofilm formation. Curli formation by *E. coli* was found to increase endogenous Aβ oligomer production by human neuroblastoma cells, and Aβ oligomers significantly inhibited curli

formation and reduced *E. coli* biofilm density. Further, curli and biofilm inhibition by Aβ oligomers increased *E. coli* susceptibility to gentamicin. Finally, *in vitro* experiments with Aβ and CsgA were conducted, and it was found that Aβ and CsgA neutralize one another's oligomeric toxicity via binding of their respective α-sheet toxic oligomeric form. The findings reported in this chapter suggest that exposure to toxic oligomers formed by microbial pathogens may trigger Aβ upregulation and aggregation to protect against infection via selective interactions between α-sheet oligomers to neutralize the oligomeric toxicity of both species with subsequent inhibition of fibrilization by Aβ.

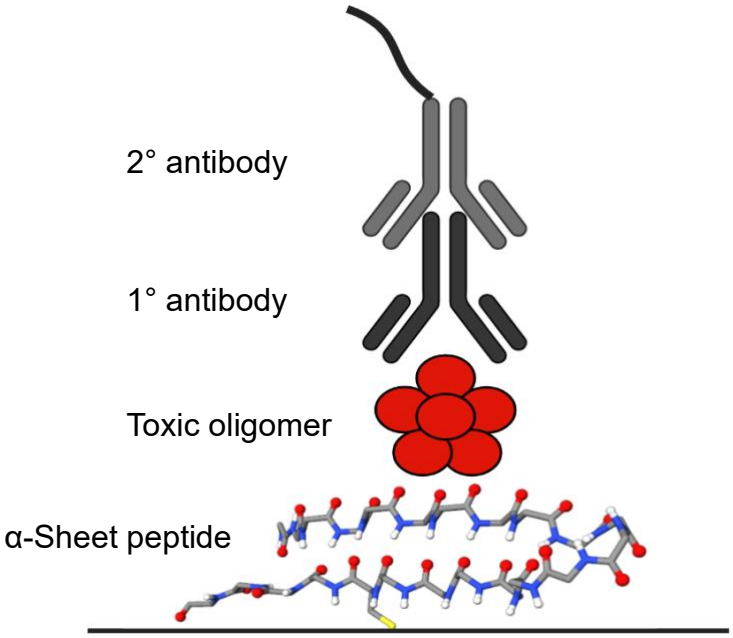


**Figure 4.1. SOBA schematic.** SOBA uses a dimeric α-sheet peptide (AP510d) as the capture agent to specifically target the α-sheet conformation present in the toxic oligomers of amyloid species. A primary (1°) antibody specific for Aβ (6E10) is then bound to the toxic oligomer. A secondary (2°) antibody is then bound to the primary antibody, and the signal is developed and can be interpreted as a quantification of the toxic Aβ oligomers present in solution.

## 4.2 Background and Motivation

Neuroinflammation has long been associated with AD and other diseases including Parkinson's disease (PD), amyotrophic lateral sclerosis (ALS), and Multiple Sclerosis (MS), suggesting a central role of a sustained inflammatory response in neurodegenerative disorders[78,170–181]. Chronic inflammation in AD is attributed to a disruption in the equilibrium of anti-inflammatory and pro-inflammatory signaling, resulting in chronic microglial cell activation and increased cytokine release[77,180–184]. Aβ aggregates are regularly degraded and phagocytosed by microglia, but when Aβ levels are significantly elevated, as is the case in AD, chronic activation of microglia results in a sustained pro-inflammatory response that exacerbates AD pathology and neuronal death[180,181,185,186]. The neuroinflammatory response then reduces Aβ degradation and phagocytosis by microglia, further elevating microglial activation and producing a cyclical loop of neurodegeneration[180,181]. The mechanism that triggers the initial upregulation of Aβ aggregation is still largely uncharacterized, but evidence of microbial pathogens in AD patient brain samples suggests that Aβ aggregation is employed as an innate immune response to microbial infection[74,82,83,86,88,176,181]. The microbial AD hypothesis postulates that although Aβ aggregation is likely a programmed immune response to microbial pathogens, excess buildup of toxic aggregates results in a chronic inflammatory response that causes AD pathology[80,88,181]. In **Chapter 4**, the molecular mechanisms that govern the role of Aβ in the innate immune response are investigated.

## 4.3 Results

*4.3.1 Upregulation of Aβ α-sheet oligomers with amyloid-forming E. coli*

Neuroblastoma cells were grown with two strains of uropathogenic *E. coli*: UTI89, a robust amyloid- and biofilm-forming clinical isolate, and UTI89 ΔCsgA (referred to below as ΔCsgA), an engineered deletion strain that lacks the cellular machinery required to form curli fibrils. Following *E. coli* biofilm maturation, the planktonic phase was removed and applied to SOBA to quantify the amount of toxic α-sheet $A\beta_{42}$ oligomers present in solution. Notably, the α-sheet peptide used as the capture agent in SOBA exhibits specificity for both *E. coli* and Aβ α-sheet oligomers. However, the use of the 6E10 anti-Aβ antibody as the primary antibody in SOBA allows for quantification of Aβ alone, as the binding epitope of 6E10 (EFRHDS) is not found in any protein produced by *E. coli*[187].

Incubation with amyloid-forming *E. coli* (UTI89) led to a threefold increase in the formation of toxic Aβ α-sheet oligomers (*p<0.0001;* **Figure 4.2**). Interestingly, the SOBA signal decreased approximately 50% when neuroblastoma cells were grown with UTI89 ΔCsgA (*p=0.04*), although it is unclear whether this is indicative of Aβ being located within the cells (or extracellular matrix) and therefore not present in the planktonic phase, or of true downregulation of toxic Aβ oligomer production.

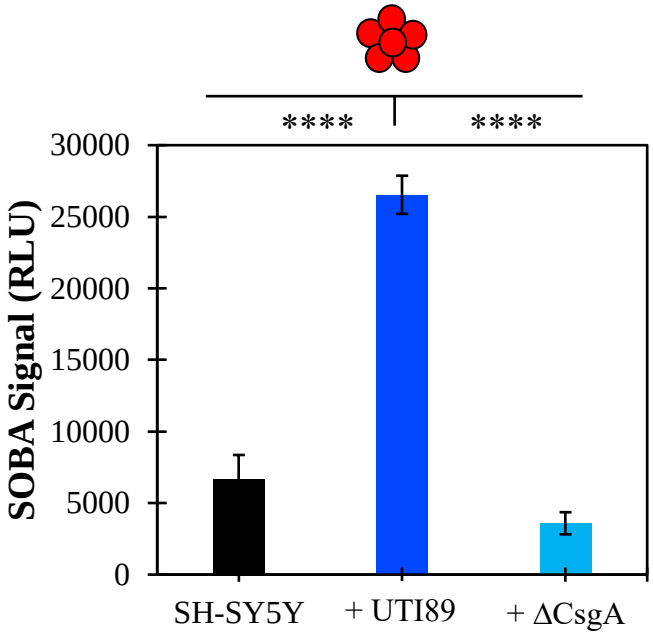


**Figure 4.2. UTI89 upregulates α-sheet containing Aβ oligomers in neuroblastoma cells.** Incubation with UTI89 results in a threefold increase ($p<0.0001$) in the production of α-sheet-containing Aβ oligomers by neuroblastoma cells as compared to the control condition (SH-SY5Y neuroblastoma cells with media in place of bacteria). Values are mean ± standard deviation for three replicates.

*4.3.2 Aβ oligomers inhibit curli formation by E. coli*

Using a protocol incorporating a ThT assay for measuring Aβ aggregation and β-sheet formation (**Figure 2.1A**), CD for determining secondary structure content (**Figure 2.1B**), and cell viability assays (**Figure 2.2**), Aβ was isolated in its three conformations: monomeric, random coil; oligomeric, α-sheet rich; and fibrillar, β-sheet rich. UTI89 and ΔCsgA were grown in biofilm forming conditions with the Aβ samples to measure the effect of Aβ secondary structure on curli formation. Curli formation was inhibited by each Aβ sample, with the most effective inhibition observed in UTI89 biofilms grown with oligomeric, α-sheet Aβ (50% ThT

signal reduction) (*p=0.0009*; **Figure 4.3A**). Biofilm amyloid content was reduced 26% and 17% by monomeric and fibrillar Aβ, respectively (*p=0.008* for monomeric Aβ and *p=0.04* for fibrillar Aβ). Oligomeric Aβ had no effect on the ThT fluorescence of UTI89 ΔCsgA biofilms (**Figure 4.3B**).

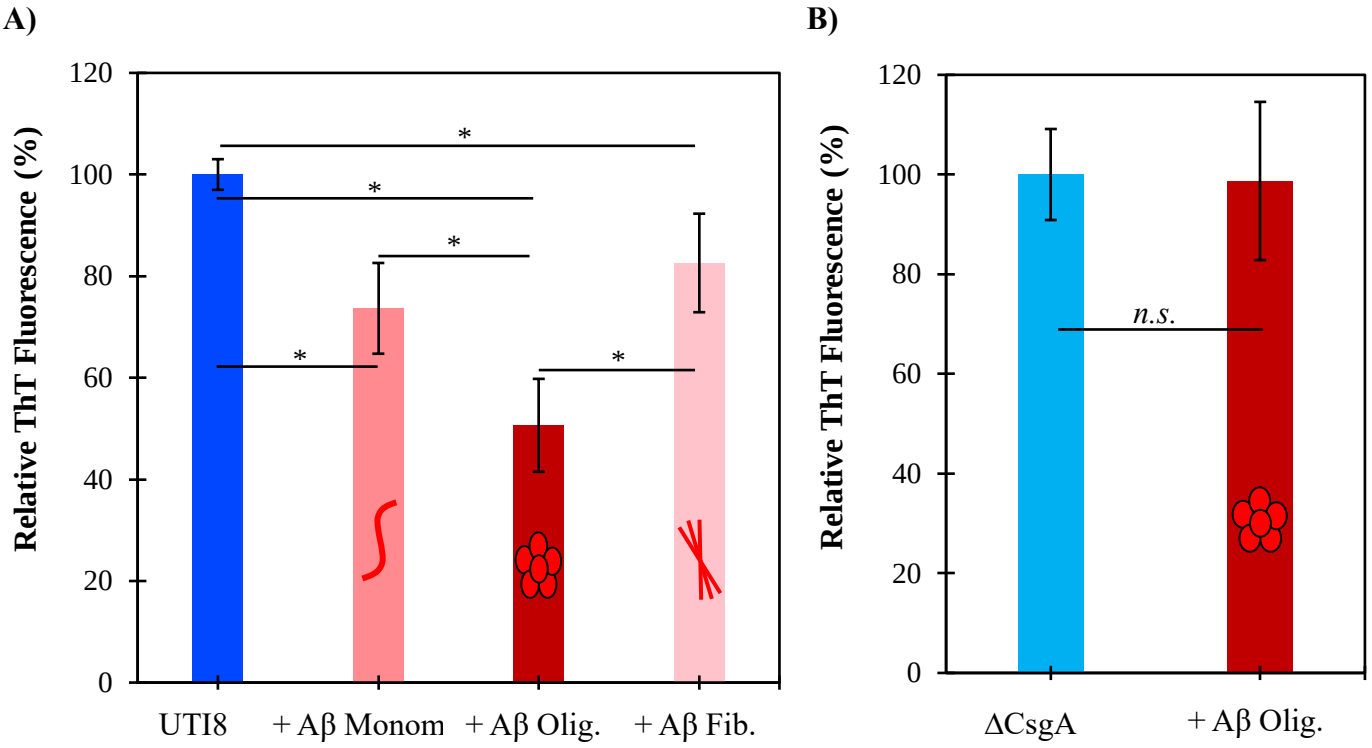


**Figure 4.3. Aβ oligomers inhibit amyloid formation in UTI89. A)** Incubation with 0.5 pg/CFU Aβ oligomers caused a 50% reduction in curli production by UTI89 (*p=0.0009*). Monomeric and fibrillar Aβ (0.5 pg/CFU) caused 26% and 17% curli inhibition, respectively (*p=0.008* for monomeric Aβ and *p=0.04* for fibrillar Aβ). Values are mean ± standard deviation for three replicates. Notably, while each sample is enriched in the respective conformation, it is likely that mixed populations are present. **B)** Incubation with 0.5 pg/CFU Aβ oligomers had no effect on the ThT signal of ΔCsgA. Values are mean ± standard deviation for three replicates.

*4.3.3 Aβ oligomers inhibit E. coli biofilm formation*

In addition to measuring the amyloid content in UTI89 biofilms, optical density at 600nm ($OD_{600}$) was measured to determine relative biofilm and cell density between the various conditions. UTI89 biofilms grown with oligomeric Aβ (0.5 pg/CFU) exhibited a 47% reduction in biofilm density (*p=0.008*; **Figure 4.4A**). Notably, planktonic cell density increased 1.5-fold (*p=0.0003*), and there was no significant difference in the summed total planktonic and biofilm $OD_{600}$ measurements between the two conditions. This suggests that by inhibiting curli formation, Aβ oligomers shift cells from the biofilm to the free-floating planktonic phase rather than causing cell death. The observed non-bactericidal activity corresponds to previous studies indicating that *de novo* α-sheet peptides inhibit amyloid formation and reduce biofilm density without promoting cell death[16]. Aβ had no effect on the cell density distribution of the non-amyloid-forming ΔCsgA strain (**Figure 5B**), suggesting that reduced UTI89 biofilm density by Aβ oligomers is due to interactions between CsgA and Aβ.

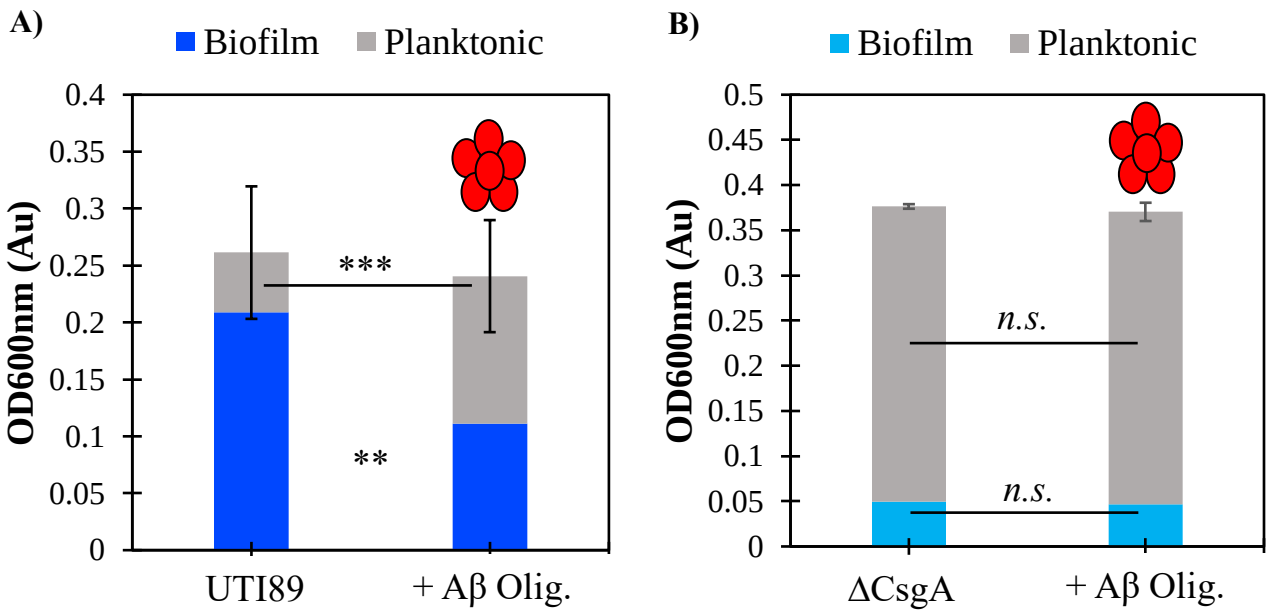


**Figure 4.4. Aβ oligomers reduce UTI89 biofilm cell density without causing cell death. A)** Incubation with 0.5 pg/CFU Aβ oligomers reduced UTI89 biofilm cell density by 47% (*p=0.008*) and increased planktonic cell density by 150% (*p=0.0003*). Aβ oligomers had no significant effect on the total summed $OD_{600}$ of UTI89. Values are mean ± standard deviation for three replicates. **B)** Incubation with 0.5 pg/CFU Aβ oligomers had no effect on the cell dispersion or total cell density of ΔCsgA, as measured by OD600. Values are mean ± standard deviation for three replicates.

*4.3.4 Aβ oligomers improve E. coli gentamicin susceptibility*

Antibiotic susceptibility experiments were then conducted to determine whether curli and biofilm inhibition by Aβ oligomers results in increased susceptibility of the *E. coli* biofilm to gentamicin. Because biofilm cells are 10-1000x less susceptible to antibiotics than planktonic cells[32], it was hypothesized that by inhibiting curli biogenesis and reducing biofilm cell density, Aβ oligomers would significantly increase the susceptibility of *E. coli* biofilms to gentamicin.

All three Aβ samples (monomeric random coil, α-sheet oligomeric, and fibrillar β-sheet) increased the susceptibility of UTI89 to gentamicin, and oligomeric Aβ had the largest effect corresponding to a 79% increase in susceptibility as measured by CFU ratios (*p<0.0001*; **Figure 4.5A**). Monomeric and fibrillar Aβ increased UTI89 gentamicin susceptibility 44% and 42%, respectively (*p<0.0001* for monomeric Aβ and *p=0.004* for fibrillar Aβ; **Figure 4.5A**). Interestingly, ΔCsgA exhibited 23% less susceptibility to gentamicin when grown with oligomeric Aβ; however, the result is not statistically significant (**Figure 4.5B**).

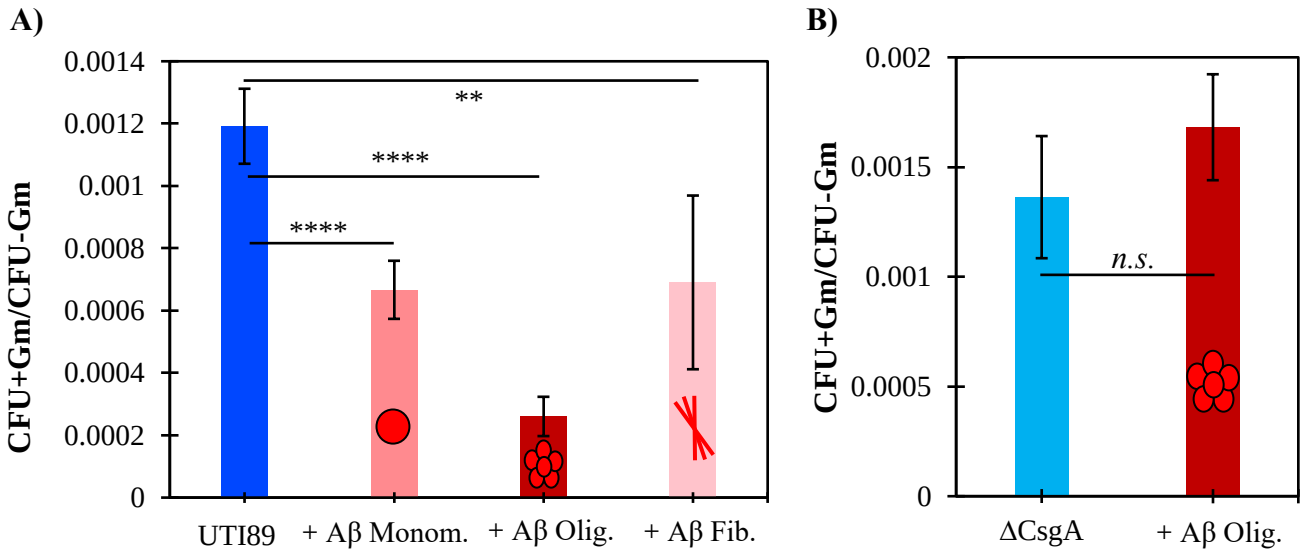


**Figure 4.5. Aβ α-sheet oligomers increase UTI89 susceptibility to gentamicin.** CFU ratios of *E. coli* with gentamicin divided by *E. coli* without gentamicin were calculated for bacteria grown in the presence and absence of 0.5 pg/CFU Aβ and compared. Values are mean ± standard deviation for three replicates. **A)** Aβ oligomers increased UTI89 susceptibility to gentamicin by 79% (*p<0.0001*). Monomeric and fibrillar Aβ increased UTI89 susceptibility to gentamicin by 44% and 42%, respectively (*p<0.0001* for monomeric Aβ and *p=0.004* for fibrillar Aβ). Notably, while each sample is enriched in the respective conformation, it is likely that mixed

populations are present. **B)** Aβ oligomers decreased ΔCsgA susceptibility to gentamicin by 23%, although the difference is not statistically significant.

*4.3.5 CsgA and Aβ α-sheet oligomers interact in vitro*

To further investigate the molecular interactions that govern *E. coli* amyloid and biofilm inhibition by Aβ, *in vitro* aggregation assays were conducted with pure CsgA and Aβ. CsgA inhibited the aggregation of Aβ (excess Aβ 7.5:1) by approximately 43% (*p=0.03*; **Figure 4.6A**). Notably, the ThT fluorescence signal of Aβ began to separate from the coincubation fluorescence signal at the end of the lag phase when α-sheet oligomeric conformers are present (**Figure 4.6A**). Further details for the structural changes observed by Aβ and CsgA during amyloidogenesis are provided in **Chapter 2** and Bleem et al., 2023[16], respectively. Cell toxicity experiments with oligomeric α-sheet Aβ and oligomeric α-sheet CsgA were also conducted to determine whether the oligomeric conformers formed by each amyloidogenic protein could neutralize one another's oligomer-associated toxicity. Aβ oligomers reduced the cell viability of SH-SY5Y human neuroblastoma cells by 28% (*p=0.002)*, and CsgA reduced the cell viability by 77% (*p=0.0004;* **Figure 4.6B**). Co-incubation of Aβ and CsgA oligomers (excess Aβ 7.5:1) led to complete recovery of neuroblastoma cell viability **(Figure 4.6B**).

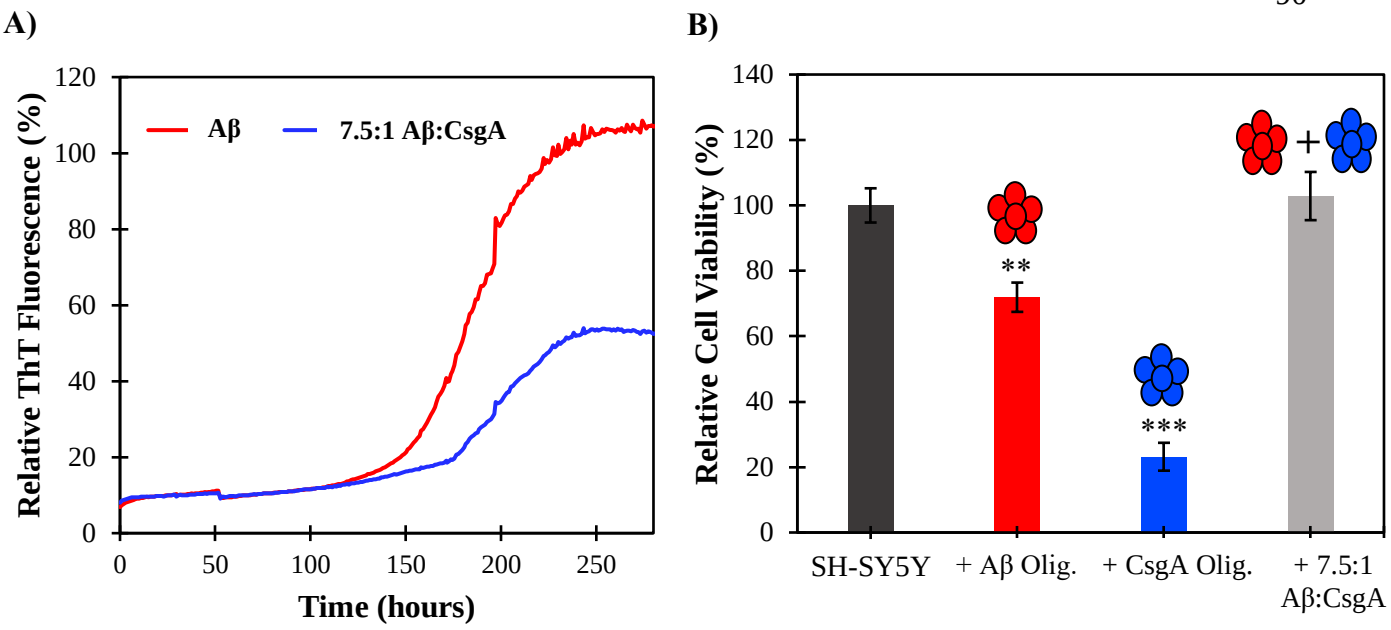


**Figure 4.6. Aβ and CsgA oligomers interact *in vitro*. A)** CsgA inhibited Aβ aggregation 47% (*p=0.03*). Inhibition begins during the late lag phase of aggregation when oligomers are formed. **B)** Aβ and CsgA oligomers reduce SH-SY5Y neuroblastoma cell viability 28% and 77%, respectively (*p=0.002* and *p=0.0004*). Co-administration of Aβ and CsgA oligomers resulted in complete recovery of cell viability (*p=0.64*).

## 4.4 Discussion

### *4.4.1 Aβ α-sheet oligomers promote E. coli biofilm clearance*

The results reported in **Chapter 4** provide mechanistic insights into the role of Aβ in the innate immune response. As shown in **Figure 4.3A** and **Figure 4.4A**, Aβ oligomers significantly inhibited curli biogenesis and weakened biofilm formation but did not promote bacterial cell death. Instead, curli and biofilm inhibition by Aβ oligomers shifted cells from the biofilm to the free-floating planktonic phase. As planktonic cells are more susceptible to clearance by the outside environment (i.e., antibiotics and host immune response), bacterial amyloid inhibition by Aβ likely serves to weaken the pathogen to promote clearance by immune cells. This non-

bactericidal activity corresponds to previous studies indicating that *de novo* α-sheet peptides inhibit amyloid formation and reduce biofilm cell density without promoting bacterial cell death[16]. Additionally, Aβ oligomers had no effect on the relative cell distribution between the planktonic and biofilm phases of the UTI89 ΔCsgA control strain (**Figure 4.4B**), suggesting that UTI89 curli and biofilm inhibition by Aβ oligomers is due to specific interactions between CsgA and Aβ.

The observed increase in gentamicin susceptibility by UTI89 (**Figure 4.5A**) when grown in the presence of toxic Aβ oligomers also support the data reported in **Figure 4.3A** and **Figure 4.4A**, and parallel the results obtained from previous experiments conducted with uropathogenic *E. coli* and *de novo* α-sheet peptides (**Chapter 3** and Bleem et al., 2023[16]). In **Chapter 3**, curli inhibition by *de novo* α-sheet peptides was shown to increase *E. coli* susceptibility to five different antibiotics. In a previous study, the α-sheet peptide inhibitors were also demonstrated to promote macrophage clearance of uropathogenic *E. coli*[16]. Findings reported in **Chapter 4** suggest that curli and biofilm inhibition by Aβ may promote similar macrophage clearance. Notably, curli inhibition and elevated *E. coli* susceptibility to gentamicin was observed by all Aβ samples, with the largest effect attributed to the sample enriched in the toxic, oligomeric α-sheet conformation. Mixed populations are present throughout the early stages of amyloidogenesis prior to the deposition of stable β-sheet fibrils (**Figure 1.1**), and it is likely that toxic Aβ α-sheet oligomers are also present in the "monomeric" and "fibrillar" samples, although to a lesser extent than in the sample obtained during the late lag phase of aggregation. Therefore, the effects observed by the "monomeric" and "fibrillar" Aβ species may be due to the presence of α-sheet oligomers.

Finally, the results reported in **Figure 4.6** provide insight into the molecular mechanisms that may govern the inhibitory properties of Aβ oligomers. ThT data from Aβ and CsgA co-incubation experiments indicate that amyloid inhibition occurs during the late lag phase of aggregation, when Aβ (**Chapter 2**) and CsgA α-sheet oligomers are present[11,16]. Additionally, oligomeric toxicity of both Aβ and CsgA was neutralized when the two amyloidogenic proteins were co-administered to human SH-SY5Y neuroblastoma cells. Therefore, the data reported in **Figure 4.6** suggest that Aβ oligomers inhibit curli and *E. coli* biofilm formation and neutralize CsgA oligomeric toxicity via specific interactions between the toxic α-sheet oligomers of both species.

While the research reported in this chapter focuses on amyloid formed by *E. coli,* it is hypothesized that Aβ α-sheet oligomers may promote immune clearance of many microbial species, including viruses and other amyloid-forming bacteria. A study by Serwer, Hunter, and Wright demonstrated that the viral capsids produced by herpes virus are rich in α-sheet structure, and they hypothesize that the presence of α-sheet structure in the capsids promotes the production of Aβ α-sheet oligomers and subsequent neurodegeneration[188]. Therefore, it is possible that the observed colocalization of Aβ plaques and HSV1 in post mortem AD brain samples reported in multiple studies[73,74,89] may be a result of specific interactions between Aβ α-sheet oligomers and the viral capsids produced by herpes virus that contain α-sheet structure.

### *4.4.2 The brain microbiome and its role in triggering various forms of dementia*

Research suggesting that microbial infection triggers various types of dementia is well documented. Enterovirus has been shown to cause rapidly progressive dementia (RPD)[189], while neuroborreliosis frequently leads to secondary dementia[190]. Other infections such as syphilis and

cysticercosis have been implicated in cases of "reversible dementia" that abate with proper treatment such as intravenous antibiotic treatment[191,192]. But despite overwhelming evidence that microbial infection can be involved in dementia, many researchers resist the idea that microbes are involved in AD disease onset.

It was previously believed that microbes entered the brain only during severe brain infections; however, a growing body of evidence suggests that various bacteria, viruses, and fungi reside even in healthy brains. The electronic tree of life (eToL) developed by Richard Lathe and colleagues uses small subunit ribosomal RNA (rRNA) probes to investigate the diversity of microorganisms in both control and AD brain samples[193,194]. An abundance of bacteria, fungi, and chloroplastida were identified in both control and AD brains, and the brain microbiome was reported to contain approximately ~20% of the diversity of the gut microbiome[193]. Notably, the spectrum of microorganisms found in the brain varied significantly between individuals, and this observed diversity is likely due to variations between environmental exposure and genetic predisposition[193]. Microorganism diversity also varied between brain regions, and there was evidence of pathogens spreading between brain regions in single individuals[193]. Certain microbial species were over-represented in AD brain samples including *Streptococcus*, *Staphylococcus*, *Altenaria*, and *Cortinarius*, suggesting that while many microorganisms may reside safely in the brain, others are more likely to trigger Aβ aggregation and AD pathology[193]. Interestingly, the concentration of brain microbes significantly increased with age[193], which may be due, in part, to $A\beta_{42}$ clearance rate decreasing with age[195], as well as other AD risk factors such as increased blood pressure and cognitive decline that are often associated with aging.

The presence of microorganisms in the brain is further supported by the fact that immunocompromised/suppressed individuals are significantly more prone to central nervous system (CNS) infections[196,197]. The susceptibility of immunocompromised individuals to CNS infections suggests that the immune system regularly defends against microbial pathogens that typically reside the brain but is unable to do so effectively when suppressed. In the case of AD, microorganisms in the brain are further elevated due to breakdown of the blood brain barrier (BBB) due to chronic inflammation from the accumulation of toxic Aβ aggregates[198].

*4.4.3 AD: an infectious disease?*

Although many posit microbial infection as a cause of sporadic AD and not genetic AD, it is possible that pathogens may be involved in familial forms of the disease as well. According to the Genome-wide association studies (GWAS), approximately 2/3 of all AD genes are associated with immunity, microglial function, and neuroinflammation[181]. The apolipoprotein E (*APOE*) ε4 allele is a genetic marker that indicates increased susceptibility to AD, and *APOE* alleles have been shown to influence the immune response to viral, bacterial, and parasitic disease[88]. APOE itself function as an immunomodulatory peptide that represses inflammation[199], presents lipid antigens to the immune system[200,201], and binds to Aβ[202]. It appears that variations in *APOE* lead to differential infection outcomes: while *APOE* ε4 exacerbates human immunodeficiency virus (HIV) infection[203], *APOE* ε3 is protective against the virus; *APOE* ε4 is correlated with severe cases of COVID infection[204,205]; *APOE* ε2/ε3 carriers with AD exhibit a significantly decreased bacterial load than homozygous *APOE* ε4 carriers[76]; *APOE* ε2 may increase susceptibility to malaria infection[206]. Therefore, it is possible that the role of *APOE* ε4 in

promoting risk to AD is due to the modulation of specific types of infections, indicating that both genetic predisposition and microbial infection can cooperatively lead to AD pathology.

The classification of AD as an infectious disease provides insight into potential prevention and therapeutic strategies. There is typically a 10–30-year window in which Aβ aggregates accumulate and trigger the formation of tau tangles prior to the onset of cognitive symptoms[181,207,208]. Proper treatment of microbial infection and the mitigation of chronic inflammation during this time may aid in reducing neuronal death and delaying disease onset, particularly in individuals genetically predisposed to AD. The findings reported in this Chapter suggest that the presence of amyloid-forming microorganisms may trigger upregulation of toxic Aβ oligomers, resulting in initial disease pathology. The data reported here also suggest that Aβ oligomers specifically inhibit curli formation via complementary α-sheet interactions between CsgA and Aβ oligomers, weaken *E. coli* biofilms, and inhibit CsgA oligomeric toxicity, thereby identifying a molecular mechanism through which Aβ functions as an antimicrobial peptide.

## 4.5 Conclusion

Numerous studies have provided evidence for a probable connection between microbial infection and AD and have postulated on the role of Aβ in the innate immune response. However, little is known about the molecular mechanisms that are involved in the aggregation of Aβ as an immune response. The research reported in **Chapter 4** investigate the capacity for Aβ to inhibit *E. coli* biofilm formation by preventing curli biogenesis and suggest that the same oligomeric species that cause neuronal cell death in AD serve a protective function against infection. Therefore, Aβ oligomers may inhibit amyloid formation of several amyloid-forming pathogens, including bacteria, viruses, and fungi, through interactions with α-sheet oligomers.

## 4.6 Materials and Methods

*4.6.1 E. coli Biofilm Growth*

A uropathogenic *E. coli* clinical isolate strain (UTI89[164]) and a control strain with a chromosomal deletion of the CsgA gene (UTI89 ΔCsgA[138]) were used for all biofilm experiments (**Appendix A, Table A.2**). Overnight cultures were grown in Luria Broth (LB, Miller, Thermo Fisher Scientific; Waltham, MA) for 16-18 hours at 37°C with shaking (180 rpm). Cultures were then "refreshed" by replacing 5 mL of culture with 5 mL fresh LB medium and grown for an additional three hours to ensure bacteria were in the exponential phase. Cultures were then spun down and diluted to an optical density ($OD_{600}$) of 0.1 (~$8x10^7$ cells/mL) in YESCA broth supplemented with 4% DMSO (Corning; Glendale, AZ), medium known to promote increased curli formation[165]. Aβ was prepared as described in **Chapter 2.6.1** and **Chapter 2.6.2** and incubated statically at 75 μM and 25°C for 0, 30, or 72 hours to obtain samples enriched in random coil, α-sheet, β-sheet structure, respectively. Diluted bacteria culture (180 μL) was plated with 20 μL Aβ (or NaOH + PBS, in the case of controls) and aliquoted in triplicate into wells of a sterile, clear 48-well polystyrene plate (Corning; Glendale, AZ). The final Aβ concentration was 0 or 7.5 μM (0.5 pg/CFU at the time of plating, assuming $8x10^7$ cells/mL). Plates were covered, sealed in a plastic bag, and statically grown at 26°C for 48 hours. Following biofilm maturation, planktonic cells and medium were removed via gentle pipetting and collected in an Eppendorf tube (Thermo Fisher Scientific; Waltham, MA). The Eppendorf tube containing planktonic cells in medium was centrifuged for 3 minutes at 8,000xg. The supernatant was then removed, and the planktonic cell pellet was resuspended in 200 μL PBS for $OD_{600}$ measurements. The biofilms were rinsed with 250 μL PBS (Sigma Aldrich; St. Louis, MO) using a pipette to gently dispense the PBS along the edge of the well. The rinse was then

removed via gentle pipetting and discarded. Biofilms were homogenized in 200 µL PBS + 20 µM ThT solution (for amyloid quantification and $OD_{600}$ reading) by vigorous pipetting (30x per well). ThT was prepared as discussed in **Chapter 2.6.2**, with exception to the final ThT concentration used for the respective experiments (20 µM in **Chapter 4** and 24 µM in **Chapter 2**). ThT and $OD_{600}$ were measured using a multimode plate reader (PerkinElmer, Waltham, MA). Each pg/CFU calculation assumes $OD_{600}$ = 0.1 corresponds to $8x10^7$ cells/mL, and that $8x10^7$ cells/mL corresponds to the initial concentration of cells seeded into each well of the 48-well plate. The pg/CFU calculations do not account for cell replication during biofilm growth, and therefore the pg/CFU ratio at the time of analysis is likely to be significantly lower.

*4.6.2 Neuroblastoma and uropathogenic E. coli co-incubation*

SH-SY5Y human neuroblastomas (American Type Culture Collection; Manassas, VA) were cultured in 1:1 DMEM:F12 (Invitrogen; Carlsbad, CA) supplemented with 10% FBS (Invitrogen; Carlsbad, CA), 100 units/mL penicillin (Invitrogen; Carlsbad, CA), and 100 µg/mL streptomycin (Invitrogen; Carlsbad, CA). The cells were seeded in a 96-well sterile tissue culture-treated plate (Corning; Glendale, AZ) at $2.4x10^5$ cells per well and cultured in $CO_2$ water-jacketed incubator (37°C, 5% $CO_2$; Thermo Fisher Scientific; Waltham, MA) for 24 hours. Overnight cultures of a clinical isolate of uropathogenic *E. coli* (UTI89) and the deletion strain (UTI89 ΔCsgA) were diluted to $OD_{600}$ = 0.3 in minimal media (YESCA broth with 4% DMSO) to promote biofilm formation as described in **Chapter 4.6.1**. The two bacterial suspensions were diluted 3-fold in 1:1 DMEM:F12 medium (without antibiotics) for a final cell density of $OD_{600}$ = 0.1. A vehicle control condition was prepared with YESCA, DMSO, and DMEM:F12 at the identical ratio. Following 24 hours of cell seeding, the cell media was removed and 100 µL of

each diluted solution (media control, UTI89, or ΔCsgA) were added directly to the surface of the adhered neuroblastomas in triplicate. The samples were grown for 48 hours at 26°C to promote biofilm formation. Cells were monitored daily to ensure that the reduced temperature did not result in neuroblastoma cell death. The supernatant was then removed from each well and individually applied to SOBA for Aβ oligomer quantification.

*4.6.3 Soluble Oligomer Binding Assay*

SOBA was conducted according to a modified protocol previously discussed in Shea et al., 2022[39] with a plate washer incorporated for several of the wash steps. Dopamine HCl (Sigma-Aldrich; St. Louis, MO) was dissolved into Tris Buffer Saline-Tween (TBS-T) (pH 7.4, 50 mM tris, 100 mM NaCl, 0.01% Tween-20) at 10 mg/mL. 150 µL of the dopamine solution was added to each well of an opaque Nunc Immobilizer Amino 96-well plate (Corning; Corning, NY) and shaken at 340 rpm at room temperature for 20-24 hours covered in foil. Following the 20-24 hour incubation, a plate washer was primed with 1 L DI $H_2O$, and the 96-well plate was aspirated and washed with DI $H_2O$ 10x. The plate washer was flushed, and the manifold sonicated for 90 minutes, and the 96-well plate was dried in a 37 °C incubator for 1 hour. α-Sheet peptide (AP510[11,16,39]) was dissolved in dimethyl sulfoxide (Sigma Aldrich; St. Louis, MO) to 36 mM, and diluted to 60 µM in carbonate buffer (pH 9.6, 100 mM $CO_3^{2-}$). The α-sheet peptide solution was incubated in a 37 °C water bath for 1 hour to dimerize. 100 µL of 60 µM AP510 in carbonate buffer was then added to each well of the 96-well plate, and the plate was shaken at 340 rpm at room temperature for 1 hour, or up to 2 hours, to couple the peptide to the 96-well plate. The plate was then aspirated and washed with PBS-T (pH 7.4, 137 mM NaCl, 2.7 mM KCl, 10 mM $Na_2HPO_4$, 1.8 mM $KH_2PO4$, 0.05% Tween-20) 3x. The washer was then

flushed with 1 L DI $H_2O$ and the manifold sonicated for 30 minutes. 150 μL of 10 mM ethanolamine (Sigma Aldrich; St. Louis, MO) in carbonate buffer was added to each well, and the 96-well plate was shaken at 340 rpm at room temperature for 2 hours while covered in foil to quench unreacted sites in each well. The plate was then washed with PBS-T 3x, and the plate washer flushed with 1 L DI $H_2O$ and the manifold sonicated for 30 minutes. 300 μL Pierce Protein-Free Blocking Buffer (Thermo Fisher Scientific; Waltham, MA) was added to each well of the plate and decanted by inverting the plate 3x. Then, 100 μL of each neuroblastoma *E. coli* co-incubation sample was applied to the surface of each well and incubated for 1 hour at 25°C without shaking. The plate washer was then primed with 2 L DI $H_2O$. The 96-well plate was then aspirated and washed with PBS 3x, the plate washer was flushed with 1 L DI $H_2O$, and the manifold sonicated for 30 minutes. 100 μL of 0.03 μg/mL of 6E10 HRP anti-β-Amyloid (BioLegend; San Diego, CA) dissolved in 3% BSA in TBS-T was added to each well, and the plate was shaken at 340 rpm for 1 hour, covered in foil. The plate washer was primed with 1 L DI H2O. Then, the plate was aspirated and washed with PBS 3x, and the plate washer was flushed with 1 L DI $H_2O$ and the manifold sonicated for 1.5 hours. 115 μL of room temperature SuperSignal ELISA Femto 9 Maximum Sensitivity Substrate (Thermo Fisher Scientific; Waltham, MA) was plated per well, and the plate was shaken for 1 minute covered in foil before reading the luminescence in a Tecan plate reader (Mannendorf, Switzerland) with a 0.2 second integration time. Chemiluminescence readings were obtained within 15 minutes for maximum signal.

*4.6.4 Antibiotic Susceptibility*

Biofilms were grown according to the methods described in **Chapter 4.6.1**. Gentamicin sulfate (Thermo Fisher Scientific; Waltham, MA) was dissolved in YESCA at a concentration of 900 µg/mL. 100 µL of antibiotic or control (YESCA media) was added to each well after 42 hours of incubation without disturbing the biofilm for a final well concentration of 300 µg/mL. Following 6 additional hours of biofilm growth (48 hours total), planktonic cells and medium were removed via gentle pipetting along the edge of the well and discarded. The biofilms were rinsed in 250 µL PBS by gently dispensing the PBS along the edge of the well. The rinse was then removed via gentle pipetting along the edge of the well and discarded. Biofilms were homogenized in 200 µL PBS by vigorous pipetting (30x per biofilm), and the biofilm suspensions were transferred to an Eppendorf tube. The biofilm suspensions were then ultra-sonicated for 5 seconds on ice and diluted in tenfold increments. The serial dilutions were then plated on LB agar plates using the drop plate method[167]. Six replicates were plated per condition. Colonies were grown for 16 hours at 37°C and CFUs were counted. Total CFUs of the biofilm suspensions were calculated using the dilution number and the number of CFUs counted in that dilution. CFU+Gm/CFU-Gm ratios were calculated by dividing the values of each of the six CFU+Gm replicates by the average CFU-Gm value and then calculate the average of the ratios.

*4.6.5 CsgA Purification*

A synthetic gene corresponding to the *E. coli* CsgA protein was designed and synthesized by Addgene (Watertown, MA). The gene was cloned into the pET-22b(+) vector, which added a C-terminal 6x His tag for purification. Plasmids were transformed into *E. coli* BL21 (DE3) cells and protein expression was carried out in 2 L shake flasks at 37°C. Cultures grew to an

OD600nm of 0.6-0.8 prior to induction with 1 mM IPTG. After 3-4 hours of additional growth, cells were harvested by centrifugation and resuspended in 30 mL denaturing buffer (8M Gnd-HCl (Thermo Fisher Scientific; Waltham, MA), 50 mM NaPi (Sigma-Aldrich; St. Louis, MO), pH 8.0) and lysed overnight with stirring at 4°C. Insoluble material was removed by centrifugation at 14,000 xg for 30 minutes and 15 mL of supernatant was incubated with 5 mL HisPur Ni-NTA beads (Thermo Fisher; Waltham, MA) for 2 hours at room temperature with end-over-end rotation. The beads were then washed twice with denaturing buffer, twice again with denaturing buffer plus 15 mM imidazole (Sigma-Aldrich; St. Louis, MO), and twice again with denaturing buffer plus 30 mM imidazole. Finally, protein was eluted with denaturing buffer plus 400 mM imidazole. Samples from each step of the purification were precipitated from guanidinium hydrochloride by trichloroacetic acid (Thermo Fisher Scientific; Waltham, MA)[209] and analyzed by SDS-PAGE.

*4.6.6 CsgA and Aβ Aggregation Studies*

CsgA aliquots were desalted immediately prior to use using the Zeba desalting column (7k MWCO) protocol (Thermo Fisher; Waltham, MA) into buffer (50 mM KCl + 50 mM NaPi, pH 7.4), transferred to an Eppendorf LoBind microcentrifuge tube (Sigma-Aldrich; St. Louis, MO), and kept on ice. Protein concentration was determined by NanoDrop 2000 Spectrometer (Thermo Fisher Scientific; Waltham, MA) at 280 nm using an extinction coefficient of 11460 $M^{-1}$ $cm^{-1}$. CsgA was aliquoted into a separate LoBind tube (volume calculated to achieve 10 µM concentration in 185 µL). Stock Aβ was prepared as described in **Chapter 2.6.1** and **Chapter 2.6.2** and slowly added to the side of the CsgA-containing tube (volume calculated to achieve 75 µM concentration in 185 µL). KCl + NaPi buffer supplemented with 24 µM ThT (ThT prepared

as discussed in **Chapter 2.6.2)** was gently added to the side of the tube (volume calculated to achieve final volume of 185 µL). The resulting solution was gently mixed 3x by pipette, and 60 µL was added to a single well in triplicate of a black 384-well plate and read every hour on a multimode plate reader (Tecan; Mannendorf, Switzerland). Relevant parameters include: $\lambda_{ex}$ 438 nm, $\lambda_{em}$ 495 nm, measurement height 7.5 mm, 8 flashes.

*4.6.7 CsgA and Aβ Cellular Toxicity Studies*

Cell viability was determined using a 3-(4,5-dimethylthiazol-2-yl)-2,5-diphenyltetrazolium bromide (MTT) assay[117]. SH-SY5Y human neuroblastomas (American Type Culture Collection; Manassas, VA) were cultured in 1:1 DMEM:F12 (Invitrogen; Carlsbad, CA) supplemented with 10% FBS (Invitrogen; Carlsbad, CA), 100 units/mL penicillin (Invitrogen; Carlsbad, CA), and 100 µg/mL streptomycin (Invitrogen; Carlsbad, CA) as described in **Chapter 2.6.9**. The cells were seeded in a 96-well sterile tissue culture-treated plate (Corning; Glendale, AZ) at $2.4x10^5$ cells per well and cultured in $CO_2$ water-jacketed incubator (37°C, 5% $CO_2$; Thermo Fisher Scientific; Waltham, MA) for 24 hours. CsgA (10 µM) and Aβ (75 µM) were prepared as described in **Chapter 4.6.6** and incubated both separately and together in KCl + NaPi buffer at 25°C until they reached the late lag phase of aggregation (t=150 hours), as informed by **Figure 4.6A**. After 24 hours of cell seeding, the cell culture media was removed and replaced with 100 µL preincubated Aβ, CsgA, or Aβ + CsgA (or NaPi + KCl, in the case of controls) diluted 1:3 in cell media. The cells were cultured with experimental solution for 24 hours at 37°C before addition of 25 µL MTT (5mg/mL in PBS; Sigma-Aldrich), then incubated for 4 hours at 37°C. After 28 hours of incubation, 100 µL lysis buffer (50% DMF, 20% SDS, 1% glacial acetic acid, and 0.2% HCl) was added to each well and incubated overnight at 25°C

covered in foil. The optical density was read at 570nm with a multimode plate reader (Tecan; Mannendorf, Switzerland). Relative cell viability values were determined by first subtracting the MTT + media blank from each signal, and then normalizing the values to the average SH-SY5Y control value.

### *4.6.8 Statistics*

All statistical significance values reported were calculated using a two-tailed T-test. A single asterisk indicates a p-value less than 0.05. Two asterisks indicate a p-value less than 0.01. Three asterisks indicate a p-value less than 0.001. Four asterisks indicate a p-value less than 0.0001.

# Chapter 5. Related and Continuing Work

The elucidation of a molecular mechanism that may govern interactions between bacterial and mammalian amyloid proteins in the context of Alzheimer's disease (**Chapter 4**) provides a framework through which to investigate the implications of infection on other mammalian diseases. Microbial pathogens have been implicated in several diseases, and recent studies suggest a possible connection between infection and type 2 diabetes (T2D)[210]. Importantly, diabetes onset typically occurs during or after acute infection[210]. Further, *Helicobacter pylori* infection is observed in many T2D patients[211–213], diabetes is more prevalent among patients infected with *B. burgdorferi*, and T2D patients have significantly more severe periodontitis than controls[214], an infection that is predominantly caused by Gram-negative bacteria[215].

As discussed in **Chapter 2**, IAPP is heavily implicated in T2D, and α-sheet oligomers are primarily responsible for pancreatic islet β-cell death. Preliminary studies conducted with IAPP and *E. coli* suggest that IAPP α-sheet oligomers significantly inhibit UTI89 curli biogenesis via a dose dependent mechanism (**Figure 5.1**). IAPP (0.7 pg/CFU) was shown to inhibit curli biogenesis by approximately 43% and these results parallel the inhibitory effects observed between Aβ and *E. coli* in **Chapter 4** (**Figure 4.3**). The results reported in **Figure 5.1** suggest a possible conserved inhibitory mechanism that mediates inhibition of *E. coli* amyloidogenesis by the oligomeric conformers of mammalian amyloid peptides.

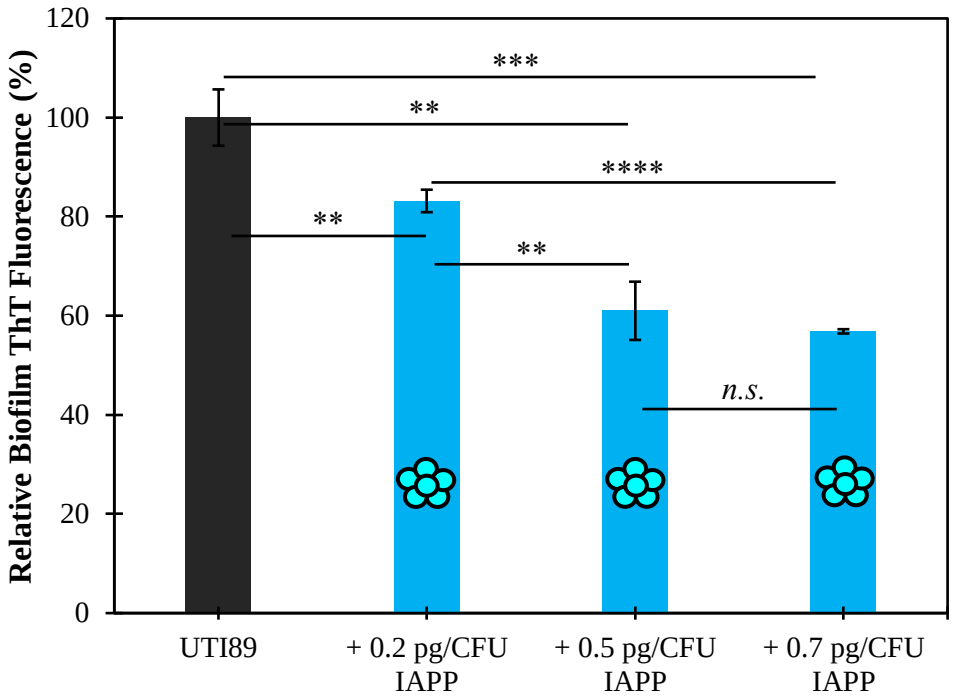


**Figure 5.1 IAPP oligomers have a dose dependent effect on UTI89 curli inhibition.** IAPP α-sheet oligomers (0.2 pg/CFU) inhibited UTI89 amyloid fibrilization by 17% (*p=0.009*) as measured by ThT. Oligomeric IAPP (0.5 pg/CFU) reduced fibrilization by 39% (*p=0.001*). IAPP oligomers (0.7 pg/CFU) inhibited aggregation 43% (*p=0.0002*). Values are mean ± standard deviation for three replicates.

Further, *in vitro* aggregation studies with pure CsgA and IAPP indicated that CsgA inhibits IAPP fibrilization by 86% (**Figure 5.2**). As was observed with CsgA and Aβ (**Figure 4.6A**), the ThT fluorescence signal of IAPP began to separate from the coincubation fluorescence signal at the end of the lag phase when α-sheet oligomeric conformers are present (**Figure 5.2**). These data suggest that IAPP and CsgA oligomers specifically interact via the shared α-sheet conformation, and this molecular mechanism likely mediates the inhibition of curli biogenesis by IAPP that was observed in *E. coli* biofilm studies (**Figure 5.1**).

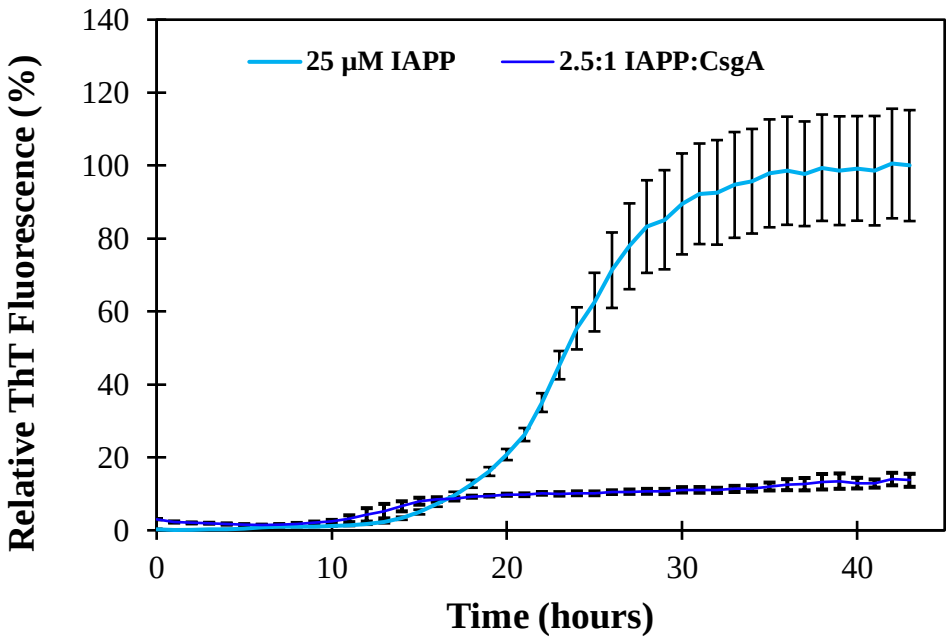


**Figure 5.2. IAPP and CsgA oligomers interact *in vitro*.** CsgA inhibited IAPP aggregation 86% as measured by ThT (*p=0.0006*). Inhibition begins during the late lag phase of aggregation when oligomers are formed. Values are mean ± standard deviation for three replicates.

The preliminary findings discussed in this Chapter indicate that the oligomeric conformers of IAPP inhibit curli biogenesis via specific α-sheet interactions with CsgA oligomers, paralleling the effects observed with Aβ in **Chapter 4**. These data suggest that mammalian amyloidogenesis may serve a protective role in targeting functional amyloid formation by bacteria and other organisms that also form amyloid, such as viruses and fungi. The identification of a conserved mechanism of functional amyloid inhibition by Aβ and IAPP posits a possible evolutionary role for amyloid formation in mammalian species, a process which is typically considered to be inherently pathological. With knowledge of a conserved inhibitory mechanism of functional amyloid inhibition by the α-sheet oligomeric conformers of mammalian amyloid peptides, future studies should be conducted to explore the interactions between other

functional and mammalian amyloid proteins in the context of human disease to further investigate a possible evolutionary role for mammalian amyloidogenesis.

# References


1. Aliyan, A., Cook, N. P. & Martí, A. A. Interrogating Amyloid Aggregates using Fluorescent Probes. *Chem Rev* **119**, 11819–11856 (2019).
2. Prosswimmer, T. & Daggett, V. The role of α-sheet structure in amyloidogenesis: characterization and implications. *Open Biology* vol. 12 Preprint at https://doi.org/10.1098/rsob.220261 (2022).
3. DePas, W. H. & Chapman, M. R. Microbial manipulation of the amyloid fold. *Res Microbiol* **163**, 592–606 (2012).
4. Bleem, A. & Daggett, V. Structural and functional diversity among amyloid proteins: Agents of disease, building blocks of biology, and implications for molecular engineering. *Biotechnol Bioeng* **114**, 7–20 (2017).
5. Knowles, T. P. J., Vendruscolo, M. & Dobson, C. M. The amyloid state and its association with protein misfolding diseases. *Nature Reviews Molecular Cell Biology* vol. 15 384–396 Preprint at https://doi.org/10.1038/nrm3810 (2014).
6. Chiti, F. & Dobson, C. M. Protein Misfolding, Amyloid Formation, and Human Disease: A Summary of Progress Over the Last Decade. *Annu Rev Biochem* **86**, 27–68 (2017).
7. Chuang, E., Hori, A. M., Hesketh, C. D. & Shorter, J. Amyloid assembly and disassembly. *J Cell Sci* **131**, (2018).
8. Ahmed, M. *et al.* Structural conversion of neurotoxic amyloid-beta(1-42) oligomers to fibrils. *Nat Struct Mol Biol* **17**, 561–7 (2010).
9. Haass, C. & Selkoe, D. J. Soluble protein oligomers in neurodegeneration: lessons from the Alzheimer's amyloid beta-peptide. *Nat Rev Mol Cell Biol* **8**, 101–12 (2007).
10. Yang, T., Li, S., Xu, H., Walsh, D. M. & Selkoe, D. J. Large Soluble Oligomers of Amyloid β-Protein from Alzheimer Brain Are Far Less Neuroactive Than the Smaller Oligomers to Which They Dissociate. *The Journal of Neuroscience* **37**, 152–163 (2017).
11. Shea, D. *et al.* α-Sheet secondary structure in amyloid β-peptide drives aggregation and toxicity in Alzheimer's disease. *Proc Natl Acad Sci U S A* **116**, 8895–8900 (2019).
12. Bleem, A., Francisco, R., Bryers, J. D. & Daggett, V. Designed α-sheet peptides suppress amyloid formation in Staphylococcus aureus biofilms. *NPJ Biofilms Microbiomes* **3**, (2017).
13. Hopping, G. *et al.* Designed α-sheet peptides inhibit amyloid formation by targeting toxic oligomers. *Elife* **3**, e01681 (2014).
14. Paranjapye, N. & Daggett, V. De Novo Designed α-Sheet Peptides Inhibit Functional Amyloid Formation of Streptococcus mutans Biofilms. *J Mol Biol* **430**, 3764–3773 (2018).
15. Kellock, J., Hopping, G., Caughey, B. & Daggett, V. Peptides Composed of Alternating L- and D-Amino Acids Inhibit Amyloidogenesis in Three Distinct Amyloid Systems Independent of Sequence. *J Mol Biol* **428**, 2317–2328 (2016).
16. Bleem, A. *et al.* Designed α-sheet peptides disrupt uropathogenic E. coli biofilms rendering bacteria susceptible to antibiotics and immune cells. *Sci Rep* **13**, 9272 (2023).
17. Cohen, S. I. A. *et al.* Proliferation of amyloid-β42 aggregates occurs through a secondary nucleation mechanism. *Proceedings of the National Academy of Sciences* **110**, 9758–9763 (2013).
18. Chiti, F. & Dobson, C. M. Protein misfolding, functional amyloid, and human disease. *Annu Rev Biochem* **75**, 333–66 (2006).

19. Jarrett, J. T. & Lansbury, P. T. Seeding “one-dimensional crystallization” of amyloid: A pathogenic mechanism in Alzheimer’s disease and scrapie? *Cell* **73**, 1055–1058 (1993).
20. Hardy, J. & Selkoe, D. J. The Amyloid Hypothesis of Alzheimer’s Disease: Progress and Problems on the Road to Therapeutics. *Science (1979)* **297**, 353–356 (2002).
21. Tomic, J. L., Pensalfini, A., Head, E. & Glabe, C. G. Soluble fibrillar oligomer levels are elevated in Alzheimer’s disease brain and correlate with cognitive dysfunction. *Neurobiol Dis* **35**, 352–358 (2009).
22. Glabe, C. G. & Kayed, R. Common structure and toxic function of amyloid oligomers implies a common mechanism of pathogenesis. *Neurology* **66**, S74-8 (2006).
23. McLean, C. A. *et al.* Soluble pool of Aβ amyloid as a determinant of severity of neurodegeneration in Alzheimer’s disease. *Ann Neurol* **46**, 860–866 (1999).
24. Janson, J., Ashley, R. H., Harrison, D., McIntyre, S. & Butler, P. C. The mechanism of islet amyloid polypeptide toxicity is membrane disruption by intermediate-sized toxic amyloid particles. *Diabetes* **48**, 491–498 (1999).
25. Salahuddin, P. *et al.* The role of amyloids in Alzheimer’s and Parkinson’s diseases. *Int J Biol Macromol* **190**, 44–55 (2021).
26. Akter, R. *et al.* Islet Amyloid Polypeptide: Structure, Function, and Pathophysiology. *J Diabetes Res* **2016**, 1–18 (2016).
27. Lin, C.-Y. *et al.* Toxic Human Islet Amyloid Polypeptide (h-IAPP) Oligomers Are Intracellular, and Vaccination to Induce Anti-Toxic Oligomer Antibodies Does Not Prevent h-IAPP–Induced β-Cell Apoptosis in h-IAPP Transgenic Mice. *Diabetes* **56**, 1324–1332 (2007).
28. Gurlo, T. *et al.* Evidence for Proteotoxicity in β Cells in Type 2 Diabetes. *Am J Pathol* **176**, 861–869 (2010).
29. Saghir, A. El, Farrugia, G. & Vassallo, N. The human islet amyloid polypeptide in protein misfolding disorders: Mechanisms of aggregation and interaction with biomembranes. *Chem Phys Lipids* **234**, 105010 (2021).
30. Haataja, L., Gurlo, T., Huang, C. J. & Butler, P. C. Islet Amyloid in Type 2 Diabetes, and the Toxic Oligomer Hypothesis. *Endocr Rev* **29**, 303–316 (2008).
31. Donlan, R. M. Biofilms: Microbial Life on Surfaces. *Emerg Infect Dis* **8**, (2002).
32. Guo, Y., Song, G., Sun, M., Wang, J. & Wang, Y. Prevalence and Therapies of Antibiotic-Resistance in Staphylococcus aureus. *Frontiers in Cellular and Infection Microbiology* vol. 10 Preprint at https://doi.org/10.3389/fcimb.2020.00107 (2020).
33. Fisher, R. A., Gollan, B. & Helaine, S. Persistent bacterial infections and persister cells. *Nature Reviews Microbiology* vol. 15 453–464 Preprint at https://doi.org/10.1038/nrmicro.2017.42 (2017).
34. Lewis, K. *Multidrug Tolerance of Biofilms and Persister Cells*.
35. Banin, E., Brady, K. M. & Greenberg, E. P. Chelator-induced dispersal and killing of Pseudomonas aeruginosa cells in a biofilm. *Appl Environ Microbiol* **72**, 2064–9 (2006).
36. Hooton, T. M. *et al.* Diagnosis, Prevention, and Treatment of Catheter-Associated Urinary Tract Infection in Adults: 2009 International Clinical Practice Guidelines from the Infectious Diseases Society of America. *Clinical Infectious Diseases* **50**, 625–663 (2010).
37. Maury, C. P. J. The emerging concept of functional amyloid. *J Intern Med* **265**, 329–334 (2009).
38. Childers, M. C. & Daggett, V. Drivers of α-Sheet Formation in Transthyretin under Amyloidogenic Conditions. *Biochemistry* **58**, 4408–4423 (2019).

39. Shea, D. *et al.* SOBA: Development and testing of a soluble oligomer binding assay for detection of amyloidogenic toxic oligomers. *Proceedings of the National Academy of Sciences* **119**, (2022).
40. Maris, N. L., Shea, D., Bleem, A., Bryers, J. D. & Daggett, V. Chemical and Physical Variability in Structural Isomers of an l/d α-Sheet Peptide Designed To Inhibit Amyloidogenesis. *Biochemistry* **57**, 507–510 (2018).
41. Armen, R. S., DeMarco, M. L., Alonso, D. O. V. & Daggett, V. Pauling and Corey's α-pleated sheet structure may define the prefibrillar amyloidogenic intermediate in amyloid disease. *Proceedings of the National Academy of Sciences* **101**, 11622–11627 (2004).
42. Armen, R. S., Alonso, D. O. V. & Daggett, V. Anatomy of an Amyloidogenic Intermediate. *Structure* **12**, 1847–1863 (2004).
43. Childers, M. C. & Daggett, V. Edge Strand Dissociation and Conformational Changes in Transthyretin under Amyloidogenic Conditions. *Biophys J* **119**, 1995–2009 (2020).
44. Steward, R. E., Armen, R. S. & Daggett, V. Different disease-causing mutations in transthyretin trigger the same conformational conversion. *Protein Engineering Design and Selection* **21**, 187–195 (2008).
45. Alonso, D. O. V., DeArmond, S. J., Cohen, F. E. & Daggett, V. Mapping the early steps in the pH-induced conformational conversion of the prion protein. *Proceedings of the National Academy of Sciences* **98**, 2985–2989 (2001).
46. Cheng, C. & Daggett, V. Molecular Dynamics Simulations Capture the Misfolding of the Bovine Prion Protein at Acidic pH. *Biomolecules* **4**, 181–201 (2014).
47. Alonso, D. O. V., An, C. & Daggett, V. Simulations of biomolecules: characterization of the early steps in the pH-induced conformational conversion of the hamster, bovine and human forms of the prion protein. *Philosophical Transactions of the Royal Society of London. Series A: Mathematical, Physical and Engineering Sciences* **360**, 1165–1178 (2002).
48. van der Kamp, M. W. & Daggett, V. Influence of pH on the Human Prion Protein: Insights into the Early Steps of Misfolding. *Biophys J* **99**, 2289–2298 (2010).
49. DeMarco, M. L. & Daggett, V. Characterization of cell-surface prion protein relative to its recombinant analogue: insights from molecular dynamics simulations of diglycosylated, membrane-bound human prion protein. *J Neurochem* **109**, 60–73 (2009).
50. DeMarco, M. L. & Daggett, V. Molecular Mechanism for Low pH Triggered Misfolding of the Human Prion Protein. *Biochemistry* **46**, 3045–3054 (2007).
51. Armen, R. S., Bernard, B. M., Day, R., Alonso, D. O. V. & Daggett, V. Characterization of a possible amyloidogenic precursor in glutamine-repeat neurodegenerative diseases. *Proceedings of the National Academy of Sciences* **102**, 13433–13438 (2005).
52. Schmidlin, T., Ploeger, K., Jonsson, A. L. & Daggett, V. Early steps in thermal unfolding of superoxide dismutase 1 are similar to the conformational changes associated with the ALS-associated A4V mutation. *Protein Engineering Design and Selection* **26**, 503–513 (2013).
53. Schmidlin, T., Kennedy, B. K. & Daggett, V. Structural Changes to Monomeric CuZn Superoxide Dismutase Caused by the Familial Amyotrophic Lateral Sclerosis-Associated Mutation A4V. *Biophys J* **97**, 1709–1718 (2009).
54. Milner-White, J. E., Watson, J. D., Qi, G. & Hayward, S. Amyloid Formation May Involve α- to β Sheet Interconversion via Peptide Plane Flipping. *Structure* **14**, 1369–1376 (2006).

55. Balupuri, A., Choi, K.-E. & Kang, N. S. Aggregation Mechanism of Alzheimer's Amyloid β-Peptide Mediated by α-Strand/α-Sheet Structure. *Int J Mol Sci* **21**, 1094 (2020).
56. Daggett, V. Alpha-sheet: The toxic conformer in amyloid diseases? *Acc Chem Res* **39**, 594–602 (2006).
57. Hayward, S. & Milner-White, E. J. The geometry of α-sheet: Implications for its possible function as amyloid precursor in proteins. *Proteins: Structure, Function, and Bioinformatics* **71**, 415–425 (2008).
58. DeMarco, M. L. & Daggett, V. From conversion to aggregation: Protofibril formation of the prion protein. *Proceedings of the National Academy of Sciences* **101**, 2293–2298 (2004).
59. Di Blasio, B. *et al.* A crystal structure with features of an antiparallel β-pleated sheet. *Biopolymers* **34**, 1463–1468 (1994).
60. Balupuri, A., Choi, K.-E. & Kang, N. S. Computational insights into the role of α-strand/sheet in aggregation of α-synuclein. *Sci Rep* **9**, 59 (2019).
61. Bi, T. M. & Daggett, V. The Role of α-sheet in Amyloid Oligomer Aggregation and Toxicity. *Yale J Biol Med* **91**, 247–255 (2018).
62. Beck, D. A. C., Alonso, D. O. V, Inoyama, D. & Daggett, V. The intrinsic conformational propensities of the 20 naturally occurring amino acids and reflection of these propensities in proteins. *Proc Natl Acad Sci U S A* **105**, 12259–64 (2008).
63. van der Kamp, M. W. *et al.* Dynameomics: a comprehensive database of protein dynamics. *Structure* **18**, 423–35 (2010).
64. Beck, D. A. C. *et al.* Dynameomics: mass annotation of protein dynamics and unfolding in water by high-throughput atomistic molecular dynamics simulations. *Protein Engineering Design and Selection* **21**, 353–368 (2008).
65. Childers, M. C., Towse, C.-L. & Daggett, V. Molecular dynamics-derived rotamer libraries for D-amino acids within homochiral and heterochiral polypeptides. *Protein Engineering, Design and Selection* **31**, 191–204 (2018).
66. Towse, C.-L., Rysavy, S. J., Vulovic, I. M. & Daggett, V. New Dynamic Rotamer Libraries: Data-Driven Analysis of Side-Chain Conformational Propensities. *Structure* **24**, 187–199 (2016).
67. Towse, C.-L., Hopping, G., Vulovic, I. & Daggett, V. Nature versus design: the conformational propensities of d-amino acids and the importance of side chain chirality. *Protein Engineering, Design and Selection* **27**, 447–455 (2014).
68. Childers, M. C., Towse, C.-L. & Daggett, V. The effect of chirality and steric hindrance on intrinsic backbone conformational propensities: tools for protein design. *Protein Engineering Design and Selection* **29**, 271–280 (2016).
69. Andrews, S. S. & Tretton, J. Physical Principles of Circular Dichroism. *J Chem Educ* **97**, 4370–4376 (2020).
70. Alzheimer's Association. 2016 Alzheimer's disease facts and figures. *Alzheimer's & Dementia* **12**, 459–509 (2016).
71. Wang, J., Dickson, D. W., Trojanowski, J. Q. & Lee, V. M.-Y. The Levels of Soluble versus Insoluble Brain Aβ Distinguish Alzheimer's Disease from Normal and Pathologic Aging. *Exp Neurol* **158**, 328–337 (1999).
72. Kelley, B. J. & Petersen, R. C. Alzheimer's disease and mild cognitive impairment. *Neurol Clin* **25**, 577–609, v (2007).

73. Itzhaki, R. F. *et al.* Herpes simplex virus type 1 in brain and risk of Alzheimer's disease. *The Lancet* **349**, 241–244 (1997).
74. Wozniak, M., Mee, A. & Itzhaki, R. Herpes simplex virus type 1 DNA is located within Alzheimer's disease amyloid plaques. *J Pathol* **217**, 131–138 (2009).
75. Harris, S. A. & Harris, E. A. Herpes Simplex Virus Type 1 and Other Pathogens are Key Causative Factors in Sporadic Alzheimer's Disease. *Journal of Alzheimer's Disease* **48**, 319–353 (2015).
76. Gérard, H. C. *et al.* The load of Chlamydia pneumoniae in the Alzheimer's brain varies with APOE genotype. *Microb Pathog* **39**, 19–26 (2005).
77. Grammas, P. Neurovascular dysfunction, inflammation and endothelial activation: Implications for the pathogenesis of Alzheimer's disease. *J Neuroinflammation* **8**, 26 (2011).
78. Mrak, R. E., Sheng, J. G. & Griffin, W. S. T. Glial cytokines in Alzheimer's disease: Review and pathogenic implications. *Hum Pathol* **26**, 816–823 (1995).
79. Allen, H. B. Alzheimer's Disease: Assessing the Role of Spirochetes, Biofilms, the Immune System, and Amyloid-β with Regard to Potential Treatment and Prevention. *Journal of Alzheimer's Disease* **53**, 1271–1276 (2016).
80. Itzhaki, R. F. *et al.* Microbes and Alzheimer's Disease. *Journal of Alzheimer's Disease* **51**, 979–984 (2016).
81. Allen, H. B. A Novel Approach to the Treatment and Prevention of Alzheimer's Disease Based on the Pathology and Microbiology. *Journal of Alzheimer's Disease* **84**, 61–67 (2021).
82. Zhan, X. *et al.* Gram-negative bacterial molecules associate with Alzheimer disease pathology. *Neurology* **87**, 2324–2332 (2016).
83. Dominy, S. S. *et al.* Porphyromonas gingivalis in Alzheimer's disease brains: Evidence for disease causation and treatment with small-molecule inhibitors. *Sci Adv* **5**, (2019).
84. Miklossy, J. Alzheimer's disease - a neurospirochetosis. Analysis of the evidence following Koch's and Hill's criteria. *J Neuroinflammation* **8**, 90 (2011).
85. Balin, B. J. *et al.* Identification and localization of Chlamydia pneumoniae in the Alzheimer's brain. *Med Microbiol Immunol* **187**, 23–42 (1998).
86. Soscia, S. J. *et al.* The Alzheimer's Disease-Associated Amyloid β-Protein Is an Antimicrobial Peptide. *PLoS One* **5**, e9505 (2010).
87. Kumar, D. K. V. *et al.* Amyloid-β peptide protects against microbial infection in mouse and worm models of Alzheimer's disease. *Sci Transl Med* **8**, (2016).
88. Lathe, R. *et al.* Establishment of a consensus protocol to explore the brain pathobiome in patients with mild cognitive impairment and Alzheimer's disease. *Alzheimer's & Dementia* (2023) doi:10.1002/alz.13076.
89. Eimer, W. A. *et al.* Alzheimer's Disease-Associated β-Amyloid Is Rapidly Seeded by Herpesviridae to Protect against Brain Infection. *Neuron* **99**, 56-63.e3 (2018).
90. Jain, N. *et al.* Inhibition of curli assembly and Escherichia coli biofilm formation by the human systemic amyloid precursor transthyretin. *Proceedings of the National Academy of Sciences* **114**, 12184–12189 (2017).
91. Jain, A. & Zahra, F. *Transthyretin Amyloid Cardiomyopathy (ATTR-CM)*. (2023).
92. Yang, T., Li, S., Xu, H., Walsh, D. M. & Selkoe, D. J. Large Soluble Oligomers of Amyloid β-Protein from Alzheimer Brain Are Far Less Neuroactive Than the Smaller Oligomers to Which They Dissociate. *The Journal of Neuroscience* **37**, 152–163 (2017).

93. Haass, C. & Selkoe, D. J. Soluble protein oligomers in neurodegeneration: lessons from the Alzheimer's amyloid beta-peptide. *Nat Rev Mol Cell Biol* **8**, 101–12 (2007).
94. McLean, C. A. *et al.* Soluble pool of Aβ amyloid as a determinant of severity of neurodegeneration in Alzheimer's disease. *Ann Neurol* **46**, 860–866 (1999).
95. CDC. *National Diabetes Statistics Report 2020. Estimates of diabetes and its burden in the United States.* (2020).
96. Li, S., Wang, J., Zhang, B., Li, X. & Liu, Y. Diabetes Mellitus and Cause-Specific Mortality: A Population-Based Study. *Diabetes Metab J* **43**, 319 (2019).
97. Hull, R. L., Westermark, G. T., Westermark, P. & Kahn, S. E. Islet Amyloid: A Critical Entity in the Pathogenesis of Type 2 Diabetes. *J Clin Endocrinol Metab* **89**, 3629–3643 (2004).
98. Kahn, S. E. *et al.* Evidence of Cosecretion of Islet Amyloid Polypeptide and Insulin by β-Cells. *Diabetes* **39**, 634–638 (1990).
99. Betsholtz, C. *et al.* Sequence divergence in a specific region of islet amyloid polypeptide (IAPP) explains differences in islet amyloid formation between species. *FEBS Lett* **251**, 261–264 (1989).
100. Cao, P., Meng, F., Abedini, A. & Raleigh, D. P. The Ability of Rodent Islet Amyloid Polypeptide To Inhibit Amyloid Formation by Human Islet Amyloid Polypeptide Has Important Implications for the Mechanism of Amyloid Formation and the Design of Inhibitors. *Biochemistry* **49**, 872–881 (2010).
101. Cooper, G. J. *et al.* Purification and characterization of a peptide from amyloid-rich pancreases of type 2 diabetic patients. *Proceedings of the National Academy of Sciences* **84**, 8628–8632 (1987).
102. Zraika, S. *et al.* Toxic oligomers and islet beta cell death: guilty by association or convicted by circumstantial evidence? *Diabetologia* **53**, 1046–1056 (2010).
103. Butler, A. E., Janson, J., Soeller, W. C. & Butler, P. C. Increased β-Cell Apoptosis Prevents Adaptive Increase in β-Cell Mass in Mouse Model of Type 2 Diabetes. *Diabetes* **52**, 2304–2314 (2003).
104. Shigihara, N. *et al.* Human IAPP–induced pancreatic β cell toxicity and its regulation by autophagy. *Journal of Clinical Investigation* **124**, 3634–3644 (2014).
105. Ritzel, R. A., Meier, J. J., Lin, C.-Y., Veldhuis, J. D. & Butler, P. C. Human Islet Amyloid Polypeptide Oligomers Disrupt Cell Coupling, Induce Apoptosis, and Impair Insulin Secretion in Isolated Human Islets. *Diabetes* **56**, 65–71 (2007).
106. Meier, J. J. *et al.* Inhibition of human IAPP fibril formation does not prevent β-cell death: evidence for distinct actions of oligomers and fibrils of human IAPP. *American Journal of Physiology-Endocrinology and Metabolism* **291**, E1317–E1324 (2006).
107. Westermark, P. *et al.* Amyloid fibrils in human insulinoma and islets of Langerhans of the diabetic cat are derived from a neuropeptide-like protein also present in normal islet cells. *Proceedings of the National Academy of Sciences* **84**, 3881–3885 (1987).
108. Tomic, J. L., Pensalfini, A., Head, E. & Glabe, C. G. Soluble fibrillar oligomer levels are elevated in Alzheimer's disease brain and correlate with cognitive dysfunction. *Neurobiol Dis* **35**, 352–8 (2009).
109. Xue, W. F. *et al.* Fibril fragmentation enhances amyloid cytotoxicity. *Journal of Biological Chemistry* **284**, 34272–34282 (2009).
110. Kayed, R. & Glabe, C. G. Conformation-Dependent Anti-Amyloid Oligomer Antibodies. in 326–344 (2006). doi:10.1016/S0076-6879(06)13017-7.

111. Kayed, R. *et al.* Common Structure of Soluble Amyloid Oligomers Implies Common Mechanism of Pathogenesis. *Science (1979)* **300**, 486–489 (2003).
112. Kazmirski, S. L. & Daggett, V. Non-native interactions in protein folding intermediates: molecular dynamics simulations of hen lysozyme. *J Mol Biol* **284**, 793–806 (1998).
113. Armen, R. S. & Daggett, V. Characterization of Two Distinct β2-Microglobulin Unfolding Intermediates that May Lead to Amyloid Fibrils of Different Morphology. *Biochemistry* **44**, 16098–16107 (2005).
114. van der Kamp, M. W. & Daggett, V. Pathogenic Mutations in the Hydrophobic Core of the Human Prion Protein Can Promote Structural Instability and Misfolding. *J Mol Biol* **404**, 732–748 (2010).
115. DeMarco, M. L., Silveira, J., Caughey, B. & Daggett, V. Structural Properties of Prion Protein Protofibrils and Fibrils: An Experimental Assessment of Atomic Models. *Biochemistry* **45**, 15573–15582 (2006).
116. Biancalana, M. & Koide, S. Molecular mechanism of Thioflavin-T binding to amyloid fibrils. *Biochimica et Biophysica Acta (BBA) - Proteins and Proteomics* **1804**, 1405–1412 (2010).
117. Kumar, P., Nagarajan, A. & Uchil, P. D. Analysis of Cell Viability by the MTT Assay. *Cold Spring Harb Protoc* **2018**, pdb.prot095505 (2018).
118. Abedini, A. *et al.* Time-resolved studies define the nature of toxic IAPP intermediates, providing insight for anti-amyloidosis therapeutics. *Elife* **5**, (2016).
119. Tam, J. P., Wu, C. R., Liu, W. & Zhang, J. W. Disulfide bond formation in peptides by dimethyl sulfoxide. Scope and applications. *J Am Chem Soc* **113**, 6657–6662 (1991).
120. Kot, B. Antibiotic Resistance among Uropathogenic Escherichia coli. *Polish Journal of Microbiology* vol. 68 403–415 Preprint at https://doi.org/10.33073/PJM-2019-048 (2019).
121. Evans, M. L. & Chapman, M. R. Curli biogenesis: Order out of disorder. *Biochim Biophys Acta Mol Cell Res* **1843**, 1551–1558 (2014).
122. Schwartz, K., Syed, A. K., Stephenson, R. E., Rickard, A. H. & Boles, B. R. Functional amyloids composed of phenol soluble modulins stabilize Staphylococcus aureus biofilms. *PLoS Pathog* **8**, (2012).
123. Khan, H. A., Baig, F. K. & Mehboob, R. Nosocomial infections: Epidemiology, prevention, control and surveillance. *Asian Pacific Journal of Tropical Biomedicine* vol. 7 478–482 Preprint at https://doi.org/10.1016/j.apjtb.2017.01.019 (2017).
124. Weiner, L. M. *et al. Morbidity and Mortality Weekly Report Vital Signs: Preventing Antibiotic-Resistant Infections in Hospitals-United States, 2014*. http://www.cdc.gov/hai/surveillance/nhsn_nationalreports.html.
125. Weiner, L. M. *et al.* Antimicrobial-Resistant Pathogens Associated with Healthcare-Associated Infections: Summary of Data Reported to the National Healthcare Safety Network at the Centers for Disease Control and Prevention, 2011-2014. *Infect Control Hosp Epidemiol* **37**, 1288–1301 (2016).
126. CDC. *Antibiotic resistance threats in the United States, 2019*. https://stacks.cdc.gov/view/cdc/82532 (2019) doi:10.15620/cdc:82532.
127. Munita, J. M. & Arias, C. A. Mechanisms of Antibiotic Resistance. *Microbiol Spectr* **4**, (2016).
128. Lewis, K. Multidrug Tolerance of Biofilms and Persister Cells. *Bacterial biofilms* 107–131 (2008) doi:10.1007/978-3-540-75418-3_6.

129. Al-Talib, H., Yean, C., Al-Jashamy, K. & Hasan, H. Methicillin-resistant Staphylococcus aureus nosocomial infection trends in Hospital Universiti Sains Malaysia during 2002-2007. *Ann Saudi Med* **30**, (2010).
130. Yu, S. *et al.* PslG, a self-produced glycosyl hydrolase, triggers biofilm disassembly by disrupting exopolysaccharide matrix. *Cell Res* **25**, 1352–1367 (2015).
131. Devlin, H., Fulaz, S., Hiebner, D. W., O'Gara, J. P. & Casey, E. Enzyme-Functionalized Mesoporous Silica Nanoparticles to Target Staphylococcus aureus and Disperse Biofilms. *Int J Nanomedicine* **Volume 16**, 1929–1942 (2021).
132. Okshevsky, M., Regina, V. R. & Meyer, R. L. Extracellular DNA as a target for biofilm control. *Curr Opin Biotechnol* **33**, 73–80 (2015).
133. Gao, L. *et al.* Nanocatalysts promote Streptococcus mutans biofilm matrix degradation and enhance bacterial killing to suppress dental caries in vivo. *Biomaterials* **101**, 272–284 (2016).
134. Wang, Y. *et al.* Anti-Biofilm Activity of Graphene Quantum Dots via Self-Assembly with Bacterial Amyloid Proteins. *ACS Nano* **13**, 4278–4289 (2019).
135. Powell, L. C. *et al.* Targeted disruption of the extracellular polymeric network of Pseudomonas aeruginosa biofilms by alginate oligosaccharides. *NPJ Biofilms Microbiomes* **4**, 13 (2018).
136. Zaman, M. & Andreasen, M. Cross-talk between individual phenol- soluble modulins in staphylococcus aureus biofilm enables rapid and efficient amyloid formation. *Elife* **9**, 1–17 (2020).
137. Schwartz, K., Syed, A. K., Stephenson, R. E., Rickard, A. H. & Boles, B. R. Functional amyloids composed of phenol soluble modulins stabilize Staphylococcus aureus biofilms. *PLoS Pathog* **8**, (2012).
138. Cegelski, L. *et al.* Small-molecule inhibitors target Escherichia coli amyloid biogenesis and biofilm formation. *Nat Chem Biol* **5**, 913–919 (2009).
139. Akhavan, B. J., Khanna, N. R. & Vijhani, P. *Amoxicillin*. (2023).
140. Sharma, D. *et al.* Interplay of the quality of ciprofloxacin and antibiotic resistance in developing countries. *Frontiers in Pharmacology* vol. 8 Preprint at https://doi.org/10.3389/fphar.2017.00546 (2017).
141. Washington, J. A. & Wilson, W. R. Erythromycin: A Microbial and Clinical Perspective After 30 Years of Clinical Use (First of Two Parts). *Mayo Clinic Proceedings* vol. 60 189–203 Preprint at https://doi.org/10.1016/S0025-6196(12)60219-5 (1985).
142. Chaves, B. J. & Tadi, P. *Gentamicin*. (2012).
143. Patel, S., Preuss, C. V. & Bernice, F. *Vancomycin*. (2023).
144. Rafaque, Z. *et al.* In-vitro investigation of antibiotics efficacy against uropathogenic escherichia coli biofilms and antibiotic induced biofilm formation at subminimum inhibitory concentration of ciprofloxacin. *Infect Drug Resist* **13**, 2801–2810 (2020).
145. Thieme, L. *et al.* MBEC Versus MBIC: the Lack of Differentiation between Biofilm Reducing and Inhibitory Effects as a Current Problem in Biofilm Methodology. *Biol Proced Online* **21**, 18 (2019).
146. Okae, Y. *et al.* Estimation of Minimum Biofilm Eradication Concentration (MBEC) on In Vivo Biofilm on Orthopedic Implants in a Rodent Femoral Infection Model. *Front Cell Infect Microbiol* **12**, (2022).

147. Mandell, J. B. *et al.* Large variations in clinical antibiotic activity against Staphylococcus aureus biofilms of periprosthetic joint infection isolates. *Journal of Orthopaedic Research* **37**, 1604–1609 (2019).
148. Pettit, R. K., Weber, C. A. & Pettit, G. R. Application of a high throughput Alamar blue biofilm susceptibility assay to Staphylococcus aureus biofilms. *Ann Clin Microbiol Antimicrob* **8**, 28 (2009).
149. Castaneda, P., McLaren, A., Tavaziva, G. & Overstreet, D. Biofilm Antimicrobial Susceptibility Increases With Antimicrobial Exposure Time. *Clin Orthop Relat Res* **474**, 1659–1664 (2016).
150. Cruz, C. D., Shah, S. & Tammela, P. Defining conditions for biofilm inhibition and eradication assays for Gram-positive clinical reference strains. *BMC Microbiol* **18**, 173 (2018).
151. Adamus-Białek, W. *et al.* Ciprofloxacin, amoxicillin, and aminoglycosides stimulate genetic and phenotypic changes in uropathogenic Escherichia coli strains. *Virulence* **10**, 260–276 (2019).
152. Verderosa, A. D., Harris, J., Dhouib, R., Totsika, M. & Fairfull-Smith, K. E. Eradicating uropathogenic Escherichia coli biofilms with a ciprofloxacin–dinitroxide conjugate. *Medchemcomm* **10**, 699–711 (2019).
153. Goneau, L. W. *et al.* Selective Target Inactivation Rather than Global Metabolic Dormancy Causes Antibiotic Tolerance in Uropathogens. *Antimicrob Agents Chemother* **58**, 2089–2097 (2014).
154. Silhavy, T. J., Kahne, D. & Walker, S. The Bacterial Cell Envelope. *Cold Spring Harb Perspect Biol* **2**, a000414–a000414 (2010).
155. Alreshidi, M. M., Dunstan, R. H., Macdonald, M. M., Gottfries, J. & Roberts, T. K. The Uptake and Release of Amino Acids by Staphylococcus aureus at Mid-Exponential and Stationary Phases and Their Corresponding Responses to Changes in Temperature, pH and Osmolality. *Front Microbiol* **10**, (2020).
156. Perov, S. *et al.* Structural Insights into Curli CsgA Cross-β Fibril Architecture Inspire Repurposing of Anti-amyloid Compounds as Anti-biofilm Agents. *PLoS Pathog* **15**, e1007978 (2019).
157. Chen, D. *et al.* The broad-spectrum antibiofilm activity of amyloid-forming hexapeptides. *Microb Biotechnol* **14**, 656–667 (2021).
158. Cegelski, L. *et al.* Small-molecule inhibitors target Escherichia coli amyloid biogenesis and biofilm formation. *Nat Chem Biol* **5**, 913–9 (2009).
159. Serra, D. O., Mika, F., Richter, A. M. & Hengge, R. The green tea polyphenol EGCG inhibits E. coli biofilm formation by impairing amyloid curli fibre assembly and downregulating the biofilm regulator CsgD via the σ(E) -dependent sRNA RybB. *Mol Microbiol* **101**, 136–51 (2016).
160. Pruteanu, M., Hernández Lobato, J. I., Stach, T. & Hengge, R. Common plant flavonoids prevent the assembly of amyloid curli fibres and can interfere with bacterial biofilm formation. *Environ Microbiol* **22**, 5280–5299 (2020).
161. Bikels-Goshen, T., Landau, E., Saguy, S. & Shapira, R. Staphylococcal strains adapted to epigallocathechin gallate (EGCG) show reduced susceptibility to vancomycin, oxacillin and ampicillin, increased heat tolerance, and altered cell morphology. *Int J Food Microbiol* **138**, 26–31 (2010).

162. O'May, C., Ciobanu, A., Lam, H. & Tufenkji, N. Tannin derived materials can block swarming motility and enhance biofilm formation in Pseudomonas aeruginosa. *Biofouling* **28**, 1063–76 (2012).
163. Stenvang, M. *et al.* Epigallocatechin Gallate Remodels Overexpressed Functional Amyloids in Pseudomonas aeruginosa and Increases Biofilm Susceptibility to Antibiotic Treatment. *Journal of Biological Chemistry* **291**, 26540–26553 (2016).
164. Mulvey, M. A., Schilling, J. D. & Hultgren, S. J. Establishment of a persistent Escherichia coli reservoir during the acute phase of a bladder infection. *Infect Immun* **69**, 4572–4579 (2001).
165. Lim, J. Y., May, J. M. & Cegelski, L. Dimethyl sulfoxide and ethanol elicit increased amyloid biogenesis and amyloid-integrated biofilm formation in Escherichia coli. *Appl Environ Microbiol* **78**, 3369–3378 (2012).
166. Blomster-Hautamaa, D. A. & Schlievert, P. M. *Preparation of Toxic Shock Syndrome Toxin-1*. (1988).
167. Herigstad, B., Hamilton, M. & Heersink, J. *How to optimize the drop plate method for enumerating bacteria*. *Journal of Microbiological Methods* vol. 44 www.elsevier.comrlocaterjmicmeth (2001).
168. Wang, X. & Chapman, M. R. Sequence Determinants of Bacterial Amyloid Formation. *J Mol Biol* **380**, 570–580 (2008).
169. Hammer, N. D., Schmidt, J. C. & Chapman, M. R. The curli nucleator protein, CsgB, contains an amyloidogenic domain that directs CsgA polymerization. *Proceedings of the National Academy of Sciences* **104**, 12494–12499 (2007).
170. Cribbs, D. H. *et al.* Extensive innate immune gene activation accompanies brain aging, increasing vulnerability to cognitive decline and neurodegeneration: a microarray study. *J Neuroinflammation* **9**, 643 (2012).
171. McGreer, P. & McGreer, E. The inflammatory response system of brain: implications for therapy of Alzheimer and other neurodegenerative diseases. *Brain Res Rev* **21**, 195–218 (1995).
172. Akiyama, H. Inflammation and Alzheimer's disease. *Neurobiol Aging* **21**, 383–421 (2000).
173. Akama, K. T. & Van Eldik, L. J. β-Amyloid Stimulation of Inducible Nitric-oxide Synthase in Astrocytes Is Interleukin-1β- and Tumor Necrosis Factor-α (TNFα)-dependent, and Involves a TNFα Receptor-associated Factor- and NFκB-inducing Kinase-dependent Signaling Mechanism. *Journal of Biological Chemistry* **275**, 7918–7924 (2000).
174. Walters, A., Phillips, E., Zheng, R., Biju, M. & Kuruvilla, T. Evidence for neuroinflammation in Alzheimer's disease. *Prog Neurol Psychiatry* **20**, 25–31 (2016).
175. Tuppo, E. E. & Arias, H. R. The role of inflammation in Alzheimer's disease. *Int J Biochem Cell Biol* **37**, 289–305 (2005).
176. Chen, W.-W., Zhang, X. & Huang, W.-J. Role of neuroinflammation in neurodegenerative diseases (Review). *Mol Med Rep* **13**, 3391–3396 (2016).
177. A. McCombe, P. & D. Henderson, R. The Role of Immune and Inflammatory Mechanisms in ALS. *Curr Mol Med* **11**, 246–254 (2011).
178. Wang, Q., Liu, Y. & Zhou, J. Neuroinflammation in Parkinson's disease and its potential as therapeutic target. *Transl Neurodegener* **4**, 19 (2015).

179. Herrero, M.-T., Estrada, C., Maatouk, L. & Vyas, S. Inflammation in Parkinson's disease: role of glucocorticoids. *Front Neuroanat* **9**, (2015).
180. Kinney, J. W. *et al.* Inflammation as a central mechanism in Alzheimer's disease. *Alzheimer's & Dementia: Translational Research & Clinical Interventions* **4**, 575–590 (2018).
181. Jorfi, M., Maaser-Hecker, A. & Tanzi, R. E. The neuroimmune axis of Alzheimer's disease. *Genome Med* **15**, 6 (2023).
182. Rubio-Perez, J. M. & Morillas-Ruiz, J. M. A Review: Inflammatory Process in Alzheimer's Disease, Role of Cytokines. *The Scientific World Journal* **2012**, 1–15 (2012).
183. Meraz-Ríos, M. A., Toral-Rios, D., Franco-Bocanegra, D., Villeda-Hernández, J. & Campos-Peña, V. Inflammatory process in Alzheimer's Disease. *Front Integr Neurosci* **7**, (2013).
184. Ferreira, S. T., Clarke, J. R., Bomfim, T. R. & De Felice, F. G. Inflammation, defective insulin signaling, and neuronal dysfunction in Alzheimer's disease. *Alzheimer's & Dementia* **10**, (2014).
185. Hickman, S. E., Allison, E. K. & El Khoury, J. Microglial Dysfunction and Defective β-Amyloid Clearance Pathways in Aging Alzheimer's Disease Mice. *The Journal of Neuroscience* **28**, 8354–8360 (2008).
186. Meda, L. *et al.* Activation of microglial cells by β-amyloid protein and interferon-γ. *Nature* **374**, 647–650 (1995).
187. Altschul, S. F., Gish, W., Miller, W., Myers, E. W. & Lipman, D. J. Basic local alignment search tool. *J Mol Biol* **215**, 403–410 (1990).
188. Serwer, P., Hunter, B. & Wright, E. T. Electron Microscopy of In-Plaque Phage T3 Assembly: Proposed Analogs of Neurodegenerative Disease Triggers. *Pharmaceuticals* **13**, 18 (2020).
189. Mantri, S. & Shah, B. B. Enterovirus causes rapidly progressive dementia in a 28-year-old immunosuppressed woman. *J Neurovirol* **22**, 538–540 (2016).
190. Kristoferitsch, W. *et al.* Secondary dementia due to Lyme neuroborreliosis. *Wien Klin Wochenschr* **130**, 468–478 (2018).
191. Vargas, A., Carod-Artal, F., Del Negro, M. & Rodrigues, M. Dementia caused by neurosyphilis: clinical and neuropsychological follow-up of a patient. *Arq Neuropsiquiatr* **58**, 578–582 (2000).
192. Wiwanitkit, V. Dementia and neurocysticercosis. *Acta Neurol Taiwan* **23**, 1–3 (2014).
193. Hu, X., Mckenzie, C.-A., Smith, C. & Haas, J. G. The remarkable complexity of the brain microbiome in health and disease. *BioRxiv* (2023) doi:10.1101/2023.02.06.527297.
194. Hu, X., Haas, J. G. & Lathe, R. The electronic tree of life (eToL): a net of long probes to characterize the microbiome from RNA-seq data. *BMC Microbiol* **22**, 317 (2022).
195. Patterson, B. W. *et al.* Age and amyloid effects on human central nervous system amyloid-beta kinetics. *Ann Neurol* **78**, 439–453 (2015).
196. Zunt, J. R. Central Nervous System Infection During Immunosuppression. *Neurol Clin* **20**, 1–22 (2002).
197. Pruitt, A. A. Central Nervous System Infections in Immunocompromised Patients. *Curr Neurol Neurosci Rep* **21**, 37 (2021).
198. Sweeney, M. D., Sagare, A. P. & Zlokovic, B. V. Blood–brain barrier breakdown in Alzheimer disease and other neurodegenerative disorders. *Nat Rev Neurol* **14**, 133–150 (2018).

199. Yin, C. *et al.* ApoE attenuates unresolvable inflammation by complex formation with activated C1q. *Nat Med* **25**, 496–506 (2019).
200. Allan, L. L. *et al.* Apolipoprotein-mediated lipid antigen presentation in B cells provides a pathway for innate help by NKT cells. *Blood* **114**, 2411–2416 (2009).
201. Elzen, P. van den *et al.* Apolipoprotein-mediated pathways of lipid antigen presentation. *Nature* **437**, 906–910 (2005).
202. Strittmatter, W. J. *et al.* Apolipoprotein E: high-avidity binding to beta-amyloid and increased frequency of type 4 allele in late-onset familial Alzheimer disease. *Proceedings of the National Academy of Sciences* **90**, 1977–1981 (1993).
203. Burt, T. D. *et al.* Apolipoprotein (apo) E4 enhances HIV-1 cell entry in vitro, and the APOE ε4/ε4 genotype accelerates HIV disease progression. *Proceedings of the National Academy of Sciences* **105**, 8718–8723 (2008).
204. Kuo, C.-L. *et al.* APOE e4 Genotype Predicts Severe COVID-19 in the UK Biobank Community Cohort. *The Journals of Gerontology: Series A* **75**, 2231–2232 (2020).
205. Safdari Lord, J., Soltani Rezaiezadeh, J., Yekaninejad, M. S. & Izadi, P. The association of APOE genotype with COVID-19 disease severity. *Sci Rep* **12**, 13483 (2022).
206. Fujioka, H. *et al.* Apolipoprotein E4 Prevents Growth of Malaria at the Intraerythrocyte Stage: Implications For Diff erences in Racial Susceptibility to Alzheimer's Disease. *J Health Care Poor Underserved* **24**, 70–78 (2014).
207. Whitson, H. E. *et al.* Infection and inflammation: New perspectives on Alzheimer's disease. *Brain Behav Immun Health* **22**, 100462 (2022).
208. Long, J. M. & Holtzman, D. M. Alzheimer Disease: An Update on Pathobiology and Treatment Strategies. *Cell* **179**, 312–339 (2019).
209. Arnold, U. & Ulbrich-Hofmann, R. Quantitative Protein Precipitation from Guanidine Hydrochloride-Containing Solutions by Sodium Deoxycholate/Trichloroacetic Acid. *Anal Biochem* **271**, 197–199 (1999).
210. Miklossy, J. & McGeer, P. L. Common mechanisms involved in Alzheimer's disease and type 2 diabetes: a key role of chronic bacterial infection and inflammation. *Aging* **8**, 575–588 (2016).
211. Bener, A. *et al.* Association between type 2 diabetes mellitus and Helicobacter pylori infection. *Turk J Gastroenterol* **18**, 225–9 (2007).
212. Gulcelik, N. E. *et al.* Helicobacter pylori prevalence in diabetic patients and its relationship with dyspepsia and autonomic neuropathy. *J Endocrinol Invest* **28**, 214–217 (2005).
213. Bjerkhoel, A., Carlsson, M. & Ohlsson, J. Peripheral Facial Palsy Caused by the Borrelia Spirochete. *Acta Otolaryngol* **108**, 424–430 (1989).
214. Gurav, A. & Jadhav, V. Periodontitis and risk of diabetes mellitus. *J Diabetes* **3**, 21–28 (2011).
215. Niemiec, B. A. Periodontal Disease. *Top Companion Anim Med* **23**, 72–80 (2008).

# Appendix A: Peptide Sequences and Bacterial Strains

## Table A.1 *De novo* α-sheet peptide sequences.

| **Peptide Sequences** | | |
|---|---|---|
| **Name[a]** | **Sequence[b]** | **Extinction Coefficient ($M^{-1}$ $cm^{-1}$)** |
| AP5 | Ac-RGNwNeSkMNEYSGWmLmLtMGR-NH2 | 12660 |
| AP90 | Ac-RGEmNlSwMNEYSGWtMnLkMGR-NH2 | 12660 |
| AP401 | Ac-rGeMnLsWmneysGwTmNlKmGr-NH2 | 12660 |
| AP500 | Ac-RGNwNeSkMNEYSGWmLmCtMGR-NH2 | 12660 |
| AP501 | Ac-RGNwNeSkMNEYYGWmLmCtMGR-NH2 | 13940 |
| AP502 | Ac-RGNwNeSkMneyygWmLmCtMGR-NH2 | 13940 |
| AP503 | Ac-RGNwNeSkMNEYYGWmLmTcMGR-NH2 | 13940 |
| AP504 | Ac-RGNcNeSkMNEYYGWmLmLtMGR-NH2 | 8250 |
| AP505 | Ac-RGNwCeSkMNEYYGWmLmLtMGR-NH2 | 13940 |
| AP510 | Ac-RGEmNyFwMNEYYGWtMnCkMGR-NH2 | 15220 |
| AP516 | Ac-rgeMnYfWmneyygwTmNcKmgr-NH2 | 15220 |
| AP520 | Ac-RGEmNlSwMNEYSGWtMnCkMGR-NH2 | 12660 |
| AP521 | Ac-RGEcNlSwMNEYSGWtMnMkMGR-NH2 | 12660 |
| AP522 | Ac-RGEcNlSwMNEYYGWtMnMkMGR-NH2 | 13940 |
| AP523 | Ac-RGEcNlSwMneyyGWtMnMkMGR-NH2 | 13940 |
| AP524 | Ac-RCEmNlSwMneyyGWtMnMkMGR-NH2 | 13940 |
| AP525 | Ac-RGEmNlSwMneyyGWtMnMkCGR-NH2 | 13940 |
| AP530 | Ac-RGEcNyFwMNEYYGWtMnMrMGK-NH2 | 15220 |
| AP531 | Ac-RGEcNyFwMNEYYGWtMnMrXGK-NH2 | 15220 |
| AP532 | Ac-RGEmCyFwMNEYYGWtMnMrXGK-NH2 | 15220 |
| AP533 | Ac-RGExNyFwMNEYYGWtMnMrCGK-NH2 | 15220 |
| AP534 | Ac-RGExNyFwMNEYYGWtMnMcRGK-NH2 | 15220 |
| AP535 | Ac-RGEyNcFwMNEYYGWtMnMrMGK-NH2 | 15220 |

| | | |
|---|---|---|
| AP536 | Ac-RGElNyFwMNEYYGWtCnMrMGK-NH2 | 15220 |

Dimeric α-sheet peptides are produced by incubating the respective monomeric peptide in carbonate buffer to promote oxidation of the cysteine residue and dimerization via intermolecular disulfide bridges. The dimer extinction coefficient is equal to double that of the corresponding monomer. [a] "AP" refers to "Alternating Peptide", which indicates alternating L- and D- amino acid templating. [b] L- amino acids are displayed in all upper case; D-amino acids are displayed in lower case.

## Table A.2 Bacterial Strains

| Name | Description | Source |
|---|---|---|
| ***E. coli* Strains** | | |
| UTI89 | UPEC strain; cystitis isolate | Mulvey et al., 2001 |
| UTI89 Δ*CsgA* | UPEC strain; cystitis isolate with chromosomal deletion of *csgA* gene | Cegelski et al., 2009 |
| ***S. aureus* Strain** | | |
| MN8 | Clinically relevant strain; toxic shock isolate, urogenital tract | |

# Appendix B: Supplemental Figures

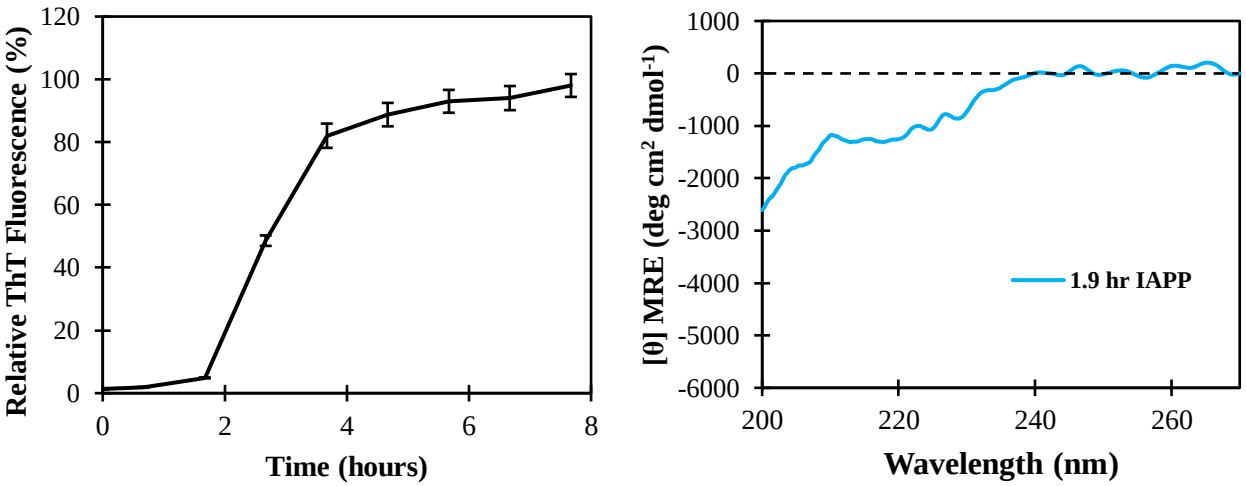


**Figure B.1. Characterization of 150 µM IAPP. A)** ThT kinetics of 150 µM IAPP in PBS indicate that the peptide has an aggregation lag phase of approximately 1.9 hours. **B)** CD spectroscopy of pre-incubated IAPP (t=1.9 hours) is representative of α-sheet structure.

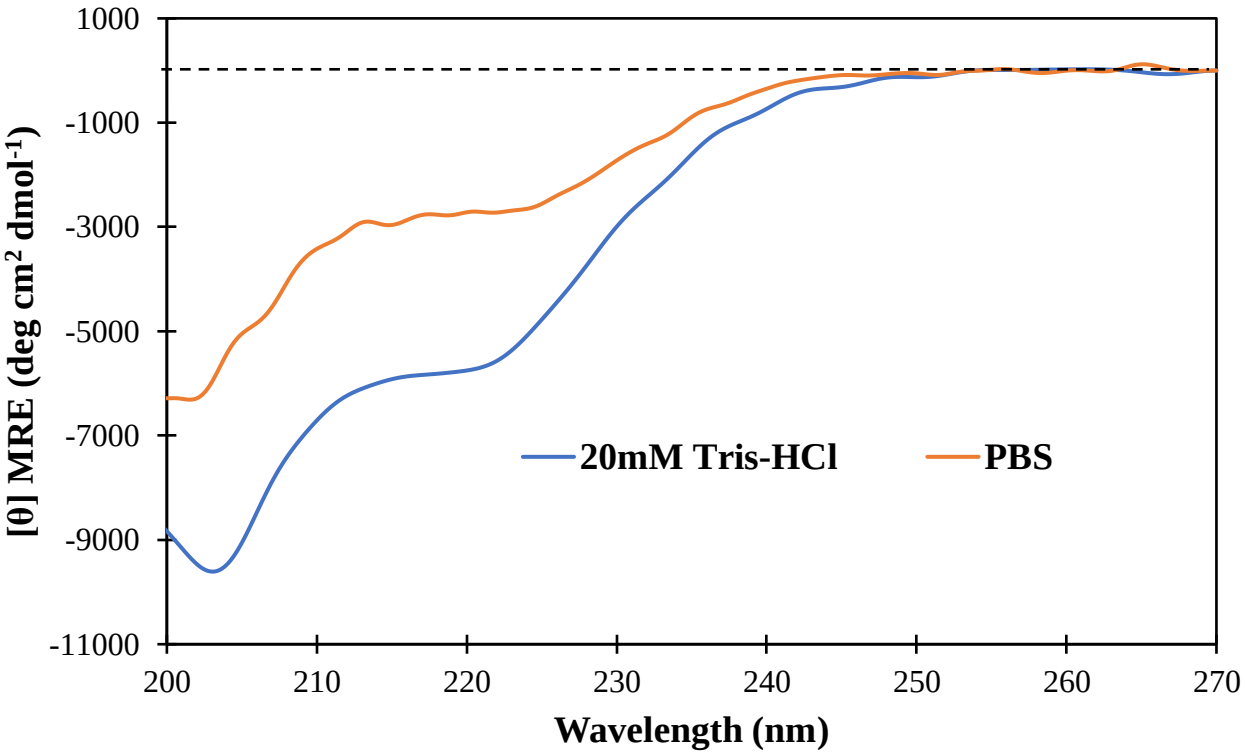


**Figure B.2. Secondary structure characterization of monomeric IAPP.** IAPP prepared in PBS (orange) produced a CD spectrum indicative of random coil structure while the CD spectrum of IAPP prepared in 20 mM Tris-HCl buffer is indicative of α-helical structure.

# Appendix C: Bacterial Minimum Inhibitory Concentrations

### C.1. Uropathogenic *Escherichia coli* (UPEC)

| | MIC (ug/mL) | bMIC (ug/mL) | bMEC (ug/mL) |
|---|---|---|---|
| **Amoxicillin** | | 60-120[151] | |
| **Ciprofloxacin** | 0.01875[153]<br>0.0215[152]<br>0.008-0.016[151] | 128-2048[144] | 382[152], >160[150] |
| **Gentamicin** | 1.25[153]<br>0.12-16[144] | 64-1024[144] | |
| **Vancomycin** | | | >8000[149] |

### C.2. Methicillin Susceptible *Staphylococcus aureus* (MSSA)

| | bMIC (ug/mL) | bMEC (ug/mL) |
|---|---|---|
| **Ciprofloxacin** | >128[147,148] | |
| **Gentamicin** | 10-1000[147], >2048[148] | 64-512[146] |
| **Vancomycin** | 50-100 (max at over 1000)[147], >2048[148] | 128-2048[146] |

MIC: the lowest concentration of an antibacterial agent necessary to inhibit visible growth. bMIC: minimum biofilm inhibitory concentration. bMEC: minimum biofilm eradication concentration (minimum concentration required to eradicate 99.9% of viable cells)[145].

# Copyright Permissions

**Chapter 1** reproduced in part with permission from:

Prosswimmer, T. and Daggett, V., 2022. The role of α-sheet structure in amyloidogenesis: characterization and implications. *Open Biology*, *12*(11), p.220261.

**Chapter 3** reproduced in part with permission from:

Bleem, A., *et al*. 2023. Designed α-sheet peptides disrupt uropathogenic *E. coli* biofilms rendering bacteria susceptible to antibiotics and immune cells. *Scientific Reports*, *13*(1), p.9272.

# VITA

Tatum Soleil Prosswimmer was born in Santa Monica, California and raised in Orange County, California. She received her Bachelor of Science in Bioengineering in 2018 from Santa Clara University in Santa Clara, CA. In 2023, she earned her Doctor of Philosophy from the University of Washington through the Molecular Engineering and Sciences Program. Her publications include:

**Prosswimmer, T.** and Daggett, V., 2022. The role of α-sheet structure in amyloidogenesis: characterization and implications. *Open Biology*, *12*(11), p.220261.

**Prosswimmer, T.,** Heng, A., Daggett, V. Mechanistic Insights into the Role of Amyloid-β in Innate Immunity. In Preparation.

**Prosswimmer, T.,** Nick, S., Bryers, J., Daggett, V. *De novo* α-sheet peptides destabilize bacterial biofilms and increase the susceptibility of *E. coli* and *S. aureus* to antibiotics**.** In Preparation.

Bleem, A., **Prosswimmer, T.,** Chen, R., Hady, T.F., Li, J., Bryers, J.D. and Daggett, V., 2023. Designed α-sheet peptides disrupt uropathogenic *E. coli* biofilms rendering bacteria susceptible to antibiotics and immune cells. *Scientific Reports*, *13*(1), p.9272.

Hsu, C., Templin, A., **Prosswimmer, T.,** Shea, D., Li, J., Brooks-Worrell, B., Kahn, S., Daggett, V. Human islet amyloid polypeptide-induced β-cell cytotoxicity is linked to formation of α-sheet structure. Submitted for publication.